Numerical investigation of lateral behaviour of a large pile group supporting an LNG tank

by

Kimberly Jones

B.Sc., University of Calgary, 2019

A Thesis Submitted in Partial Fulfillment of the

Requirements for the Degree of

MASTER OF APPLIED SCIENCE

in the Department of Civil Engineering

University of Victoria

Numerical investigation of lateral behaviour of a large pile group supporting an LNG tank

by

Kimberly Jones

B.Sc., University of Calgary, 2019

Supervisory Committee

Dr. Cheng Lin, Co-Supervisor

Department of Civil Engineering

Dr. Min Sun, Co-Supervisor

Department of Civil Engineering

Abstract

Liquefied natural gas (LNG) storage tanks are often supported by very large pile groups (≥ 100 piles). As these superstructures tend to be located along coastal areas, there is often a high risk of extreme lateral loading caused by either seismic, flooding or hurricane activity. In many cases, the foundation design can be governed by the required lateral resistance. At present, the responses of large pile groups subjected to lateral loading are not well understood. Published guidance for design is premised upon experimental testing of smaller pile groups (< 25 piles), and no additional commentary is provided to advise the design for groups of a larger scale.

A typical approach for design of laterally loaded pile groups uses the beam on Winkler foundations method, where nonlinear *p*-*y* curves are reduced by a *p*-multiplier to account for the group effects. Alternatively, an average *p*-multiplier known as a group reduction factor (GRF) can be used. Chapter 1 details the study of using 3D continuum finite element (FE) models to measure the group effects in large pile groups using *p*-multipliers and GRF. Soil conditions, pile spacing, pile number, and pile head condition were varied to observe their effects. The study also looked at the effect of the circular configuration of pile groups used in LNG tank foundations. The design standards and prevailing methods were shown to overestimate trailing row *p*-multipliers for large pile groups, particularly with larger pile spacing. Based on the study data and published data, a predictive equation was proposed for estimating GRF of a laterally loaded large pile group.

In addition, geotechnical engineers tend to evaluate the lateral responses of pile groups regardless of the presence of superstructures. It is not known whether this approach is suited for large infrastructure such as LNG storage tanks and their respective foundations. Chapter 2 captures the results from 3D finite element (FE) models used to observe the integrated tank and piled foundation behaviour and evaluate whether the current design approach used in practice is suitable. In addition, changes to soil-foundation stiffness, including varying soil conditions and pile spacing, were made to observe their effects. The results found that the foundation responses in the integrated model varied significantly from models which only considered the foundation. It was also found that the amount of LNG in the tank, soil conditions, and pile spacing also affected the lateral pile responses, particularly the leading and trailing piles.

Table of Contents

List of Tables

List of Figures

List of Publications

Jones, K., Sun, M., and Lin, C. 2021. Numerical analysis of group effects of a large pile group under lateral loading. Computers and Geotechnics (under review)

Jones, K., Sun, M., and Lin, C. 2021. Integrated analysis of LNG tank superstructures and foundations under lateral loading. Engineering Structures (under review)

Jones, K., Sun, M., and Lin, C. 2021. Numerical modeling of a large pile group under lateral loads. GeoNiagara 2021 (accepted)

Lin, C., Jones, K., and Sun, M. 2021. Lateral behavior of a large pile group supporting an LNG tank. Geo-Congress 2022 (under review)

Acknowledgements

I wish to express my gratitude to my supervisors, Dr. Min Sun and Dr. Cheng Lin, for their continuous support and guidance. Without their support, this thesis would not have been possible. I am thankful for the time and resources they provided me throughout the research project. Because of them, I was able to learn the research process as well as the procedures of publishing. Their encouragement helped me succeed as a MASc student.

I am also thankful to my fellow graduate students in our research team for their feedback and suggestions. I thoroughly looked forward to connecting with them each week. Having the opportunity to share my research made me a better presenter and helped me develop skills in addressing comments. I also gained a better, broader understanding of geotechnical engineering from hearing about their projects as well. While I am thankful to the entire group, I am particularly grateful to Owen and Jay who shared their experiences and provided me valuable advice in conducting my numeric research

Appreciation is also given to the University of Victoria and the National Sciences and Engineering Research Council of Canada (NSERC) who provided funding for this research.

Chapter 1. Numerical analysis of group effects of a large pile group under lateral loading

Jones, K., Sun, M., and Lin, C. 2021. Numerical analysis of group effects of a large pile group under lateral loading. Computers and Geotechnics (under review)

1.1. Introduction

Lateral responses of a pile group are commonly determined by using the beam on Winkler foundation (BWF) method with consideration of group effect, where the pile is modelled as a beam supported by nonlinear Winkler-springs positioned along its length. The soil resistance is simulated as pre-defined nonlinear springs using *p*-*y* curves which relate soil resistance, *p*, and horizontal pile deflection, *y*. For pile groups, the soil resistance is reduced by a *p*-multiplier, f_m, to reflect the decrease in lateral resistance caused by "group effect". Influence zones are developed behind individual piles within a pile group as they push the soil in front while the load is transferred to the soil. The overlapping of these zones in pile groups results in less soil resistance, and a reduction in the amount of load each pile can carry. The term "shadowing effect" is employed to describe the overlapping zones between piles in different rows, and the term "edge effect" is used to describe the overlapping shear zones between piles in the same row. The closer the piles are spaced, the more overlapping of the influence zones occurs, which creates a greater reduction of soil resistance.

Current design recommendations, such as those in FHWA (2016), AASHTO (2012), and FEMA P-751 (2012), suggest *p*-multiplier values in pile groups row-by-row, relative to the loading direction and the spacing between pile rows. "Leading-row" piles have larger *p*-multipliers than "trailing rows" since the soil in front of trailing piles has been weakened by the movement of the leading piles away from the soil mass. Additionally, the recommended *p*-multipliers for piles in closely spaced groups are smaller because of the greater overlap in the shear zones. An alternative approach to defining *p*-multipliers row-by-row is to instead define a group reduction factor which is applied to all piles in the group. The group reduction factor is the average *p*-multiplier for the group and is currently acceptable in practice for design considering seismic and cyclic loading as the "leading rows" and "trailing rows" alternate with a continual change in load direction (Brown et al. 2001). Group reduction factors may also be appropriate for large pile groups, where a majority of piles would be considered "trailing piles". Additionally, for liquefied natural gas

Table 1-1 Previous experimental studies of laterally loaded pile groups

References	Type of test	Soil type	Pile type	Pile head condition	Group size	Pile spacing	Deflection of pile head (inch/cm)
Brown (1987)	Full Scale	Stiff Clay	Steel Pipe	Free	3 × 3	3*D*	2/5.1
Brown (1988)	Full Scale	Med. Dense Sand	Steel Pile (grout-filled)	Free	3 × 3	3*D*	1.5/3.8
McVay et al. (1995)	Centrifuge	Sand	Steel Pipe	Free	3 × 3	3*D*, 5*D*	3/7.6
Ruesta and Townsend (1997)	Full Scale	Loose Sand	Prestressed Concrete Piles	Free	4 × 4	3*D*	3/7.6
Rollins et al. (1998)	Full Scale	Clay	Steel Pipe	Free	3 × 3	3*D*	2/5.1
McVay et al. (1998)	Centrifuge	Sand	Square Aluminum	Fixed	3 × 3 3 × 4 3 × 5 3 × 6 3 × 7	3*D*	3/7.6
Rollins et al. (2005)	Full Scale	Silts and Clays	Steel Pipe	Free	3 × 5	3.92*D*	3.5/8.9
Walsh (2005)	Full Scale	Sand	Steel Pipe	Free	3 × 5	3.92*D*	3.5/8.9
Rollins et al. (2006)	Full Scale	Stiff Clay	Steel Pipe	Free	3 × 3	5.65*D*	2.5/6.4
Christensen (2006)	Full Scale	Sand	Steel Pipe	Free	3 × 3	5.65*D*[1]	2/5.1
Taghavi and Muraleetharan (2017)	Centrifuge	Clay	Steel Pipe	Fixed	2 × 2	3*D* 7*D*	14/35

[1]3.29D spacing between piles in row

(LNG) tank foundations it is difficult to define pile rows due to their circular configuration. These foundations also have a higher expectation for design due to their importance and extremely high consequence of failure. Thus, it is of utmost importance for designing engineers to understand the lateral behaviour as well as the group effect for large pile groups.

The objective of this study is to quantify the group effect of large-scale pile groups by observing *p*-multipliers and group reduction factors. Within this paper, large scale pile groups are defined as those with ≥100 piles. Existing knowledge on laterally loaded pile groups is primarily derived from previous field testing as well as centrifuge testing performed in a lab. No experimental research exists, which is specific to large pile groups due to the great expense such testing would cost, and other logistic complexities of testing large foundations. Table 1-1 lists previous experimental studies on laterally loaded pile groups. All these tests have been performed on small groups (< 25 piles), with most limited to 3 × 3 arrangements, and pile spacing of 3 times pile diameter (3*D*). Also, most testing has focused on square or rectangular shape of pile groups, but no testing has been conducted for a circular pile group. Thus, there is no experimental data to suggest reliable *p*-multipliers for large pile group with circular configuration such as those used for LNG storage tank foundations. Published design manuals (Table 1-2) suggest *p*-multipliers based on the results of the published experimental work for small pile groups (Table 1-1). However, there is no comment on the range of validity for *p*-multipliers so it is left to the judgement of practicing design engineers to quantify the impact large pile groups may have on these values.

Table 1-2 Recommended *p*-multipliers from design manuals

Design Manual	Recommended *p*-Multiplier	
	Pile Spacing	f_m (from leading to trailing row)
AASHTO (2012)[1] & FHWA (2016)[1]	3*D*	0.70 0.50 0.35
	5*D*	1.00 0.85 0.70
FEMA P-751 (2012)[2]	3*D*	0.79 0.57 0.41
	5*D*	0.92 0.84 0.72
	6*D*	0.97 0.93 0.83
	≥8*D*	1.00 1.00 1.00
U.S Army (1991)[3]	3*D*	0.33 0.33 0.33
	4*D*	0.38 0.38 0.38
	5*D*	0.45 0.45 0.45
	6*D*	0.56 0.56 0.56
	7*D*	0.71 0.71 0.71
	≥8*D*	1.00 1.00 1.00

[1]Design manual recommends interpolation between values for other pile spacings
[2]Design manual recommends use of empirical formulas from Rollins et al. (2006)
[3]Design manual recommends group reduction factors

Numerical models are developed and validated by comparison to the experimental data from previous full-scale testing of a 7 × 9 pile group from an out-of-service LNG foundation in Japan, the largest test pile group ever reported. Parametric analyses are then performed to observe the large pile group behaviour affected by varying conditions, including soil condition, pile spacing, pile number, group shape, and pile head fixity. Current design recommendations and prevailing methods are then assessed for their applicability to large-scale pile groups. Through regression analyses of the collated data from this study as well as the experimental and numerical studies by others, a predictive equation is proposed for estimation of group reduction factor (GRF) of a pile group with the number of piles up to 1600.

1.2. Model validation

1.2.1. Three-dimensional continuum finite element (3D FE) Model

Continuum models of varying pile groups were evaluated in this study and were built using PLAXIS 3D. Prior to parametric analyses, a baseline model was validated through the simulation of a 7 × 9 pile group load test, which was once part of a 496-pile LNG foundation at the Osaka Gas Senboku Receiving Terminal 1 (Teramoto et al. 2018). This is the largest lateral load test to date and the study provided useful insights on the lateral effects of large pile groups, including the load-displacement of the pile group as well as pile deformation and bending moments at varying loading levels. However, *p*-multipliers and GRF were not derived in that study. For the 7 × 9 pile group, as well as a 2 × 1 pile group which was also tested on site, the loading was applied perpendicular to the larger dimension. The soil at the site is multilayered and was modeled as an elastic perfectly plastic material with Mohr-Coulomb as failure criteria while piles and pile cap as elastic materials in the 3D FE models. In all simulations, the water table is 1.225 m below ground surface as was encountered at the site. Soil parameters were back calculated by matching the calculated load-displacement curves at pile head of the 2 × 1 pile group to the field test results (Fig. 1-1(a)), and these are presented in Table 1-3.

Table 1-3 Input parameters (layered) used in the 3D FE model

Soil	Depth (m)	Average SPT N	γ[1] (kN/m^3)	E[2] (MPa)	ν[3]	c'_{ref}[4] (kPa)	φ'[5] (°)	ψ[6] (°)	k_0[7]
Filling soil (Gravel)	0-1.225	17	16.0	47.6	0.3	1	33.4	0.0	0.43
Filling soil (Gravel)	1.225-2.2	13	17.9	36.4	0.3	1	31.1	0.0	0.43
Silty sand	2.2-5.5	5.25	17.9	14.7	0.3	10	25.3	0.0	0.43
Silty clay	5.5-10.5	5	17.9	14.0	0.3	25.5	19.0	0.0	0.43
Gravel	10.5-14.0	8	17.9	22.4	0.3	10	27.7	0.0	0.43
Gravel sand	14.0-18.0	36	17.9	100.8	0.3	1	35.8	3.5	0.43
Silty clay	18.0-22.0	13	17.9	36.4	0.3	63.75	25.1	0.0	0.43
Gravel	22.0-26.7	46	17.9	128.8	0.3	1	39.3	3.5	0.43

[1]unit weight; [2]elastic modulus; [3]Poisson's ratio; [4]cohesion; [5]friction angle; [6]dilation angle; [7]coefficient of lateral earth pressure

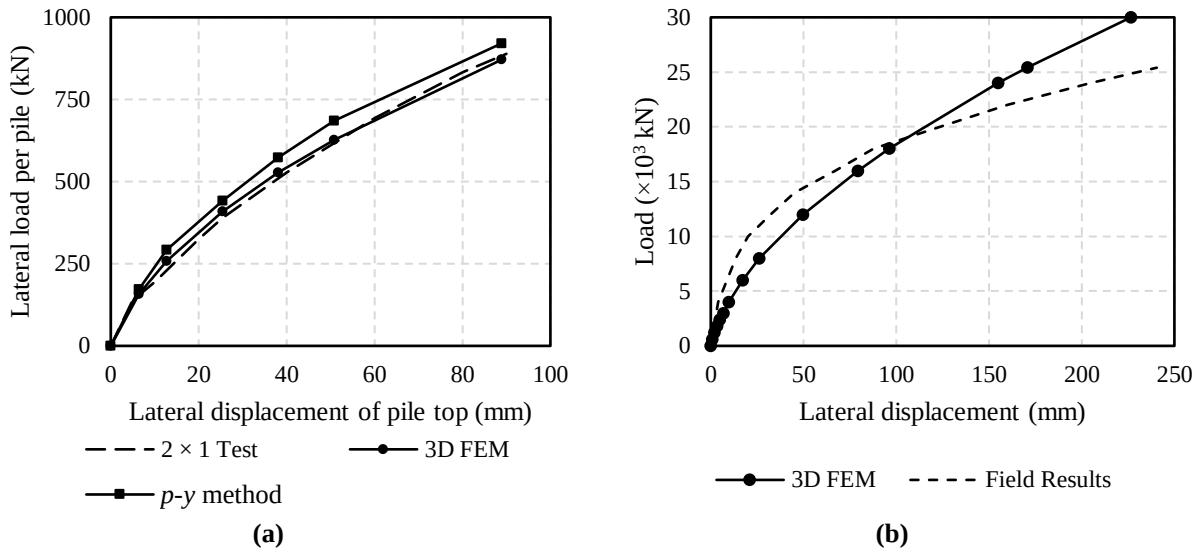

Figure 1-1 Comparison of load-deflection curves between numerical modeling and load tests: (a) 2 × 1 pile group (lateral load perpendicular to a larger dimension), (b) 7 × 9 pile group (lateral load perpendicular to a larger dimensions)

For the 7 × 9 pile group, in the preliminary study, four different baseline models (Cases I – IV) were constructed in the process of validation against the large pile group test. All were considered as half-models due to the symmetry of the foundation, as well as the applied loading. Fig. 1-2 illustrates the arrangements of the models. Case I is the simplest model since it only considers the 7 × 9 pile group. Case II is an extension of Case I, where the surrounding piles which remained in the soil during load tests are considered. Case III best reflects the in-situ loading conditions as a portion of the remaining piles are treated as reaction piles which experience equal loading in the opposite direction as the piles in the 7 × 9 group. Finally, Case IV assumes the reaction piles behave as a boundary. Cases II – IV obtained similar load-displacement behaviour results, as shown in Fig. A-1 in Appendix A. Ultimately Case III was considered herein since it best replicated the in-situ conditions during the loading tests.

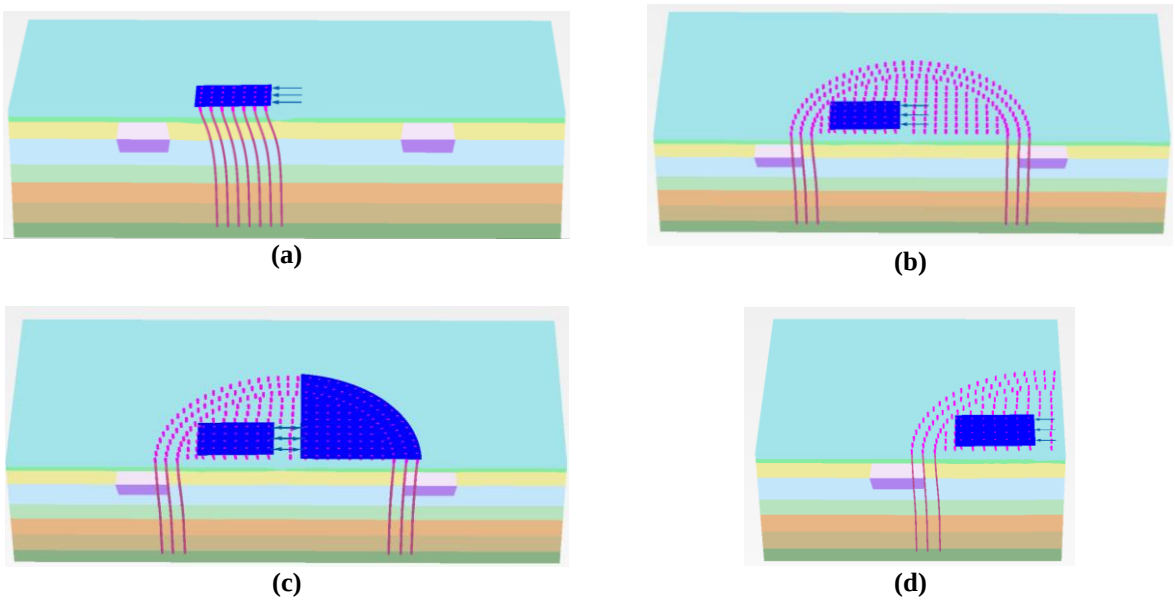

Figure 1-2 Construction of a 3D FE model validated against the field test: (a) Case I-test pile group without surrounding piles, (b) Case II-test pile group with surrounding piles, (c) Case III-full replication of the field test, and (d) Case IV-treating reaction pile group as a boundary

The piles supporting the LNG storage tank are steel pipe piles, with an outer diameter of 406.4 mm and a pipe thickness of 12.7 mm. The piles have a total length of 23.5 m with the top-most 6 m portion filled with reinforced concrete with 0.9 m of stick-up. The reinforced concrete pile cap is positioned above ground and has a thickness of 0.8 m. Within the 3D FE model, the foundation is modeled using structural elements only. Previous FE studies on smaller pile groups often model piles using volume elements, or a hybrid of a structural element (beam) and a volume element (e.g., Teramoto et al. 2018; Lin and Lin 2020). However, creation of piles using such elements is computationally expensive, particularly in the number of piles evaluated in this study (up to 1600). Instead, this study modelled the piles as embedded beams, and the stick up is modeled as a beam. The pile cap in the baseline models is modeled as a plate. Table 1-4 lists the input parameters used in the creation of the 3D FE models. The use of embedded beam structural element also requires input of skin friction and end bearing forces to simulate the vertical soil-pile interaction at failure. Values for these parameters were determined using recommended procedures provided by American Petroleum Institute (API 2011). Stiffness parameters were determined using the material and geometric properties of the pile. Within PLAXIS 3D, “medium” coarseness of soil elements was selected for the meshing of the soil. However, for the soil within the pile group, it was necessary to refine the mesh for more accurate results. The

zone of increased refinement extended 2*D* from the edge of the pile group, and 10*D* below the ground surface (Fig. A-2). For all models, vertical boundary was extended 10*D* below the tips of the piles while horizontal boundary ranged from 30*D* – 100*D* from the nearest edge of pile groups. For the single pile models and the smallest pile groups (2 × 2 and 3 × 3), the horizontal boundary used is 30*D*. The larger pile groups (4 × 4, 10 × 10 and 22 × 22) use horizontal boundaries of 50*D*, and the largest pile group models (40 × 40) uses a horizontal boundary of 100*D*. These boundaries were found to have negligible impact on numerical analysis results.

Table 1-4 Structural element parameters used in the 3D FE model

Structural Element	Element type	Depth below pile head (m)	E^1 (GPa)	γ^2 (kN/m^3)	A^3 (m^2)	I^4(10^{-3}) (m^4)	$T_{skin}{}^5$ (kN/m	$F_{end}{}^6$ (kN)	ν^7	d^8 (m)
Pile stickup	Beam	0-0.9	49.0	30.2	0.1295	1.334	-	-	-	-
Concrete-filled segment	Embedded Beam	0.9-6.0	49.0	30.2	0.1295	1.334	12	-	-	-
Hollow segment	Embedded Beam	6.0-23.5	200.0	78.5	0.01569	0.03037	55	125	-	-
Pile cap	Plate	-	28.2	24.0	-	-	-	-	0.15	0.8

[1]elastic modulus; [2]unit weight; [3]cross-sectional area; [4]moment of inertia; [5]skin resistance; [6]base resistance; [7]Poisson's ratio; [8]thickness

Using the back-calculated soil parameters in Table 1-3, the structural parameters in Table 1-4, and the forgoing model setup, the 7 × 9 pile group was simulated. Comparison of the load-displacement curves of the 3D FE models and results from the field test for are presented in Fig. 1-1(b). In general, the results are agreeable, although slight discrepancy is seen particularly at the higher loading levels. During the field testing, the researchers noted the falling of the pile heads from the pile cap (Teramoto et al. 2018). This was not considered in the numerical simulations and thus deflection is slightly underestimated in the 3D FE model results. In addition, a comparison can also be made to the load share of the piles in the 7 × 9 group as measured during testing. As shown in Fig. 1-3, load carried by each pile is normalized to the leading pile which carries the largest amount of load. The 3D FE model replicated the decrease in load share carried by the trailing piles (pile rows 4-7) as the applied load to the group increased. However, the 3D FE model results were unable to show a significant increase in load share in row 7 (trailing row) as was apparent

in the field results. The discrepancy may be a result of uncertainties in the field that could not be captured in the numerical modelling: for example, the above-mentioned pile-cap connection failures in some locations might cause redistribution of load share between piles. Overall, the results of the numerical model agree reasonably well with those of the field tests; therefore, the baseline numerical model is validated, which can be used for the further parametric analyses.

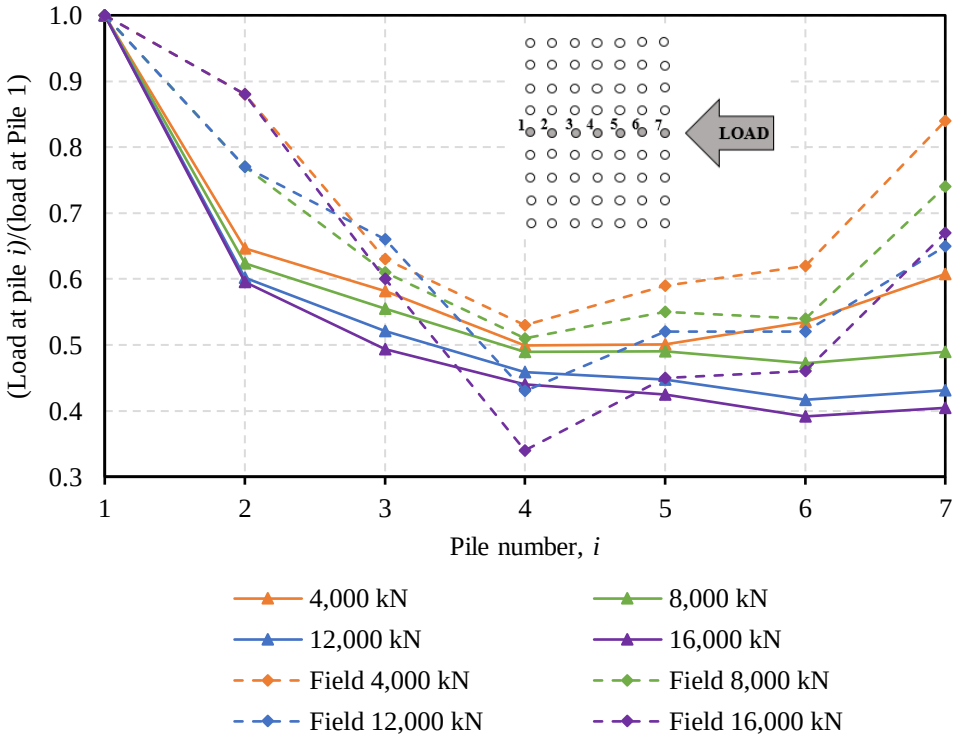

Figure 1-3 Load share of piles in the group subjected to varying lateral-load levels

1.2.2. Beam on Winkler foundation (BWF) model

A BWF model was created to back-calculate *p*-multipliers (f_m) for the 3D FE model as the direct derivation of soil resistance, *p* from the 3D FE model results to show reasonable variation along depth is often challenging. Similar approach is also employed by Rollins et al. (1998), Rollins et al. (2005), and Fayyazi et al. (2014). In general, a baseline BWF model for a single isolated pile is established by validating against the 3D FE model. Subsequently, BWF models for individual piles in a pile group are established from the baseline BWF model by assigning a reduction factor (*p*-multiplier) to account for the group effect. The *p*-multiplier in the BWF model is adjusted until the calculated results for individual piles matched the FE model results.

The BWF model was implemented in the software, LPILE. Instead of elements, soil is modeled as nonlinear Winkler-springs distributed along the length of the pile. Behaviour of an individual pile is based on the solution of fourth order differential equation for a beam with nonlinear support. Different *p-y* curves were selected to represent nonlinear spring supports to pile based on the different classifications of soils at the site. Therefore, the BWF model is also called *p-y* method in this study.

A baseline BWF for a single isolated pile was established using the 2 × 1 pile group. Since the lateral load was applied perpendicular to the length of the 2 × 1 pile group and the pile spacing was equal to 4*D*, a pile in the 2 × 1 test under lateral loading was properly modelled by a single isolated pile. For both the concrete-filled and hollow segments of the pile, input parameters of area, moment of inertia and modulus were identical to those used in the 3D FE models. For the soils, similar values of friction angle and shear strength as the 3D FE model were initially selected as input parameters to simulate the 2 × 1 pile group under lateral loading. However, for good agreement between the 3D FE and *p-y* methods, it was necessary to increase the friction angle of the two surficial layers by 5° within the baseline BWF model to closer relate the two models in load-displacement characteristics (agreement within 8%). Fig. 1-1(a) shows the calculated load-displacement curves of the 2 × 1 pile group from *p-y* method and 3D FE model, where both models show a good comparison with the field test results. As the 3D FE and BWF models rely on different constitutive relationships, different numerical solutions are expected. Thus, it is not unreasonable that different friction angles would be back calculated, and the difference is consistent with previous numerical studies (Lin and Lin 2020). Table 1-5 lists the *p-y* curves selected, as well as the other input soil parameters for the multilayered soil. Adjustments of the parameters below the two surficial layers had a negligible effect on load capacity of the pile and remained identical to the input parameters of the 3D FE model.

Table 1-5 Input parameters for BWF model

Soil	Depth (m)	*p-y* Curve	γ[1] (kN/m^3)	k[2] (kN/m^3)	c[3] (kPa)	φ[4] (°)	ε_{50}[5]
Filling soil (Gravel)	0 - 1.225	Sand (Reese)	16.0	24400	-	38	-
Filling soil (Gravel)	1.225 - 2.2	Sand (Reese)	8.1	16300	-	36	-
Silty sand	2.2 - 5.5	Sand (Reese)	8.1	5400	-	25	-
Silty clay	5.5 - 10.5	Soft Clay (Matlock)	8.1	-	30	-	0.020
Gravel	10.5 - 14.0	Sand (Reese)	8.1	16300	-	28	-
Gravel sand	14.0 - 18.0	Sand (Reese)	8.1	16300	-	36	-
Silty clay	18.0 - 22.0	Stiff Clay with Free Water (Reese)	8.1	135000	65	-	0.007
Gravel	22.0 - 26.7	Sand (Reese)	8.1	61000	-	39	-

[1]unit weight; [2]initial modulus of subgrade reaction; [3]undrained shear strength; [4]friction angle; [5]strain corresponding to one-half the maximum principal stress difference

1.3. Parametric analysis

A parametric study was conducted to observe the group effect of large laterally loaded pile groups. Table 1-6 details the extent of the study, where a total of 45 simulations were performed. Soil conditions, pile group size (i.e., number of piles), pile spacing, shape configuration, and pile head fixity were varied through the study to establish their impact on large pile group behaviour. In the study 3D FE models were created and simulated, while the *p-y* method (or BWF model) was employed to back-calculate *p*-multipliers for the individual piles in the groups using the procedure as described previously in the BWF model section. With *p*-multipliers determined for each individual pile, an average *p*-multiplier for each pile group is calculated and referred to as the group reduction factor (GRF). As with the baseline 3D FE model analysis, 3D FE models for parametric analyses were built as half models because of the symmetry of the pile groups and loading conditions considered herein.

Table 1-6 Details of 3D FE parametric analysis

Evaluation	Pile arrangement	Soil condition	Pile spacing	Pile-head fixity
Effect of soil conditions	10 × 10, 22 × 22, 40 × 40	Loose, medium dense, and dense sand, plus layered sand	5*D*	Free
Effect of number of piles	2 × 2, 3 × 3, 4 × 4, 10 × 10, 22 × 22, 40 × 40	Layered	3*D*, 5*D*, 6*D*, 8*D*	Free
Effect of pile spacing				
Effect of group shape	496 (circular) vs. 484 (square) 1600 (circular) vs. 1600 (square)	Layered	3*D*, 5*D*	Free
Effect of pile head fixity	3 × 3, 10 × 10, 22 × 22, 40 × 40	Layered	3*D*, 5*D*	Free, fixed

The lateral load needed to mobilize the pile head by 25.4 mm (1") is used to estimate *p*-multipliers in this study. It is also used to define lateral capacity (Lin and Wu 2019) herein when group efficiency (average lateral capacity of individual piles in a pile group divided by the capacity of a single isolated pile) is to be determined. Previous research on laterally loaded pile groups has found the *p*-multiplier, and thus group reduction factor, to be constant once a displacement of at least 20 – 30 mm is reached (McVay et al. 1998). Thus, the results presented are expected to also be valid at larger pile mobilization as well. The majority of the continuum simulations considered free pile head condition, where point displacements were applied at the top of the pile without any restriction of rotation. For the simulations which did consider fixed-head condition, the models connected the top of the piles to a "rigid body" in the 3D FE model where all three rotational degrees of freedom were set to zero.

1.4. Results

1.4.1. Effect of soil conditions

Previous experimental and numerical studies have shown that the soil conditions, specifically the density of sands, affects the lateral responses of pile groups (e.g., McVay et al. 1995; Fayyazi et al. 2014). The Japanese LNG terminal site studied by Teramoto et al. (2018) has multilayered soil, in which limited experimental derivations of *p*-multipliers has been performed (e.g., Christensen 2006). In order to observe the impact on the group effect caused by soil condition, the foundation response in multilayered soil is compared with similar foundations in uniform sand with

varying densities. Table 1-7 lists the input parameters for the uniform sand conditions used in the 3D FE models. As with the multilayered soil, results of *p*-multiplier and GRF from the uniform sand were derived by fitting load-deflection responses from BWF models for individual piles in a pile group to those of 3D FE models while varying *p*-multiplier. In the BWF models, Reese sand *p*-*y* curves were selected for the uniform soil. As with the multilayered soil, friction angles in all three densities of sand in the baseline BWF model were increased by 4° as compared to the 3D FE model to ensure agreement between the two models within 7%, 4% and 1% for loose, medium dense and dense sands, respectively. The water table was also assumed to be at an identical depth as the layered soil (i.e., 1.225 m below ground surface). With agreeable baseline BWF models with the 3D FE models for multilayered soil as well as loose, medium dense and dense uniform soil, analyses were performed to observe the impact of the different soil conditions on the pile group effect of large pile groups (*p*-multiplier and GRF). Specifically, 10 × 10, 22 × 22, and 40 × 40 pile groups with 5*D* pile spacing were created as 3D FE models and analyzed.

Table 1-7 Soil parameters for uniform soils in 3D FE model

Relative density of sand	γ[1] (kN/m^3)	E[2] (kN/m^2)	ν[3]	φ[4] (°)	ψ[5] (°)	k_0[6]
Loose	17.9	42000	0.3	30	0.0	0.50
Medium dense	17.9	55000	0.3	35	0.0	0.43
Dense	17.9	70000	0.3	40	0.0	0.36

[1]unit weight; [2]elastic modulus; [3]Poisson's ratio; [4]friction angle; [5]dilation angle; [6]cofficient of lateral earth pressure

For laterally loaded piles, it is expected that approximately the top 10*D* of soil governs the response of the piles (Brown et al. 1988). For the multilayered soil, this consists of loose-to-medium dense sand atop very loose silty sand. It is not expected that any of the deeper soil layers to have much, if any, impact on the results. This was also observed through the back calculation of soil parameters in the baseline 3D FE model (against the field test) where changes in deeper soil layer parameters had a negligible effect on the lateral responses of piles. Previous studies on smaller pile groups have shown that as density increases in cohesionless soils, *p*-multiplier decreases (e.g., McVay et al. 1995). In other words, a greater group effect is observed in dense sand than in loose sand. The results from this study do show that this is also the case with large pile groups. In particular, this trend is clear from the three uniform soil cases for *p*-multiplier, as can be seen in Fig. 1-4. The multilayered soil, however, provides a different trend of *p*-multipliers. Unlike the uniform soils, the leading row *p*-multipliers are significantly lower in all three pile groups. Additionally,

most of the trailing row *p*-multipliers are lower than all three of the uniform soil conditions. Given the loose-to-medium dense sand at the surface of the multilayered soil profile, the *p*-multiplier trend would normally be expected to be between the range outlined by the uniform sand results. The multilayered soil profile has a clear influence on group effect; however, the behaviour of a single pile appears to be unimpacted. The lateral capacity of a single isolated pile modeled in multilayered soil was found to be between the capacities obtained from loose and medium dense sands. Thus, it can be concluded that the layer (at a depth of 5.5*D*-10*D*) beneath the surficial sand (0-5.5*D* depth) plays a key role in affecting the results for pile group interaction at this site.

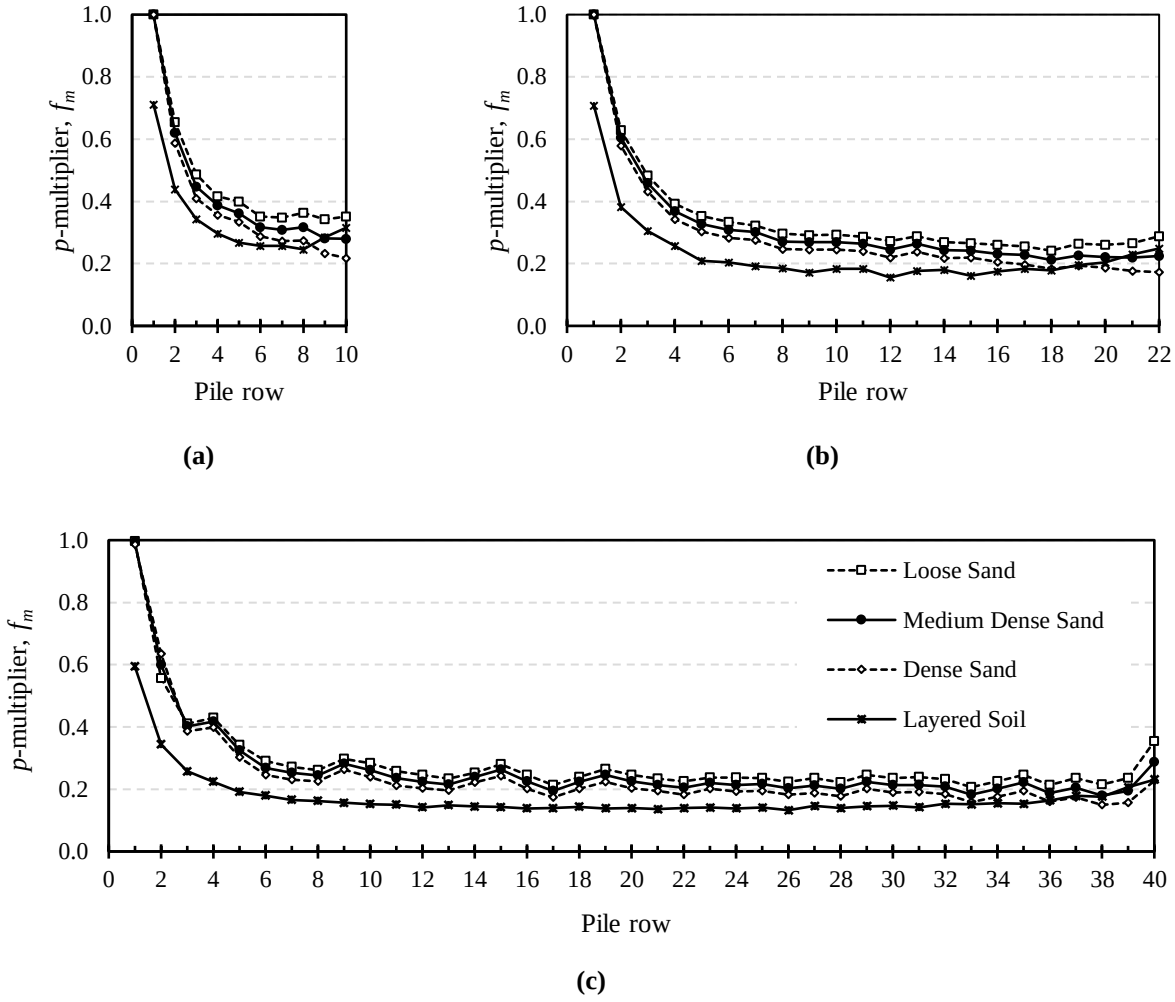

Figure 1-4 Variations of *p*-multiplier with soil conditions: (a) 10 × 10 (b) 22 × 22 and (c) 40 × 40 pile groups with Row 1 corresponding to leading row while higher row numbers corresponding to trailing rows

In a separate analysis, 3 × 3 and 10 × 10 pile groups with 3*D* pile spacing were compared in linear-elastic soil to observe the effect a significant change in the elastic modulus, *E*, has on small and large pile groups. For the comparison, three scenarios were considered: a 5.5*D*-thick higher soil modulus above a lower soil modulus soil, a 5.5*D*-thick lower soil modulus above a higher modulus soil, and a uniform higher modulus soil. Note that for this evaluation, the values of soil modulus were similar to the loose-to-medium dense (E = 42 MPa) sand and very loose silty sand (E = 14.4 MPa) from the Japanese soil. Instead of *p*-multipliers, only lateral capacity from the 3D FE model was used for the comparison. Little to no changes in the capacity were observed for the 3 × 3 pile group. However, with the higher modulus soil being above a lower modulus soil, the capacity of the piles and group efficiency of the 10 × 10 pile group were lower than the other two scenarios which obtained similar results. Details can be found in Fig. A-3. This finding is verified by a previous study which also determined stiff-over-soft soil profiles cause a reduced group efficiency (Salgado et al. 2014).

Soil conditions also affect the magnitude of GRF in large pile groups, and these results are presented in Fig. 1-5. For the uniform soil, loose sands have the highest group reduction factors for all three pile group sizes studied. Medium dense sand obtains factors slightly below loose sand, and similarly, dense sand obtains factors slightly below medium dense sand. The group reduction factors for the models in multilayered soil generate the smallest values between the four soil conditions considered. However, Fig. 1-5 shows the curves generated for the four soil conditions all follow a similar trend. This suggests GRF may be less impacted by the soil conditions than *p*-multipliers.

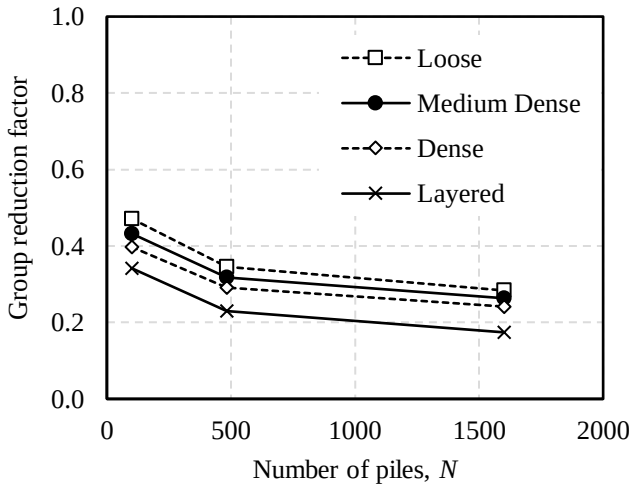

Figure 1-5 Group reduction factors of a pile group in uniform soils and layered soil

1.4.2. Effect of pile spacing

It is well known that pile spacing has a significant effect on the lateral capacity of pile groups. However, existing research, listed in Table 1-1, has mainly focused on small pile groups (< 25 piles) with a spacing of 3 times pile diameter (i.e., S=3D). However, it is common to see larger piles spacings used in larger foundations. In this study, pile spacings of S=3D, 5D, 6D and 8D are compared for both smaller (2 × 2, 3 × 3, and 4 × 4) and larger (10 × 10, 22 × 22, and 40 × 40) pile groups. All results were obtained by considering pile groups in the multilayered soil from the Japanese LNG Terminal site (Teramoto et al. 2018).

As expected, pile spacing does affect the values of p-multipliers for small and large pile groups. Fig. 1-6 compares p-multipliers by row for groups with different pile spacings. With 3D, 5D, and 6D pile spacings, the leading row p-multiplier decreases as the pile group becomes larger. At S=8D, the leading row p-multiplier appears to stay consistent at unity. Thus, the leading row p-multiplier is not only a function of spacing, but also of the pile group size. Although, this may be caused by the multilayered soil since all the large pile groups in uniform soil found identical p-multiplier value for all leading rows. For the larger pile groups, the value of p-multipliers plateaus after about the 4th or 5th pile row, which is consistent with previous findings (McVay et al. 1998). Additionally, the plateau appears to slightly vary between the three large pile groups which suggests that the total number of piles and rows influences trailing row p-multipliers. For the 22 × 22 pile groups, this plateau is observed to be approximately 0.06, 0.19, 0.28, and 0.53 for 3D, 5D, 6D and 8D pile spacings, respectively. Even with 8D pile spacing, the p-multipliers in the trailing rows are much lower than what would be expected. It is normally understood that piles at such a significant spacing would not experience interaction and design would not require any decrease in soil resistance (i.e., f_m = 1 for all piles).

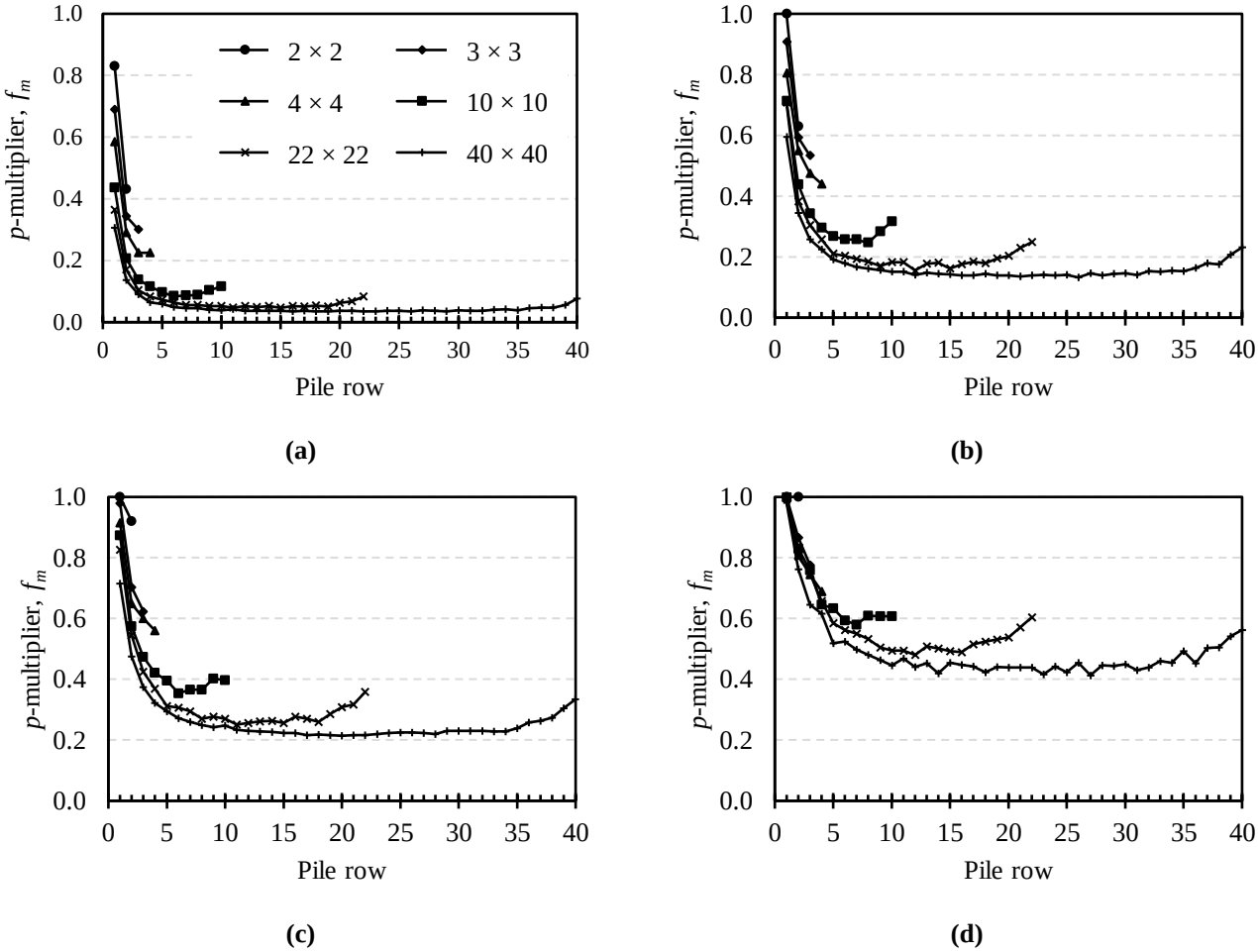

Figure 1-6 Variations of *p*-multiplier with pile spacing: (a) *S*=3*D*; (b) *S* =5*D*; (c) *S* =6*D*; (d) *S* =8*D*

Since *p*-multipliers of the piles vary by spacing, so do group reduction factors. Fig. 1-7(a) displays the change in GRF as the pile spacing changes, with each curve representing a different number of piles. Each curve is shown to have a similar trend between small pile groups and large pile group: i.e., GRF approximately increases linearly with the increase in pile spacing. This relationship is also observed in small pile groups by others as discussed later.

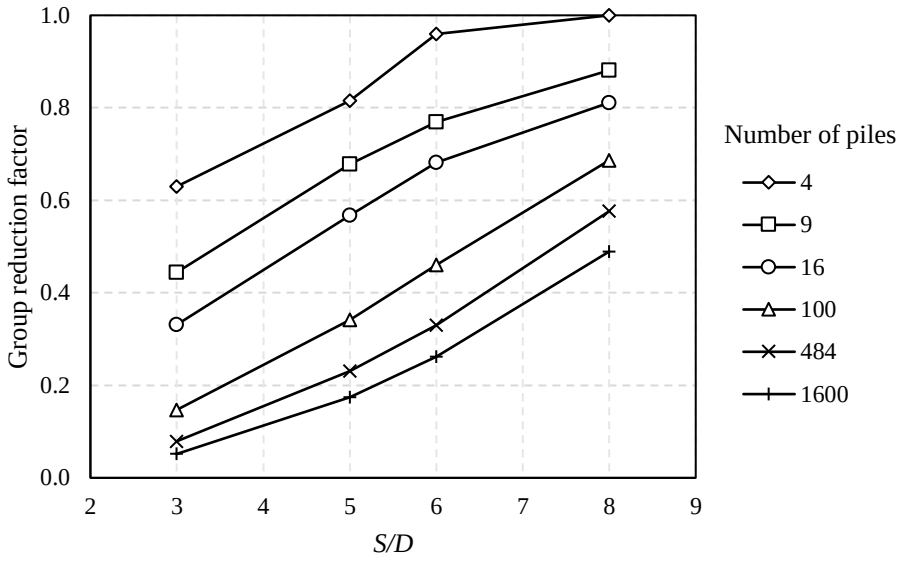

(a)

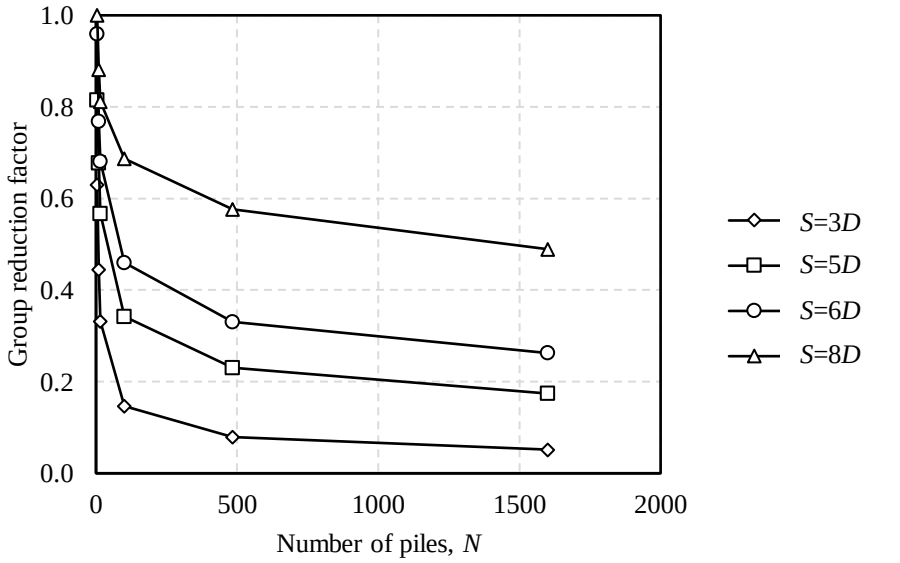

(b)

Figure 1-7 Group reduction factor varied with (a) pile spacing and (b) number of piles

1.4.3. Effect of pile number

Fig. 1-7(b) presents variations of GRF with the number of piles using the same set of data as Fig.1-7(a). Only the GRF is evaluated since the results are independent of the number of rows in the pile group. Fig. 1-7(b) shows that as the number of piles increases, the GRF decreases. This is consistent with previous studies (Fayyazi et al. 2014).

Nevertheless, it is interesting that the precipitous reduction in GRF occurs when the number of piles is less than 100 but the rate of reduction becomes smaller as the number of piles exceeds 100. The decrease appears to follow a negative exponential power relationship. It should be noted that the results are obtained in multilayered soil. As observed earlier, the multilayered soil yielded slightly lower group reduction factors than the uniform soil but the trend of GRF varied with the number of piles is similar between the layered soil and the uniform soil (Fig. 1-5).

1.4.4. Effect of pile group (shape) configuration

One application of large pile group foundations is to support liquefied natural gas (LNG) storage tanks. These pile groups typically have orthogonally arranged piles surrounded by two or three rings of piles as shown in Fig. 1-8, where the rings are positioned to carry the load of the tank walls and most efficiently support the superstructure. The 496-pile foundation from the Osaka Gas Senboku Receiving Terminal 1 is one example of this (Teramoto et al. 2018). However, it is also possible for the LNG tanks, and the supporting pile foundation, to be much larger. Another example of an LNG storage tank foundation layout can be found in Savannah, GA, USA (Lin and Lin 2019) where the number of piles in the foundation totals 1600. As most pile groups used in practice are rectangular in configuration, no experimental research has been conducted to observe the behaviour of pile groups in circular or other arrangements. For this aspect of the parametric study, 496- and 1600- pile group LNG foundations were considered with 3*D* and 5*D* pile spacing. Arrangement layouts are shown in Fig. 1-8. These LNG foundation arrangements were compared with rectangular arrangements to observe the effect of the shape configuration. The 496-pile LNG foundations were compared with 22 × 22 foundations (484 piles), and the 1600-pile LNG foundations were compared with 40 × 40 foundations.

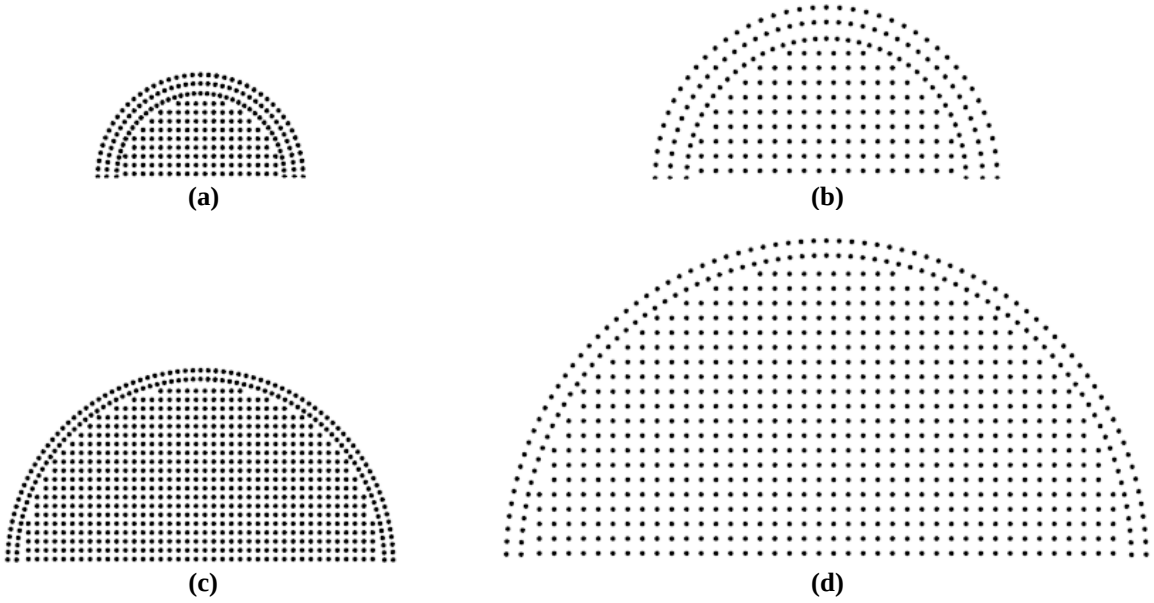

Figure 1-8 Circular pile group arrangements in half model: (a) 494 piles, *S*=3*D*, (b) 494 piles, *S*=5*D*, (c) 1600 piles *S*=3*D*, (d) 1600 piles, *S*=5*D*

Previously, the *p*-multipliers presented were the average for an entire row in a pile group. However, considering the circular configuration of the outer rings of piles in the LNG foundation, it is difficult to average *p*-multipliers by row due to the misalignment of outer rings and inner orthogonal rows of piles. Also, the number of piles in the outer rings typically exceeds the number of internal rows, meaning two piles in the same "row" may in fact be parallel to the load direction which contradicts the meaning of a pile row. Even if the averages by row were determined, it may not be practical or useful to compare to the square arrangements. Alternatively, Fig. 1-9 shows the distribution of *p*-multipliers for the piles along the midline of the foundation as well as those along the edge and perimeter. The plots in Fig. 1-9 compare the *p*-multipliers against the distance from the front-most pile (leading pile). For all four LNG foundations, the *p*-multipliers along the midline piles are identical to those from the corresponding square models. Thus, the group effect of the midline piles appears to be independent of configuration. However, the piles along the edge of the square foundation and the piles along the perimeter of the LNG foundation display different trends in *p*-multipliers. The piles along the edge of the square foundations show a similar trend of *p*-multipliers as the midline piles, with the difference being an increase in value (approximately 0.05 for trailing piles in Fig 1-9(a, c), 0.10 in Fig. 1-9(b, d)). In contrast, the *p*-multipliers from the piles along the perimeter of the LNG foundation display a unique trend. For all the LNG models, the *p*-multipliers appear to degrade linearly before plateauing in value. The front-most

half of the perimeter piles appear to experience less "shadowing" from piles in front compared to traditional rectangular foundations. Conversely, the trailing half of the perimeter piles experiences more "shadowing" from leading piles and thus display lower lateral soil resistance, and *p*-multiplier values, than the square models.

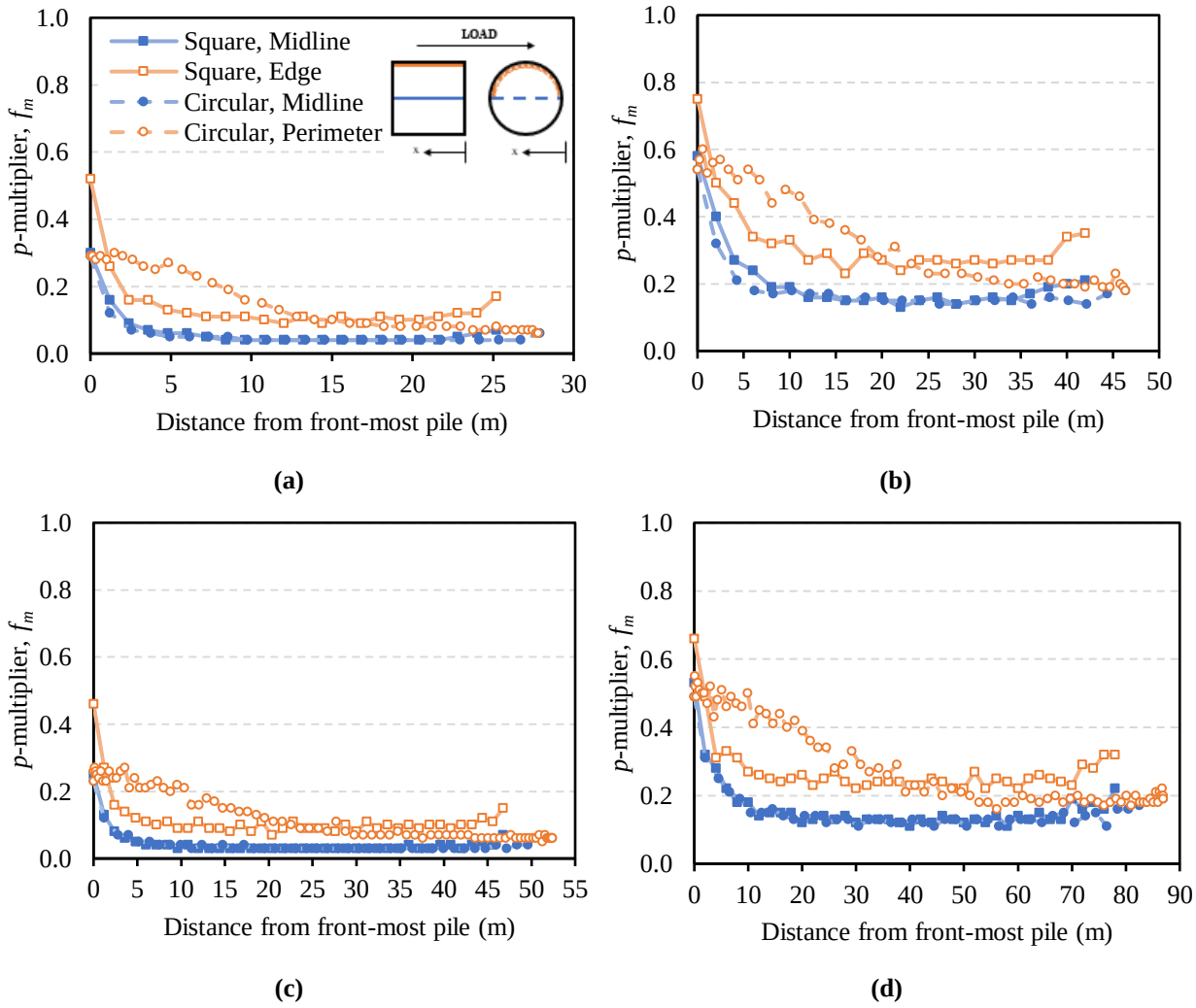

Figure 1-9 *p*-multiplier for square and circular large pile groups: 22 × 22 and 496 piles with (a) *S*=3*D* and (b) *S*=5*D*, 40 × 40 and 1600 piles with (c) *S*=3*D* and (d) *S*=5*D*

While there are important differences noted in *p*-multipliers for perimeter piles, this study observed that group reduction factors between the circular and square arrangements are approximately equal, as seen in Fig. 1-10. This suggests that for large pile groups, GRF is independent of the group configuration, and GRF derived from square configuration can be used for circular configuration.

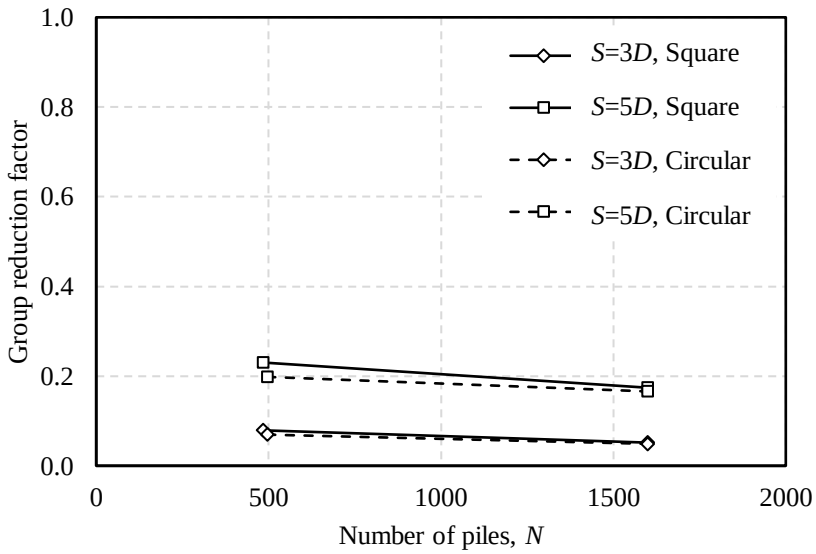

Figure 1-10 Group reduction factor for square and circular pile groups

1.4.5. Effect of pile head condition

All the previous 3D FE model simulation results have been based on an assumed free-head condition for all piles. Free-head condition allows the pile head to freely translate and rotate in any direction. Thus, there are no restrictions on the three translational degrees of freedom (DOFs) (i.e., free to translate) and the three rotational DOFs (i.e., free to rotate). Fixed-head condition on the other hand restricts only the three rotational DOFs but imposes no translational restrains to pile head. As with the free-head condition, the lateral translation is set at 25.4 mm for the fixed-head conditions. While most previous research has focused on free-head condition, it is often more practical to assume a certain level of pile head fixity as most pile groups are used in conjunction with a pile cap to complete the foundation. For the LNG foundations considered in this study, the pile caps are elevated over the ground surface. This means that while the pile cap does not directly transfer load to the soil, it does provide some fixity to the pile head but may not the full fixity (i.e., fixed-head condition). The degree of fixity depends on the embedment of pile reinforcement into the pile cap, rigidity of pile cap, pile spacing, etc. It is important to understand any impacts additional fixity has in design as compared to the free-head condition. For the purposes of this study, changes in *p*-multiplier and group reduction factor are used to measure the effect of pile head conditions. A small pile group (3 × 3) is compared to large

pile groups (10 × 10, 22 × 22, and 40 × 40) under fixed-head and free-head conditions. Additionally, these analyses were performed with both 3*D* and 5*D* pile spacing.

Fig. 1-11 presents the resulting *p*-multipliers for free- and fixed-head conditions. For the 3 × 3 pile groups, an increased group effect (corresponding to a reduced *p*-multiplier) is noted with the fixed-head condition for both 3*D* and 5*D* pile spacing (Fig. 1-11(a)). Additionally, all the larger pile groups are affected by head fixity as well (Fig. 1-11(b, c, d)). However, the effect appears more significant when the piles are spaced 5*D* apart. For the larger models, particularly the 22 × 22 and 40 × 40 pile groups, the *p*-multipliers for free- and fixed-head condition nearly converge with 3*D* pile spacing. This suggests the group effect is already very significant and a threshold in reduction of lateral soil resistance may have been reached. Moreover, fixity is seen to affect both leading and trailing row *p*-multipliers. Observations are focused on the results from the 5*D* spacing models since they do not appear to encounter a resistance reduction threshold. The leading row *p*-multipliers are the most significantly impacted. For fixed-head condition, leading row *p*-multiplier values are reduced by 0.26-0.31 for the four pile group sizes studied. The reduction does not seem to follow a particular trend with respect to group size. In contrast, the reduction in trailing row *p*-multipliers appear to be smaller and correlate to pile group size. For the 3 × 3 pile group, trailing row *p*-multiplier values are reduced by approximately 0.2 with fixed-head condition. This becomes less significant in the larger 10 × 10 model (*p*-multiplier reduced by 0.15), as well as the 22 × 22 and 40 × 40 models (*p*-multiplier reduced by 0.1).

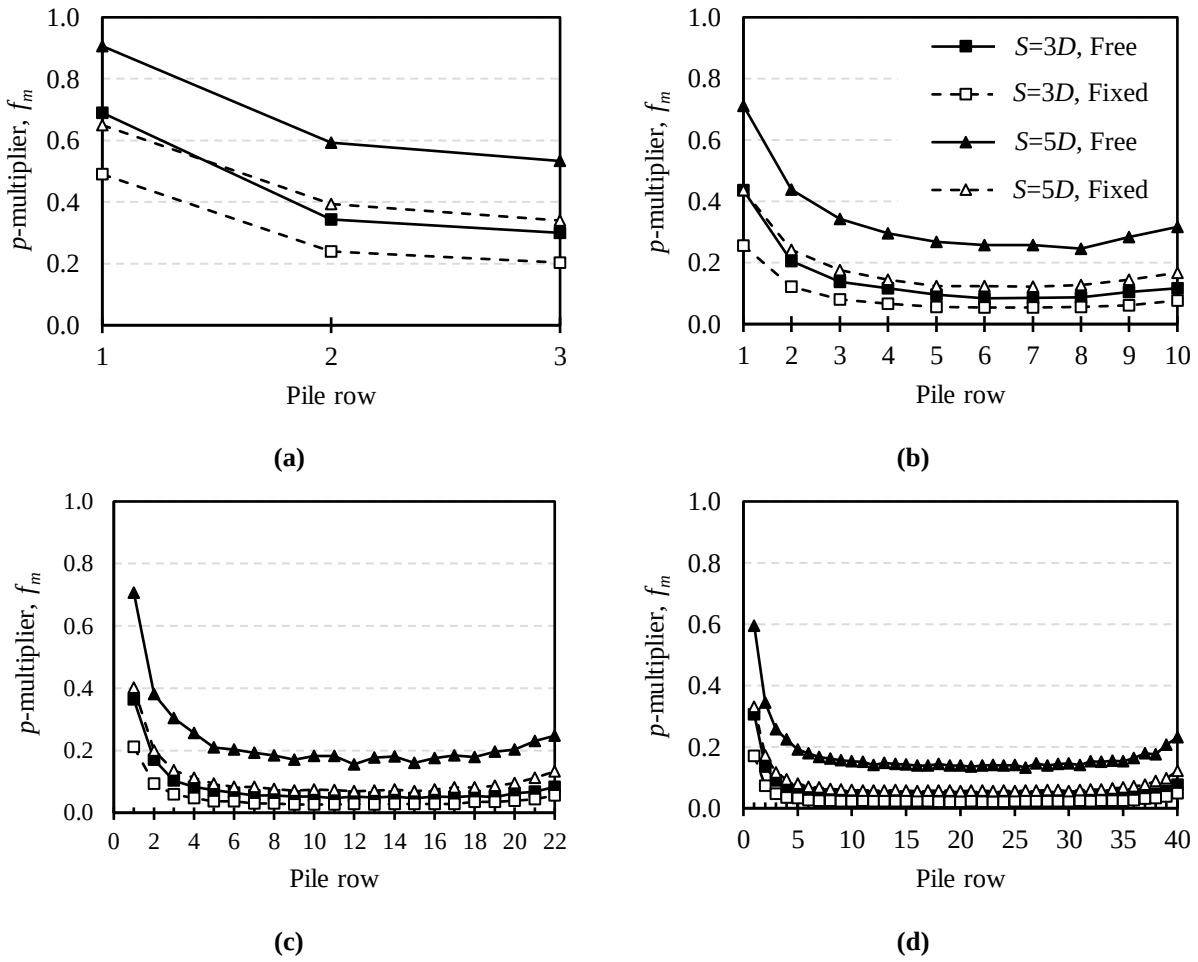

Figure 1-11 Effect of pile head fixity on *p*-multiplier for pile groups of: (a) 3 × 3, (b) 10 × 10, (c) 22 × 22, and (d) 40 × 40

Pile groups with fixed-head condition also experience a reduction in group reduction factors as the number of piles in the group increases. Fig. 1-12 shows the group reduction factors for the four pile groups considering free- and fixed-head conditions, where similar reduction trends are observed. This figure shows there is a more significant difference between free- and fixed-head conditions for the larger spacing of 5*D* than 3*D*, as was observed with *p*-multipliers. However, a slight convergence as the number of piles increases is observed with 5*D* pile spacing for the different head fixities as well. With 3*D* pile spacing, the convergence appears more significant. Additionally, the group reduction factor was determined from Case I of the 7 × 9 baseline model where the piles were spaced at 5*D*. The value appears to nearly overlap the interpolated line between the results from the 3 × 3 and 10 × 10 pile groups under fixed-head condition. Thus, it appears the group effect for a pile group with a pile cap is close to a pile group with fixed pile head.

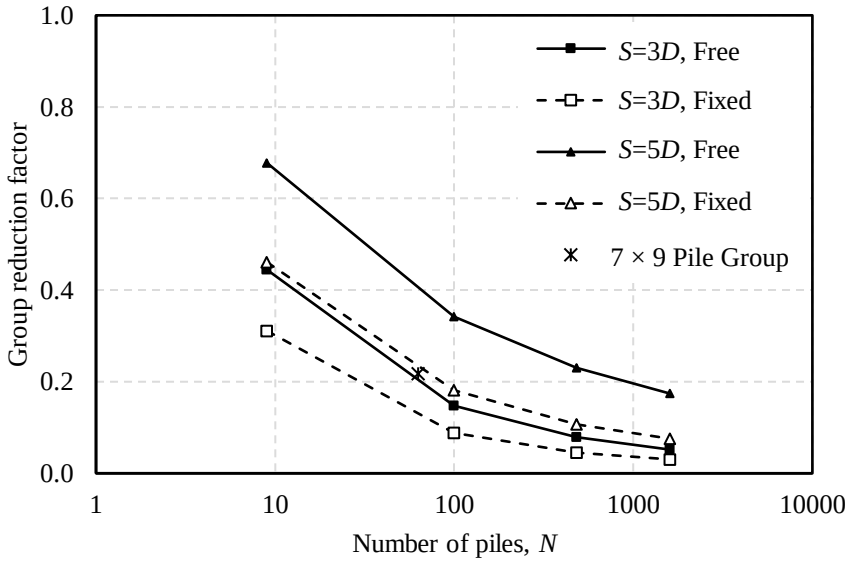

Figure 1-12 Group reduction factor considering free- and fixed-head conditions

1.5. Discussion

This section focuses on elucidating the mechanisms behind the observed group effects through analyses of the stress field in surrounding soil, comparing the present study results to the published experimental and numerical results for small to medium sizes of pile groups, assessing the recommendations from the existing standards and prevailing methods, and proposing a predictive equation suitable for large pile groups.

1.5.1. Multilayered effect

The observed multilayered soil effect is believed to be due to having a significant change in soil properties at a depth of approximately 5.5*D* below surface within the upper 10*D* influence depth. The contours of lateral stress (Fig. 1-13) depict that the lateral stress of soils surrounding the leading piles is smaller in multilayered soil than in uniform soil, and the corresponding stress field extends horizontally to a greater extent but vertically more localized in the upper layer (above a depth of 5.5*D*). Overall, these results indicate that the contrast of soil properties between the two layers in upper 10*D* depth results in that the upper strong layer (depth <5.5*D*) attracts more lateral load from piles than the lower weaker layer (depth of 5.5*D*-10*D*), thus engaging more soils to resist the load and developing a larger shallow soil reaction zone (Fig. 1-13). The larger soil reaction would cause more overlaps of soil reactions, resulting in an

increase in the shallowing effect. Therefore, the group effect is more significant in the layered soil with a strong layer underlain by a weak layer in the upper 10*D* influence depth.

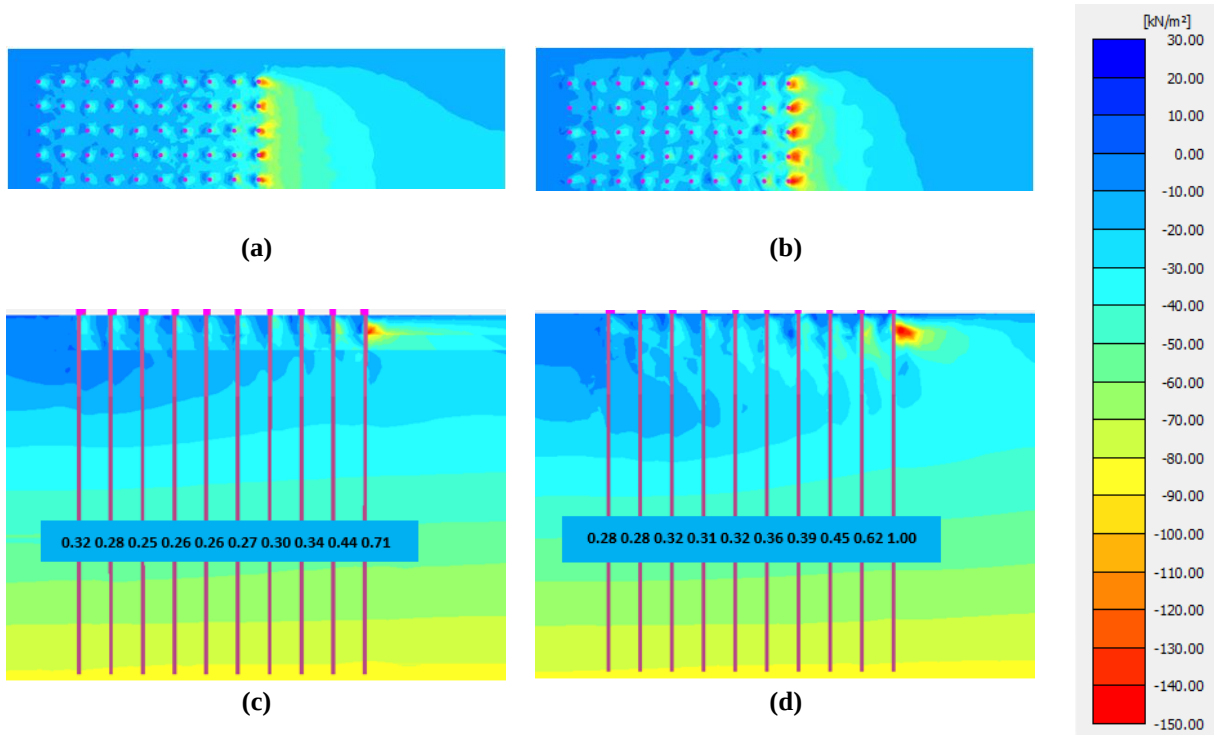

Figure 1-13 Plan view (2.5*D* below ground surface) and cross-sectional view (central piles) of lateral effective stress of a 10 × 10 pile group with (a, c) layered soil and (b, d) uniform medium dense sand

It is interesting to note that the multilayered soil effect is manifested when defining the group effect through *p*-multipliers, group reduction factors, or group efficiency as discussed previously. In the present study, when observing load share of pile row (i.e., load carried by pile rows normalized by that carried by the leading row) for the large pile groups (10 × 10, 22 × 22, and 40 × 40), the results (Fig. 1-14) were much more consistent between the different soil conditions. The trend in pile row load share from the multilayered and uniform medium dense soil profiles obtained similar results. This indicates that the multilayered effect vanishes when the load share is used to evaluate the group effect. In other words, it is not proper to define the group effect using the load share.

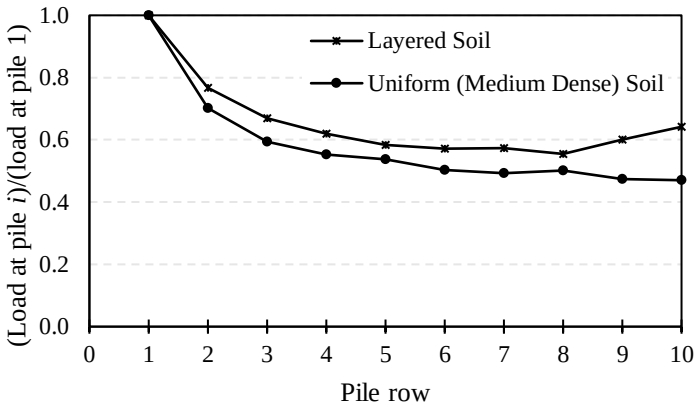

(a)

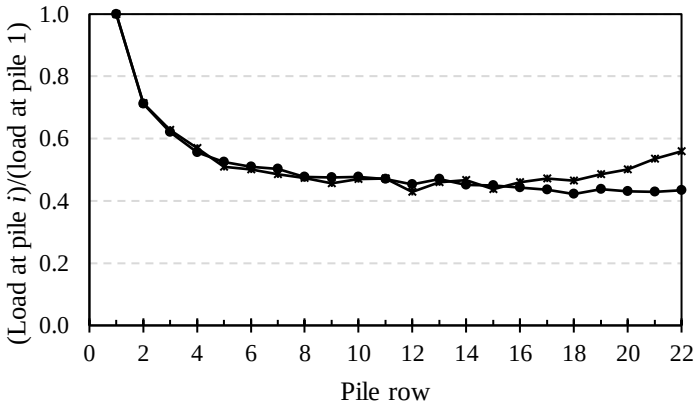

(b)

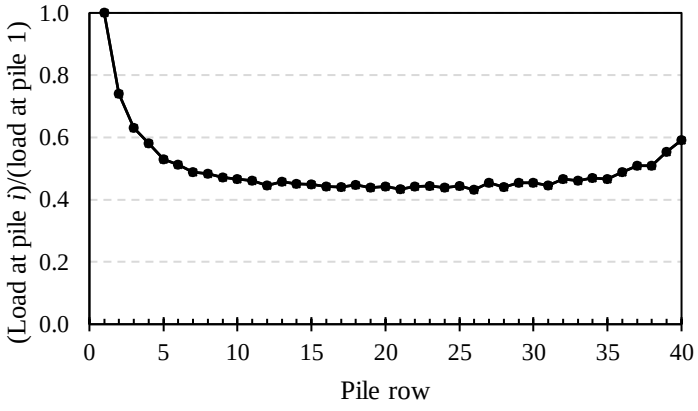

(c)

Figure 1-14 Normalized load share of (a) 10 × 10, (b) 22 × 22, and (c) 40 × 40 pile groups with 5*D* pile spacing in layered soil and uniform medium dense soil

1.5.2. Pile spacing

Pile spacing was also observed to have a significant impact on the group effect for large pile groups. Fig. 1-15 presents the effect of pile spacing for this study compared to previous experimental and numerical testing, where each subfigure summarizes the results for different pile group sizes. Fayyazi et al. (2014) is used as a comparison to these results as they also observed GRF for large pile groups (up to 100 piles) with varying soil conditions, including loose, medium dense and dense sands. Here, only the results for loose and medium dense sands are shown from the previous study since the surficial layer of the multilayered Japanese soil (Teramoto et al. 2018) falls within this density range. The results from this 3D FE study found a more significant group effect when compared to all the other results. This is likely due to the multilayered soil effect. While the values of GRF are lower than the previous studies, the overall near-linear trend between GRF and pile spacing is identical to those observed experimentally and numerically for small pile groups in Fig. 1-15. Comparisons cannot be made to the results from the pile group sizes of 22 × 22 and 40 × 40 as these sizes have not been studied previously. However, the agreeable results for the smaller groups suggest the GRFs obtained from the 3D FE model for the large pile groups are reliable as well.

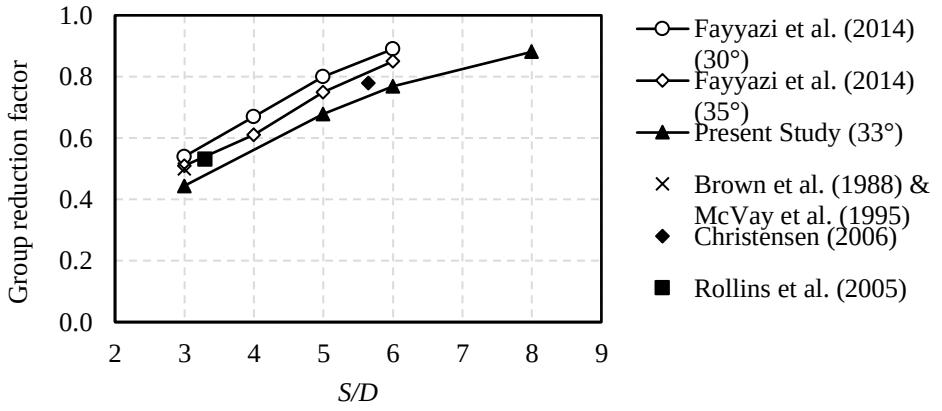

(a)

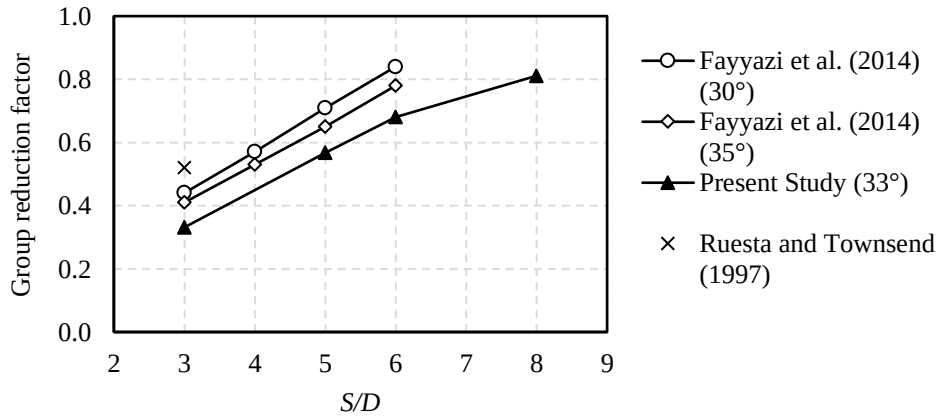

(b)

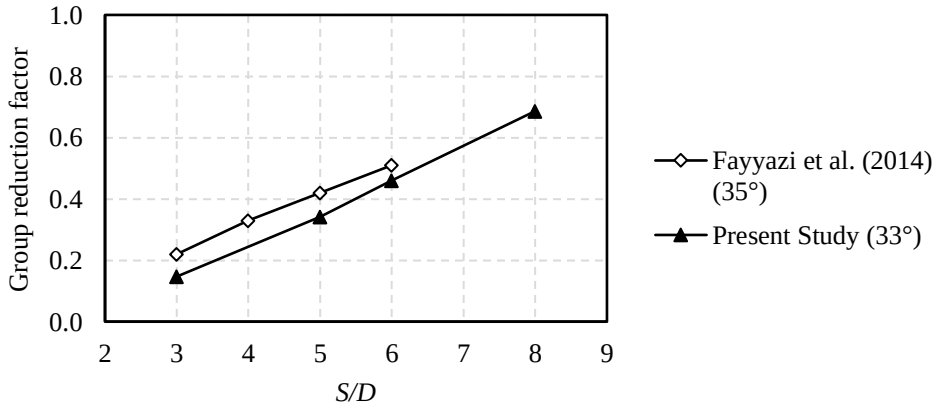

(c)

Figure 1-15 Group reduction factor calculated from the present, previous experimental (a, b), and previous numerical (a, b, c) studies considering spacing effect: (a) 3 × 3, (b) 4 × 4, (c) 10 × 10

The contours of lateral effective stress also help observe the group effect as influenced by pile spacing. As noted by the comparison between the layered and uniform soil models, pile groups which engage more soil have a more significant group effect with smaller group reduction factors. Similarly, this study also observes that pile groups with smaller spacing engage more soil in front of the leading piles, resulting in smaller corresponding group reduction factors. A comparison of 3*D* and 8*D* spacing models is shown in Fig. 1-16. A full comparison between 3*D*, 5*D*, 6*D*, and 8*D* spacing can be found in Figures A-4 and A-5. The stress contour also shows higher stress in trailing row piles with larger spacing which correlates to the larger lateral soil resistance and *p*-multipliers for those piles.

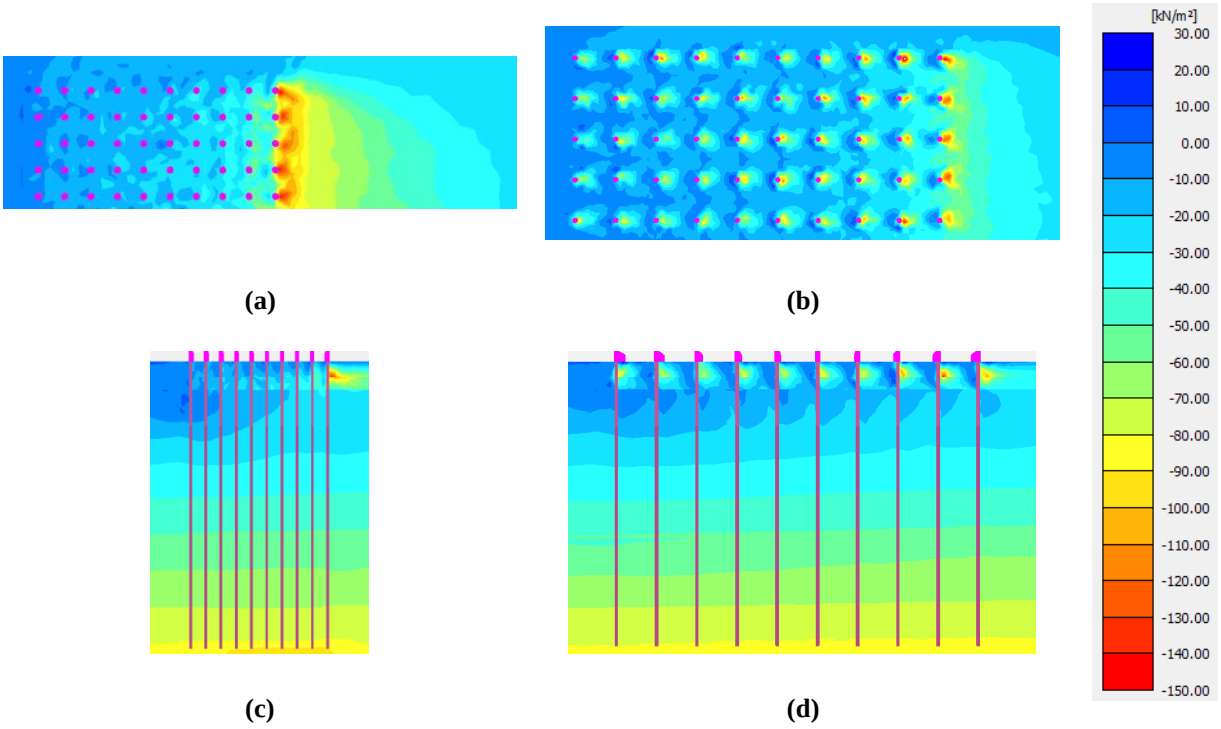

Figure 1-16 Plan view (3*D* below ground surface) and cross-sectional view of effective stress of a 10 × 10 pile group with varying pile spacings: (a, c) *S*=3*D*; (b, d) *S*=8*D*

1.5.3. The number of piles

The effect of pile number (i.e., pile group size) can also be compared to Fayyazi et al. (2014) in terms of GRF, which is presented in Fig. 1-17. Note that Fayyazi et al. (2014) investigated only GRF for small to medium sizes of pile groups (≤100 piles) while no discussion of *p*-multipliers was given. These numerical studies are compared with pile spacings of 3*D* and 5*D*. Here, only the medium dense sand case is shown from the previous study. In Fig. 1-17, the

trends of both numerical studies are very similar, with group reduction factors continually decreasing as the pile number increases. As shown in Fig. 1-16, the multilayered soil effect is also clearly observed as the GRFs determined for layered soil are lower than for the uniform soil at identical spacing. However, the GRF from the 10 × 10 pile group in medium dense uniform soil from this 3D FE study nearly overlaps the value obtained by Fayyazi et al. (2014). Combining these two results creates a continuous trend, where this study appears to be an extension of the previous results. Thus, there is agreement between the two studies, and suggests a similar relationship of GRF with increasing the number of piles.

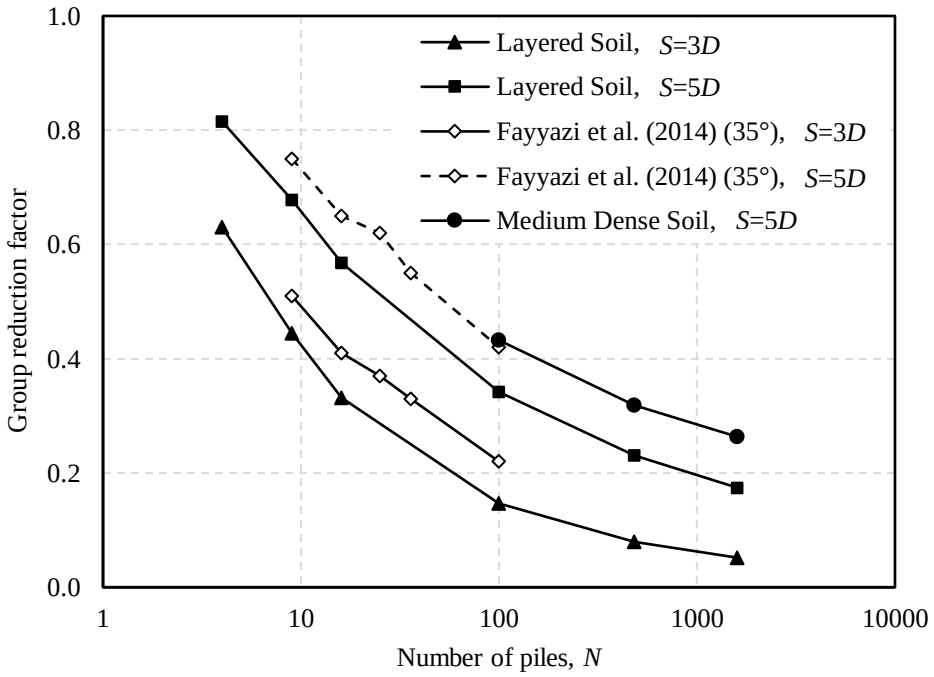

Figure 1-17 Group reduction factor from the present study and previous numerical study considering group size effect

1.5.4. Pile head conditions

The results from this study showed that pile head fixity also influenced the group effect for large pile groups. Fig. 1-18 compares this present numerical study to Fayyazi et al. (2014) again as their study included pile head fixity in their parametric analysis. The multilayered soil effect is again evident with both 3*D* pile spacing (Fig. 1-18(a)) and 5*D* pile spacing (Fig. 1-18(b)) as the group reduction factors from this study are less than those found in Fayyazi et al. (2014) for both pile head fixity conditions. Compared with Fayyazi et al. (2014), this study observed a similar fixity effect.

The increased group effect caused by head fixity can also be explained by the lateral effective stress contours (Figures A-6 and A-7) obtained from this study. It is observed that the pile group with fixed-head condition engages more soil than the same group with free-head piles. The larger influence zone correlates to a larger group effect, with lower *p*-multipliers and group reduction factors.

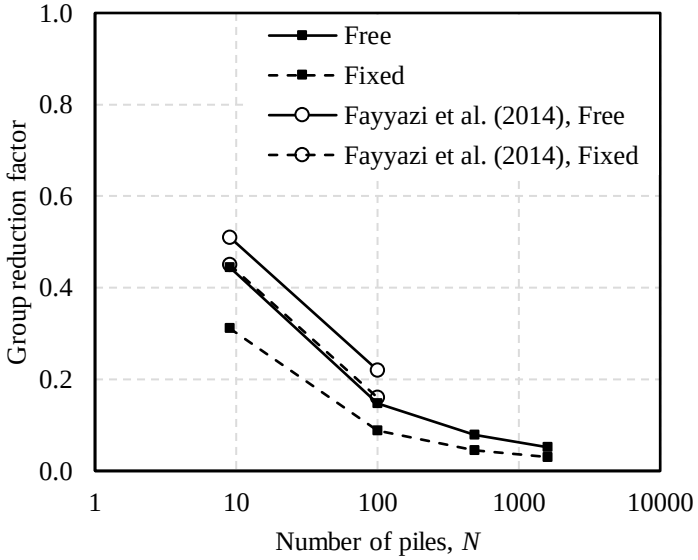

(a)

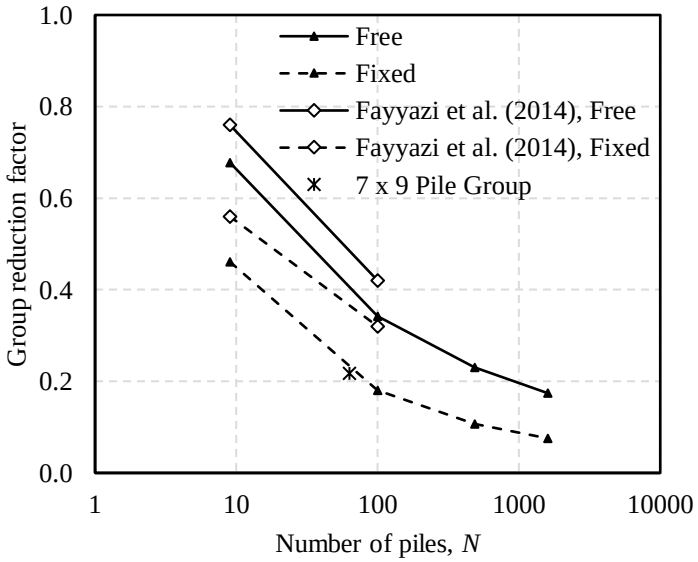

(b)

Figure 1-18 Group reduction factors calculated by the present study versus previous numerical study considering pile-head conditions (a) *S*=3*D*, (b) *S*=5*D*

1.5.5. Assessment of the existing standards and prevailing methods

The results of the present study are compared with design standards (FHWA 2016; AASHTO (2012); FEMA P-751 (2012); U.S. Army (1991)) and prevailing methods (Mokwa et al. 2000; Reese et al. 2006). Note that these design recommendations are derived from the experimental data for small pile groups (<25 piles) in Table 1-1. The use of these recommendations for large pile groups (≥100 piles) is subjected to extrapolation.

Fig. 1-19 compiles the *p*-multipliers from the present study (multilayered soil), the design standards, and the prevailing methods. The comparison in the figure is made for pile spacings of 3*D*, 5*D* and 6*D*. For *S*=8*D*, all design manuals (Table 1-2) suggest no group effect so all *p*-multiplier values can be compared against unity. As described previously, the *p*-multipliers from this study for varied sizes of pile group all plateau in value after approximately four pile rows. This result is consistent with the design manuals and prevailing methods. Therefore, in Fig. 1-19, the first ten rows of the large 22 × 22 and 40 × 40 pile groups are shown in the figures for clarity. For all spacings, the recommended *p*-multipliers are higher than obtained in this numerical study for large pile groups (10 × 10, 22 × 22, and 40 × 40). The exception to this is the comparison to the relevant provisions in the design manual by U.S. Army Corps of Engineers (1991) as it recommends group reduction factors instead of *p*-multipliers by row. So, the recommended value for the first row (leading row) is near or above the obtained values. However, this standard overestimated most of the other trailing rows. The difference between the recommended values and the ones determined in this study becomes more significant at the larger pile spacings. For example, for the 22 × 22 pile group models, there is a difference in *p*-multiplier of approximately 0.24 between this study and FHWA (2016) & AASHTO (2012) for the trailing rows (row 5 – 22) at 3*D* spacing. However, this difference increases to 0.51 at 5*D*, and 0.62 at 6*D*. This indicates that group effect that may be negligible for a small pile group with a large pile spacing (e.g., $S \geq 6D$) can be developed for a large pile group with the same large pile spacing. In other words, extrapolating the recommendations to large pile groups is unconservative, in particular for large pile groups with a large pile spacing.

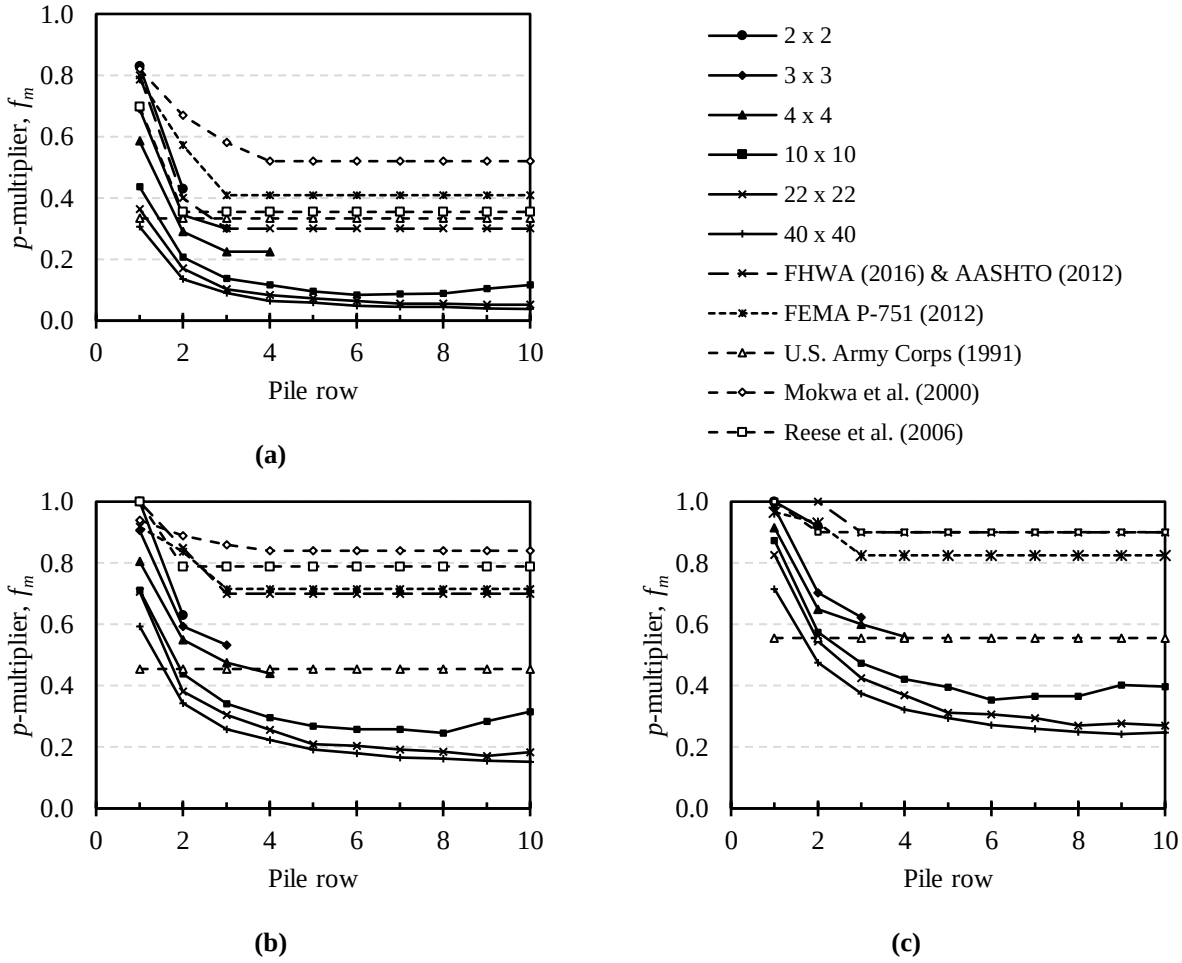

Figure 1-19 Comparison of *p*-multiplier calculated by design standards and prevailing methods to 3D FE analyses for pile groups with pile spacing (a) *S*=3*D*, (b) *S*=5*D*, and (c) *S*=6*D*

Similarly, a comparison to design standards and prevailing methods can also be made for the GRF results of this study (Fig. 1-20). Fig 1-20(a) makes this comparison for the pile groups with 3*D* pile spacing. There is fair agreement in this figure between the numerical results and the recommended values for small pile groups. The lower values obtained by this study are likely explained by the effect of multilayered soil, as previously discussed in this paper as the recommended values are in general obtained from on uniform soil conditions. However, the numerical results become significantly lower than the recommendations as the number of piles in the group increases. This large gap can also be seen in Fig 1-20(b) as well, which shows the comparison for pile groups with 5*D* pile spacing. This gap is even noticeable for small pile groups, where the GRF values determined in this study with 5*D* spacing are less than the recommended values. This highlights the lack of experimental testing with larger pile spacing for pile groups of

all sizes. While not shown directly in any figure, the overestimation of GRF also exists for the 6*D* and 8*D* pile spacings also observed in this study.

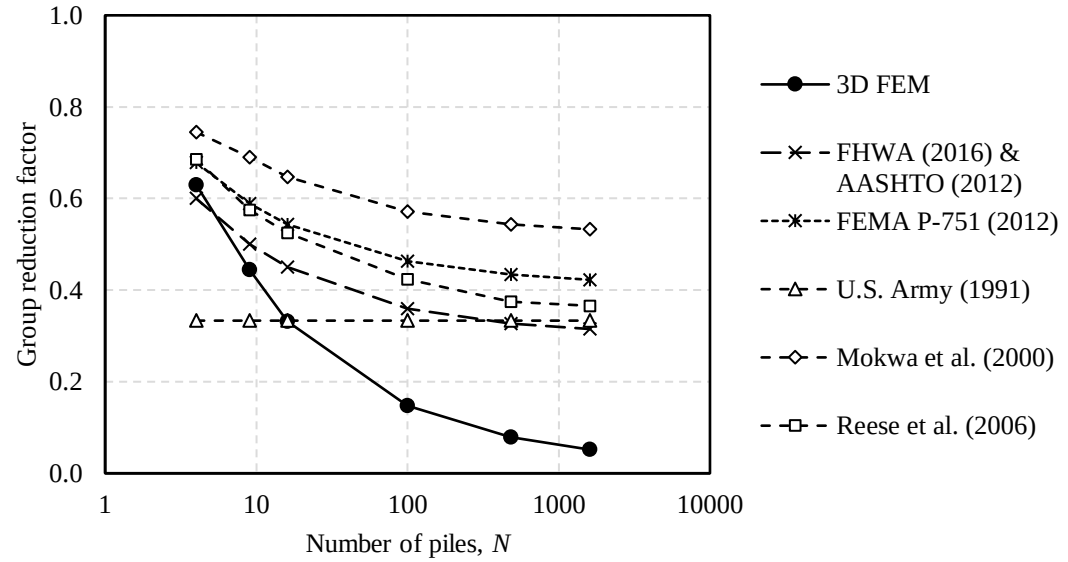

(a)

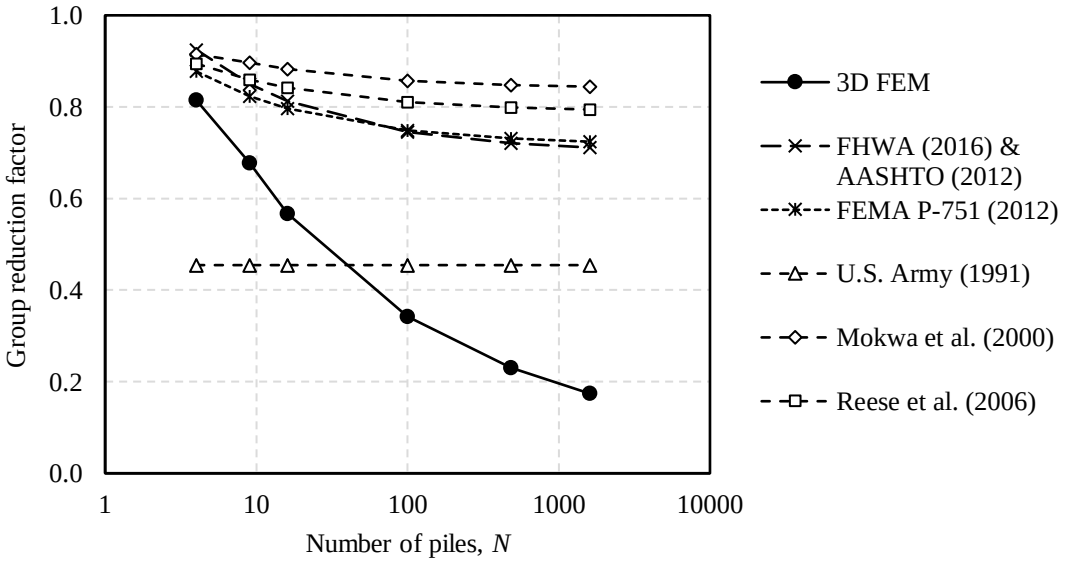

(b)

Figure 1-20 Group reduction factor calculated by 3D FE model versus design standards and prevailing methods: (a) *S*=3*D*, (b) *S*=5*D*

1.5.6. Recommendations of group reduction factors for large pile groups

The current recommendations of *p*-multipliers or GRF for large pile groups are extrapolated from those for small pile groups; therefore, they overestimate GRF or underestimate group effect of large pile groups, which is unsafe for design. There is a need for development of recommendations which can more accurately estimate the group effect for large pile groups. Using the results from this study combined with numerical and experimental data published by others (e.g., Table 1-1 and Fayyazi et al. 2014), a predictive equation is proposed based on a regression analysis. Fig. 1-21 shows the collated GRF data as well as the curves generated by the predictive equation. There are 101 data points of GRF which cover a range of the pile group sizes (4 to 1600 piles), pile spacings from 3*D* to 8*D*, and various soil conditions (layered soil in Teramoto et al. 2018, loose sand, medium dense sand, and dense sand). The regression analysis was performed using the results from free pile head conditions only (i.e., the fixed-head model results were neglected). As pile number and pile spacing appear to have the most significant impact on group reduction factors, only these parameters are included in the proposed function. This predicted equation is regressed with $R^2 > 0.8$.

$$GRF = \frac{0.262}{N^{0.251}}\left(\frac{S}{D}\right) \leq 1 \quad (1\text{-}1)$$

where GRF is group reduction factor, *N* is the number of piles for a pile group, *S* is pile spacing, and *D* is pile diameter or side width. The calculated GRF using Eq. (1-1) should be positive and is cut off by an upper limit of 1.0. Moreover, Eq. (1-1) can be applicable to both square shape and circular shape of pile groups as the shape configuration is found to have a negligible effect. It is valid for a pile group of no more than 1600 piles and pile spacing ranging between 3*D* and 8*D* (inclusive). Since Eq. (1-1) is developed based on the results from sandy soil, it may be cautious for use for pile groups in clayey soil. Moreover, Eq. (1-1) may yield a slightly larger GRF when used for fixed-head conditions, while the difference would be small for a large pile group.

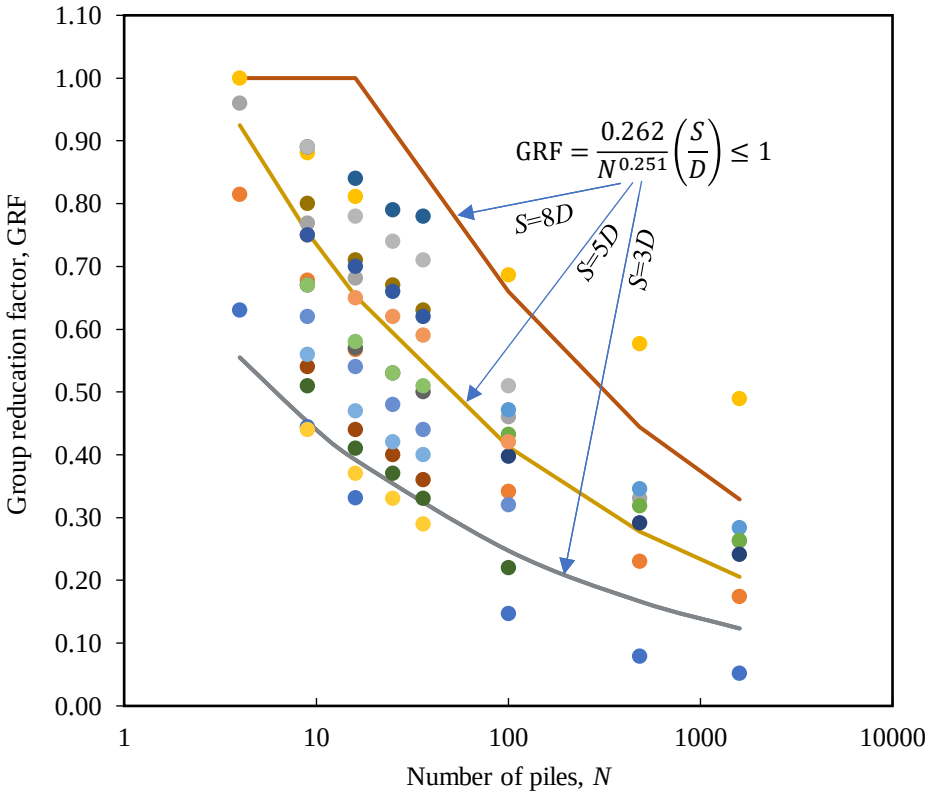

Figure 1-21 Compiled GRF data and proposed predictive equation for GRF

1.6. Conclusions

This study investigated the impact various pile group parameters have on the "group effect" on laterally loaded large pile groups, as measured by *p*-multipliers and group reduction factors. A baseline 3D FE numerical model was established and validated against the largest lateral load test in the world, a 7 × 9 pile group from an out-of-service LNG tank foundation. Additional 3D FE models were also created to systematically observe the various factors (soil condition, pile spacing, number of piles, pile group shape configuration, and pile head fixity) affecting the group effect of large pile groups. Recommendations from existing design standards and prevailing methods were then critically assessed against the results of the parametric study. The following conclusions were made from this study:

(1) The investigated factors of pile spacing, pile number, soil condition, and pile head fixity are all relevant design considerations for large-scale pile foundations. In comparison, the effects of the pile spacing and the number of piles appeared to be more significant than soil condition and pile head fixity. A large pile group

($\geq$ 100 piles) with a large spacing of $S \geq 6D$ (D = pile diameter) showed an appreciable group effect, which, however, is normally considered to develop no group effect in conventional design practice.

(2) The layered soil consisting of a strong layer atop a weak layer in the upper $10D$ influence depth was found to develop a greater group effect than the uniform soil. This is because the strong layer attracted more lateral load from piles, engaging more soils to react, and therefore a more shallowing effect was developed in this soil condition.

(3) The shape arrangement of the large pile groups affected the distribution of *p*-multipliers for piles along the edge and perimeters of pile groups but had a negligible impact on the overall group reduction factor. Thus, providing a design recommendation for group reduction factors based on pile group size and inter-pile spacing may be an accurate and computationally efficient way to design large pile groups, including those used for LNG tank foundations.

(4) Existing design standards and prevailing methods greatly overestimated trailing row *p*-multipliers and group reduction factors for large pile groups. Use of the recommended values would significantly overestimate the lateral capacity of large pile groups and could be unsafe for the foundations during extreme loading events such as during hurricanes and earthquakes.

(5) Based on the present study data and the collated published data, a predictive equation is proposed to estimate group reduction factors for pile groups with the number of piles up to 1600 and pile spacing between $3D$ and $8D$.

References

AASHTO 2012. AASHTO LRFD bridge design specifications. American Association of State Highway and Transportation Officials (AASHTO), Washington, D.C., USA.

API 2011. Geotechnical and foundation design considerations, ANSI/API recommended practice 2GEO. American Petroleum Institute (API), Washington, D.C., USA.

Brown, D. A., Reese, L. C., & O'Neill, M. W. 1987. Cyclic lateral loading of a large-scale pile group. Journal of Geotechnical Engineering (ASCE), **113**(11), 1326–1343.

Brown, D.A., Morrison, C., and Reese, L.C. 1988. Lateral load behavior of pile group in sand. Journal of Geotechnical Engineering (ASCE), **114**(11): 1261–1276.

Brown, D.A., ONeill, M.W., Hoit, M., McVay, M., El-Naggar, M.H., and Chakraborty, S. 2001. Static and dynamic lateral loading of pile groups. Technical Report NCHRP Report No.461. National Cooperative Highway Research Program, Washington, D.C.

Christensen, D. 2006. Full scale lateral load test of a 9 pile group in sand. Master's thesis. Brigham Young University.

FEMA 2012. Foundation analysis and design (No. FEMA P-751), NEHRP recommended provisions: design examples. Federal Emergency Management Agency (FEMA). National Institute of Building Sciences, Building Seismic Safety Council, Washington, D.C., USA.

FHWA 2016. Design and construction of driven pile foundations – volume 1. National Highway Institute U.S. Department of Transportation, Federal Highway Administration, Washington, D.C., U.S.A.

Lin, G.M., and Lin, C. 2019. Driven pile supported LNG tank in Savannah, Georgia. *Deep Foundation Institute Magazine*, 2019 Jan/Feb Issue

Lin, Y., and Lin, C. 2020. Scour effects on lateral behavior of pile groups in sand. Ocean Engineering, **208**: 1–17. doi:10.1016/j.oceaneng.2020.107420.

Lin, C., and Wu, R. (2019). Evaluation of vertical effective stress and pile lateral capacities considering scour-hole dimensions. Canadian Geotechnical Journal, **56**(1), 135-143.

McVay, M., Casper, R., & Shang, T.-I. 1995. Lateral response of three-row groups in loose to dense sands at 3d and 5d pile spacing. Journal of Geotechnical Engineering (ASCE), **121**(5), 436–441.

McVay, M., Zhang, L., Molnit, T., and Peter, L. 1998. Centrifuge testing of large laterally loaded pile groups in sand. Journal of Geotechnical and Geoenvironmental Engineering, **124**(10): 1016–1026. doi:10.1061/(ASCE)1090-0241(1998)124:10(1016).

Mokwa, R. L., Duncan, J. M., and Charles, E. V. 2000. Investigation of the resistance of pile caps and integral abutments to lateral loading. FHWA/VTRC 00-CR4, Virginia Transportation Research Council, Charlottesville, Virginia.

Reese, L.C., Isenhower, W. M., and Wang, S. 2006. Analysis and design of shallow and deep foundations. John Wiley & Sons Inc., Hoboken, U.S.A.

Reese, L.C., Wang, S.T., Isenhower, W.M., and Arrellaga, J.A. 2000. Computer program LPILE plus version 4.0 technical manual, Ensoft, Inc., Austin, Texas.

Rollins, K., Peterson, K., & Weaver, T. 1998. Lateral load behavior of full-scale pile group in clay. Journal of Geotechnical and Geoenvironmental Engineering, **124**(6), 468–478. https://doi.org/10.1061/(ASCE)1090-0241(1998)124:6(468)

Rollins, K., Snyder, J., & Broderick, R. 2005. Static and dynamic lateral response of a 15 pile group. Proceedings of the 16th International Conference on Soil Mechanics and Geotechnical Engineering, Vols 1-5: Geotechnology in Harmony with the Global Environment, 2035–2039.

Rollins, K., Olsen, K., Jensen, D., Garrett, B., Olsen, R., & Egbert, J. 2006. Pile spacing effects on lateral pile group behavior: Analysis. Journal of Geotechnical and Geoenvironmental Engineering, **132**(10), 1272–1283. https://doi.org/10.1061/(ASCE)1090-0241(2006)132:10(1272)

Ruesta, P., & Townsend, F. 1997. Evaluation of laterally loaded pile group at Roosevelt Bridge. Journal of Geotechnical and Geoenvironmental Engineering, **123**(12), 1153–1161. https://doi.org/10.1061/(ASCE)1090-0241(1997)123:12(1153)

Salgado, R., Tehrani, F.S., and Prezzi, M. 2014. Analysis of laterally loaded pile groups in multilayered elastic soil. Computers and Geotechnics, **62**: 136–153.

Taghavi, A., & Muraleetharan, K. 2017. Analysis of laterally loaded pile groups in improved soft clay. International Journal of Geomechanics, **17**(4).

Teramoto, S., Niimura, T., Akutsu, T., and Kimura, M. 2018. Evaluation of ultimate behavior of actual large-scale pile group foundation by in-situ lateral loading tests and numerical analysis. Soils and Foundations, **58**(4): 819–837. doi:10.1016/j.sandf.2018.03.011.

U.S. Army Corps of Engineers 1991. Engineering and design: design of pile foundations (Engineering manual No. EM 1110-2-2906). U.S. Army Corps of Engineers, Washington, D.C., USA.

Walsh, J. 2005. Full scale lateral load test of a 3x5 pile group in sand. Master's thesis. Brigham Young University.

Chapter 2. Integrated analysis of LNG tank superstructure and foundation under lateral loading

Jones, K., Sun, M., and Lin, C. 2021. Integrated analysis of LNG tank superstructures and foundations under lateral loading. Engineering Structures (under review)

2.1. Introduction

Liquified natural gas (LNG) storage tanks are an integral part of the gas supply chains around the world. Many of these tanks are positioned in for use in coastal regions within LNG import and export facilities. These locations tend to be at greater risk of experiencing significant lateral loading events including earthquakes, hurricanes, flooding, or even tsunamis. As such, the design of the tanks and foundations often needs to consider very significant lateral loading levels. Additionally, soft alluvial deposits are widespread in coastal areas at shallow depths which results in a decreased lateral capacity of piles. Due to these factors, the lateral loading requirement can govern the design. As the tank superstructures are very large, substantial foundations are required to support them. Commonly, large pile groups with piles in the hundreds, or even thousands, are used in the design in order to meet design requirements and minimize settlements. Previous experimental testing of the lateral pile group response has been limited to much smaller pile groups (fewer than 25 piles) (Brown et al. 1988; McVay et al. 1995; Ruesta and Townsend 1997; McVay et al. 1998; Rollins et al. 1998). Thus, the large-scale pile group performance during service life or during an extreme event is unclear.

In practice, superstructure and foundation are often analysed and designed independently. Using the traditional approach, structural engineers at the initial design stage often analyse the superstructure assuming a rigid foundation, and geotechnical engineers subsequently analyse the foundation using the loadings provided by structural engineers. When analysing the superstructure using a frame analysis program, the definitions of boundary conditions are critical in the assembly of stiffness matrices. The underlying assumptions (e.g., pinned, semi-rigid, or rigid supports) affects the static and dynamic responses of the superstructure model, and subsequently the support reactions required by geotechnical engineers for foundation analysis. For a complete foundation analysis, loading and support conditions at pile heads need to be defined in the special-purpose foundation analysis programs. However, such pile head loading

and boundary conditions cannot be determined accurately until the superstructure analysis is completed which requires the input from the foundation analysis. Therefore, in the absence of a very intensive iteration process, crude assumptions are often made by the structural and geotechnical engineers throughout the analysis when using the traditional approach (Lin et al. 2010; Lin et al. 2012). In addition, it is common to consider lateral loading on foundations without the vertical loading effects. In all, the current design practices often do not consider sufficiently the interaction between LNG storage tank and foundation. The integrated problem is complex and is variable on many aspects of the structure and foundation, including structural materials, pile group geometry and soil conditions. Thus, research and updates on practical approaches for integrated analysis are particularly useful in this regard, as this has been a practical problem encountered by engineers. Fraser and Wardle (1976) analysed a two-bay portal frame and rectangular rafts. Luo et al. (2016) conducted numeric research on a high-rise structure using thick-shell elements supported by a piled foundation. Ko et al. (2017) investigated a 10-storey framed superstructure supported by a piled raft foundation. This list is not exhaustive given the particular interest in this topic, and wide range of structures, foundations, and loading conditions which require study. Some of these previous studies have proposed new analysis methodologies which provide a more coupled approach for the investigated structures (e.g., Viladkar et al. 1994; Ko et al. 2017). Comparing to the traditional approaches in current practice, these coupled approaches in general do not involve crude assumptions or intensive iteration until convergence since all computation integrates superstructure and foundation.

To this day, research on the integrated behaviour of LNG tank infrastructure is limited. The tank structures are different from the framed systems traditionally analysed. The load transfer from the LNG tank structure is through tank walls in combination with the direct pressure of LNG at the base of the tank. Also, the foundations for these structures are often significantly larger, particularly in the number of piles used, than those used to support a standard building. Additionally, the tank can be elevated above the ground surface, as supported by the pile cap. While the pile cap serves to help transfer load to the foundation, it does not directly transfer load to the soil as in more common piled-raft foundations. It also adds more complexity to the integrated behaviour of the tank and foundation as the relatively flexible pile cap can more easily deform which is expected to result in changes in the load transfer to the piled foundation. This also varies from the traditional decoupled approach which would assume a rigid boundary where deformations would not occur.

This research assesses the foundational response of an LNG tank structure using an integrated approach, where the full interaction among superstructure, pile foundation and soil is considered in a single computer model. This avoids crude assumptions on boundary conditions and intensive iteration until convergence as all elements are coupled during the entire computation. In this research, a 1,000,000 BBL-capacity LNG storage tank supported by a 1600-pile foundation, located on Elba Island in Savannah, Georgia, USA (Lin and Lin 2019) is selected as a case study. Three-dimensional finite element continuum models simulate this LNG tank being subjected to wind pressures consistent with those from a Category 3 hurricane, as determined by AASHTO procedures (AASHTO 2012). The LNG foundation is also analysed using the conventional (decoupled) approach. The results are compared to observe whether the traditional approach is valid for assessing the LNG storage tank superstructure-foundation infrastructure. In addition, the integrated computer models are expanded to consider additional gravitational effects as the amount of LNG present in the tank changes. Also, the response is observed with changes in soil-foundation stiffness. General observations with respect to load transfer to the foundation are made.

2.2. Model creation

2.2.1. Three-dimensional continuum finite element (3D FE) Model

The 3D FE program PLAXIS 3D (Brinkgrieve et al. 2018) was used to study the response of large pile groups supporting an LNG storage tank subjected to lateral loading. While the program PLAXIS 3D is used primarily as a geotechnical software package, it also provides the ability to consider structural elements. Thus, it can easily be implemented to study integrated superstructure-foundation problems and was utilized in this study. Typical integrated and decoupled models are shown in Fig. 2-1. In all cases, half-models are developed and analysed (by taking advantage of the symmetries of geometry, loading and boundary conditions) to save computational time. Symmetry boundary conditions were applied along the cut face.

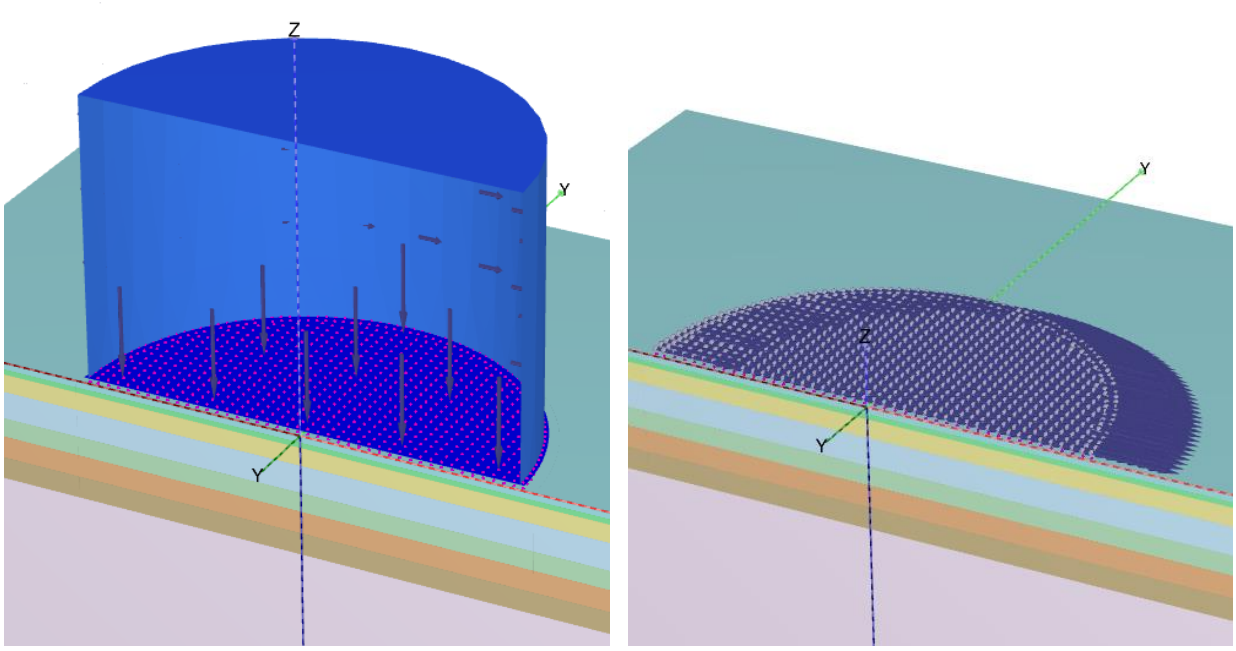

(a) **(b)**

Figure 2-1 Typical PLAXIS 3D (a) integrated model and (b) decoupled model

2.2.1.1. Structure and foundation model

The 1,000,000 BBL, or approximately 160,000 m^3, capacity storage tank in Savannah, GA, USA is a double-walled steel tank with insulation filled between the steel. As the natural gas is stored in liquified form at or below -160°C, the inner steel wall, and the steel at the bottom of the tank must be able to tolerate cryogenic temperatures. As such, nickel alloy steel is utilized for these elements to ensure performance at the colder temperatures. The thicknesses of each steel wall, as well as the insulation layer between them, are 1 ft thick, or 0.30 m. The outer diameter of the tank extends 78.6 m, and total height is 51.8 m. In the 3D FE model, the cylindrical tank is modeled using elastic plate elements. For numerical modelling purposes, the inner and outer tank walls are assumed to be behave as one element. This assumption is verified by the negligible effect in stiffness (less than 2%) given the large diameters of the tank walls and the relatively small distance separating them. Also, the tank bottom and pile cap are modelled as one element, with thickness-weighted averages used for elastic properties. The tank bottom is considered as a 0.30 m thick nickel steel layer, while the pile cap is comprised of 0.76 m of reinforced concrete. The roof is modelled as a 0.30 m-thick

steel flat surface. Loading conditions are further discussed later in this paper. Input parameters used for each of these plates are listed in Table 2-1.

Table 2-1 Structural element parameters used in 3D FE model

Structural Element	Element type	Depth below pile head (m)	E^1 (GPa)	γ^2 (kN/m^3)	A^3 (m^2)	I^4(10^{-3}) (m^4)	$T_{skin}{}^5$ (kN/m)	$F_{end}{}^6$ (kN)	ν^7	d^8 (m)
Pile stickup	Beam	0 – 1.0	28	24	0.2090	3.641	-	-	-	-
Pile	Embedded Beam	1.0 – 19.7	28	24	0.2090	3.641	500	10000	-	-
Pile cap/tank bottom	Plate	-	75.7	39.6	-	-	-	-	0.23	1.07
Tank walls	Plate	-	200	78.5	-	-	-	-	0.3	0.61
Tank roof	Plate	-	200	78.5	-	-	-	-	0.3	0.30

[1]elastic modulus; [2]unit weight; [3]cross-sectional area; [4]moment of inertia; [5]skin resistance; [6]base resistance; [7]Poisson's ratio; [8]thickness

The foundation supporting the LNG storage tank consists of 1600 piles joined together with a pile cap elevated above the ground surface by 0.61 m. Elevating the structure above the ground surface helps to mitigate concerns with ground freeze and thaw as the gas is stored at -160°C or colder. The piles used in the foundation are square prestressed concrete piles, 457.2 mm inside width. They are 20.7 m in total length and embedded 19.7 m into the soil. The piles are orthogonally arranged with 4*D* spacing (*D* = 457.2 mm), surrounded by two outer rings of piles (320 piles per ring) to support the tank walls. The layout of the piles is presented in Fig. 2-2(a). In the 3D FE models, each pile is modelled as an embedded beam with the stick up as a beam. The embedded beam structural element simulates the vertical soil-pile interaction using defined end bearing and skin friction as input parameters. Input values for these components were selected based on values used in a previous study validating the use of these embedded beam elements for lateral loading problems and modelling using PLAXIS 3D (Dao 2011). A summary of input parameters for the piles are included in Table 2-1. Given the large number of piles used in the model (up to 800 in the half model), the embedded beam provides a computationally efficient means of performing the analyses in comparison to using volume or hybrid elements (beam and volume element) more commonly used to study laterally loaded pile groups.

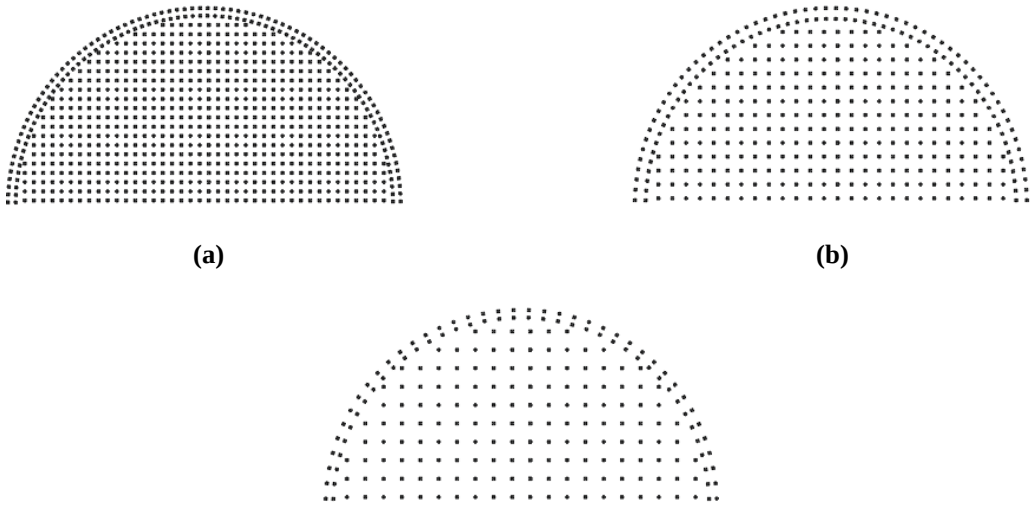

Figure 2-2 Layout of piles for parametric study; (a) 4*D* spacing, (b) 6*D* spacing, and (c) 8*D* spacing

2.2.1.2. Soil model

Boundaries of the soil models were established based on preliminary sensitivity analyses, which observed changes in lateral load pile response of large pile groups. Lateral soil boundaries were extended 100 pile side width (*D*) from the edges of the pile group. Additionally, the vertical soil boundary was extended 100*D* below the pile tips. While "*D*" typically refers to pile diameter, the piles used to support the LNG tank considered in this study are square in cross-section, instead of circular. Thus, "*D*" herein will refer to the pile side lengths of each pile. The mesh is automatically generated by PLAXIS 3D using a "medium" coarseness setting. To improve pile response accuracy and reduce numeric irregularities, a finer mesh was used surrounding the pile group. The refined soil zone extends laterally 5*D* from the edge of the pile group, and vertically the entire length of the embedded pile plus 5*D*.

Soil in the 3D mesh is simulated through the use of 10-node tetrahedral solid elements. The soil constitutive model uses the Mohr-Coulomb failure criterion. Input parameters are based on those previously back-calculated from the full-scale lateral load test of a 7 × 9 pile group located at the Osaka Gas Senboku Receiving Terminal 1 (Teramoto et al. 2018). The numerical model using Mohr-Coulomb soil has been validated in a previous study, and the input parameters can be referenced from Jones et al. (2021). The soil is characterized as multilayered with primarily cohesionless soils. The water table is assumed to be 1.225 m below ground surface, based on soil investigations

conducted on-site. Uniform, cohesionless soil with varying strengths are also considered in the parametric study to observe the effect of soil conditions. This is further discussed with the results.

2.2.1.3. Loading conditions

Lateral loading is applied to the superstructure using surface loads on the tank walls. Windward and leeward pressures are approximated using procedures outlined by AASHTO for bridge design (AASHTO 2012). This study considers a Category 3 hurricane event, where wind velocity is assumed to be 53.6 m/s, or 120 mph. The AASHTO specification (2012) contains recommendations for calculations of design wind velocities and pressures for structural elements 9.1 m above sea level. The ground surface where the Savannah, GA tank is located is approximately 2.9 m below sea level. Thus, the design wind pressures are applied to the tank walls 12.0 m above ground surface. The tank is assumed to be in "open country", where the local terrain and LNG facility provides few obstructions. This classification defines meteorological wind characteristics, including a friction velocity of 3.7 m/s, and a friction length of upstream fetch of 0.07 m. Using these, the design wind velocity is determined as a function of elevation above sea level. Next, the design wind pressures are be determined using the calculated wind velocity values and a base wind pressure. The base wind pressures are assumed to be 2.4 kN/m^2 and 1.2 kN/m^2 for windward and leeward loads, respectively. The values selected are consistent with recommended values for the design of bridge trusses, columns, and arches. Additionally, they are the most conservative pressures suggested in AASHTO (2012). As the resulting design wind pressure is a function of elevation, the average pressure over the height of the structure is determined. In this case study, windward and leeward wind pressures were calculated and applied as 5.14 kN/m^2 and 2.57 kN/m^2, respectively.

In addition to the wind pressure, part of the parametric study also observes changes in lateral response as the tank stores differing amounts of LNG. This aspect is considered in the relevant simulations as an additional vertical surface pressure applied to the tank bottom and pile cap element. Following the construction of the tank, hydrostatic pressure testing, which is more commonly known as hydrotesting, was performed on the tanks to ensure structural integrity and serviceability prior to operation with LNG. During the hydrotest, water is incrementally filled into the tank to generate pressures identical to those expected during the service life. Thus, this study utilizes these pressures generated during the test to simulate half-full and full tank scenarios. The maximum hydrostatic pressure representing a 100% full tank state is applied to the tank base as 203.6 kPa, as determined by the water head in the tank. Thus, this study applies vertical pressures of 101.8 kPa and 203.6 kPa, respectively to consider the additional vertical load interaction.

2.3. Parametric analysis

A parametric study was used to better understand the complex superstructure-foundation problem, specifically with respect to LNG storage tanks and their respective foundations subjected to lateral loading. Table 2 outlines the extent of the study. In total, 10 simulations were performed to study the integrated behaviour, where 8 of these simulations utilize an integrated model. By varying the tank internal pressure, the effects of different gravity loading levels (empty, half-full, and full tank in Table 2) on the lateral responses are investigated. Also, by varying soil conditions, the effects of varying soil density (loose, medium dense, and dense sands, and layered soil in Table 2) on the lateral responses are studied as well. Lastly, varying pile spacing (4*D*, 6*D*, and 8*D* in Table 2) allows for observations with respect to soil-pile stiffness as they affect lateral response. In addition, a typical integrated model (Fig. 2-1(a)) is compared to two decoupled foundation models (Fig. 2-1(b)). Using the traditional approach, the pile group is modeled considering both free-head and fixed-head conditions in order to identify accuracies and limitations to the traditional approach. Free-head condition is achieved by prescribing a lateral displacement at each pile head but releasing other degrees of freedom (DOFs) (i.e., each pile head is allowed to rotate). Conversely, fixed-head condition is created by prescribing a lateral displacement while restraining other DOFs (i.e., each pile head is restrained from rotating).

Table 2-2 Details of 3D FE parametric analysis

Evaluation	Model arrangement	LNG	Soil condition	Pile spacing
Effect of design analysis	Integrated superstructure and foundation, piles-only (free-head and fixed-head)	Empty tank	Layered	4*D*
Effect of LNG pressure	Integrated superstructure and foundation	Empty, half-full, and full tank	Layered	4*D*
Effect of soil condition	Integrated superstructure and foundation	Empty tank	Loose, medium dense, and dense sand, plus layered sand	4*D*
Effect of pile spacing	Integrated superstructure and foundation	Empty tank	Layered	*4D*, 6*D*, 8*D*

Shear force distribution is used to observe changes in pile group response, and load transfer from the structure to the foundation. In addition, the displacement and load profiles of key piles in the foundation are used to observe changes in pile group response as well.

2.4. Results and discussion

2.4.1. Effect of design analysis approach

The effect of the design analysis approach is studied by comparing an integrated superstructure-foundation model to similar models considering only the foundation. All models discussed in this section consider an empty tank condition, where no pressure is added to the tank bottom. The average lateral displacement of the tank bottom and pile cap plate from the integrated model is applied to each pile to observe the foundation-only lateral response. As is common in geotechnical engineering practice, this lateral effect is considered without any of the vertical loading from the tank superstructure. Both free-head (i.e., pile head allowed to rotate) and fixed-head (i.e., pile head restrained from rotation) conditions are compared in the foundation-only models.

Fig. 2-3 shows the distribution of shear forces carried by key piles in the pile arrangement, including the midline piles of the foundation as well as the outer and inner pile rings. Fig. 2-3(a) illustrates that the integrated model generates a greater lateral pile response in the leading and trailing piles along the midline of the foundation. This seems to affect approximately the 10 leading-most and 10 trailing-most piles, or 20% of both the leading piles and trailing piles. This result suggests that the added vertical loading from the tank walls increases the lateral response of the piles subjected to the wall loading. Additionally, the figure shows that piles 3 - 9 and 44 experience shear in the opposite direction (i.e., negative shear) compared to what the traditional approaches would suggest. Thus, the vertical loading from the tank walls in combination with the overturning effects of the tank influence the load distribution. Fig. 2-3(a) also indicates that the lateral capacity of the piles in the middle of the foundation are well approximated by the foundation-only design approach. However, the response of the outer perimeter piles, shown in Fig. 2-3(b), are different in the integrated and pile-only models. Here, both free- and fixed-head models underestimate the load carried by the leading piles. Additionally, the trailing pile response is in the opposite direction from the pile-only models. Again, this is likely attributed to the overturning effects of the tank. In contrast, the three simulations show pile reactions of the inner pile ring follows a similar trend and magnitude (Fig. 2-3(c)), suggesting the inner and more central piles of the foundation are the least impacted.

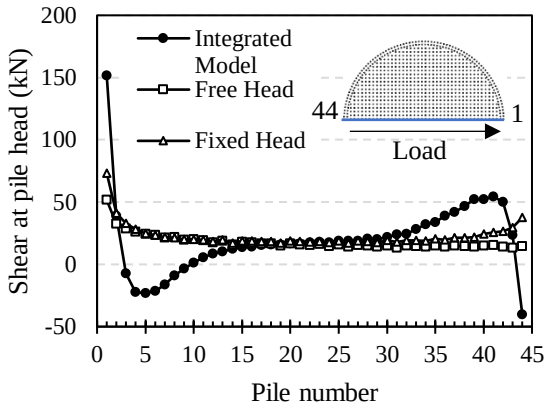

(a)

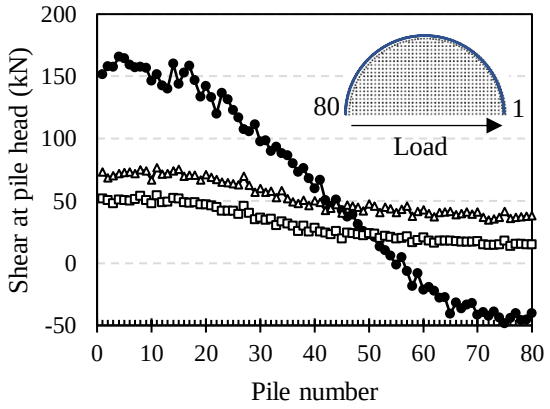

(b)

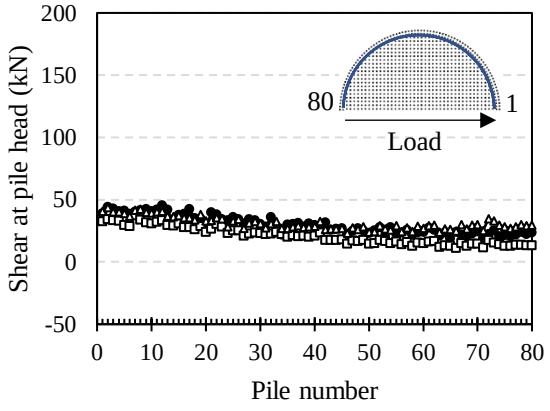

(c)

Figure 2-3 Distribution of shear at pile head for (a) midline piles, (b) outer perimeter piles, and (c) inner perimeter piles from different analysis models

The lateral displacement of the piles also highlights differences between the design approaches. Fig. 2-4 compares the lateral displacement profiles of the leading, central, trailing, and central perimeter piles in the pile group. This figure illustrates that the influence depth of each pile, regardless of its position in the group, extends the entire length (43*D*). Observations from smaller pile groups, such as a typical 3 × 3 arrangement, only observe approximately a 10*D* influence depth with laterally loaded piles (Brown et al. 1988). However, all three design approach models conclude this does not apply to piles in such a large-scale group. Fig. 2-4(b) and Fig. 2-4(d) also show that the fixed-head pile model well represents the central and central perimeter piles. However, the lateral displacement of the leading and trailing piles is much more pronounced in the integrated model. Fig. 2-4(a) and Fig. 2-4(c) shows that the pile deflections are much more cupped than the piles in the models without the superstructure. Thus, the integrated superstructure-foundation has the greatest influence on the leading and trailing piles. This is also observable in Fig. 2-5, which shows the deflected shape of the bottom of the tank and midline piles from the integrated model. Here, it appears that the additional settlement of the perimeter piles carrying the weight of the tank walls creates the unique deflected shapes in the leading and trailing piles.

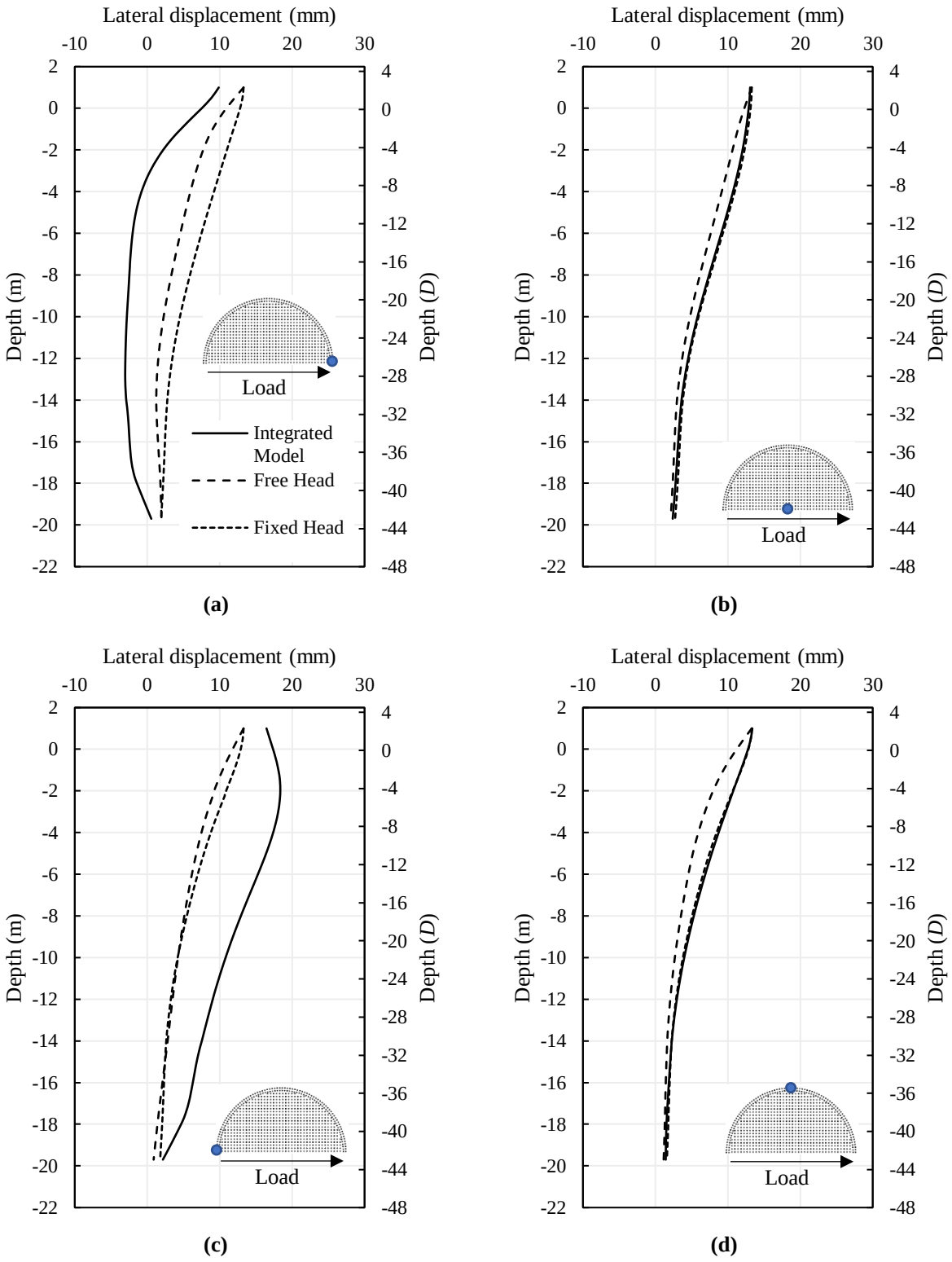

Figure 2-4 Lateral displacement profiles of the (a) leading pile, (b) central pile, (c) trailing pile, and (d) central perimeter pile from different analysis models

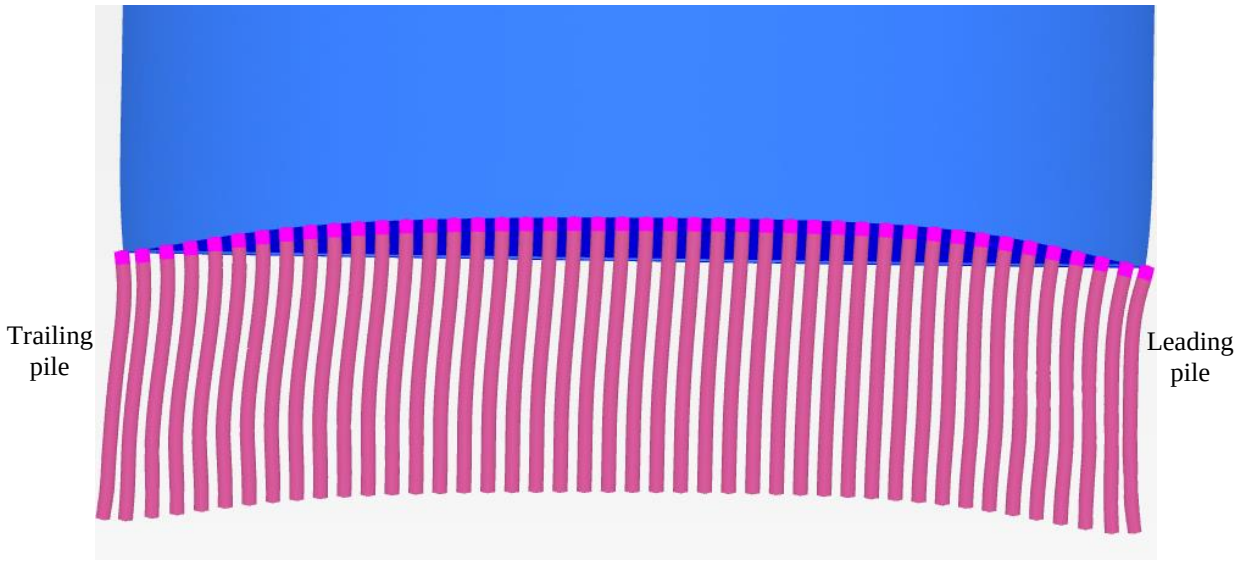

Figure 2-5 Deflected shape of the bottom of the tank and midline piles (scaled up 100 times)

Similarly, the bending moment profiles, shown in Fig. 2-6, of the same piles also demonstrate that the integrated behaviour of the superstructure and foundation is most pronounced in the leading and trailing piles. Fig 2-6(a) shows the leading pile generates a larger bending moment at the pile head than the fixed-head model. In addition, the location of maximum bending moment below surface is deeper in the integrated model than the pile-only models, approximately 4*D* and 2*D*, respectively. Although, the true maximum bending moment of the leading pile occurs at the pile head. Ultimately, both free- and fixed-head models underestimate the maximum bending moment in the leading pile. On the other hand, the trailing pile in the integrated model exhibits a bending moment profile opposite in sense to the traditional design approaches. This is also consistent with the negative loading in Fig. 2-3(a). The opposite distribution of bending moment in the integrated model is explained by the deflected shape in Fig. 2-5. While the pile experiences the loading effects created by the wind, it also experiences loading effects from the tank wall which oppose and outweigh the former. In contrast, the same mechanism appears to add loading to the leading pile given the direction of the relative forces. It is also worth noting that that central pile as well as the central perimeter pile closely reflect the behaviour observed in the fixed-head model.

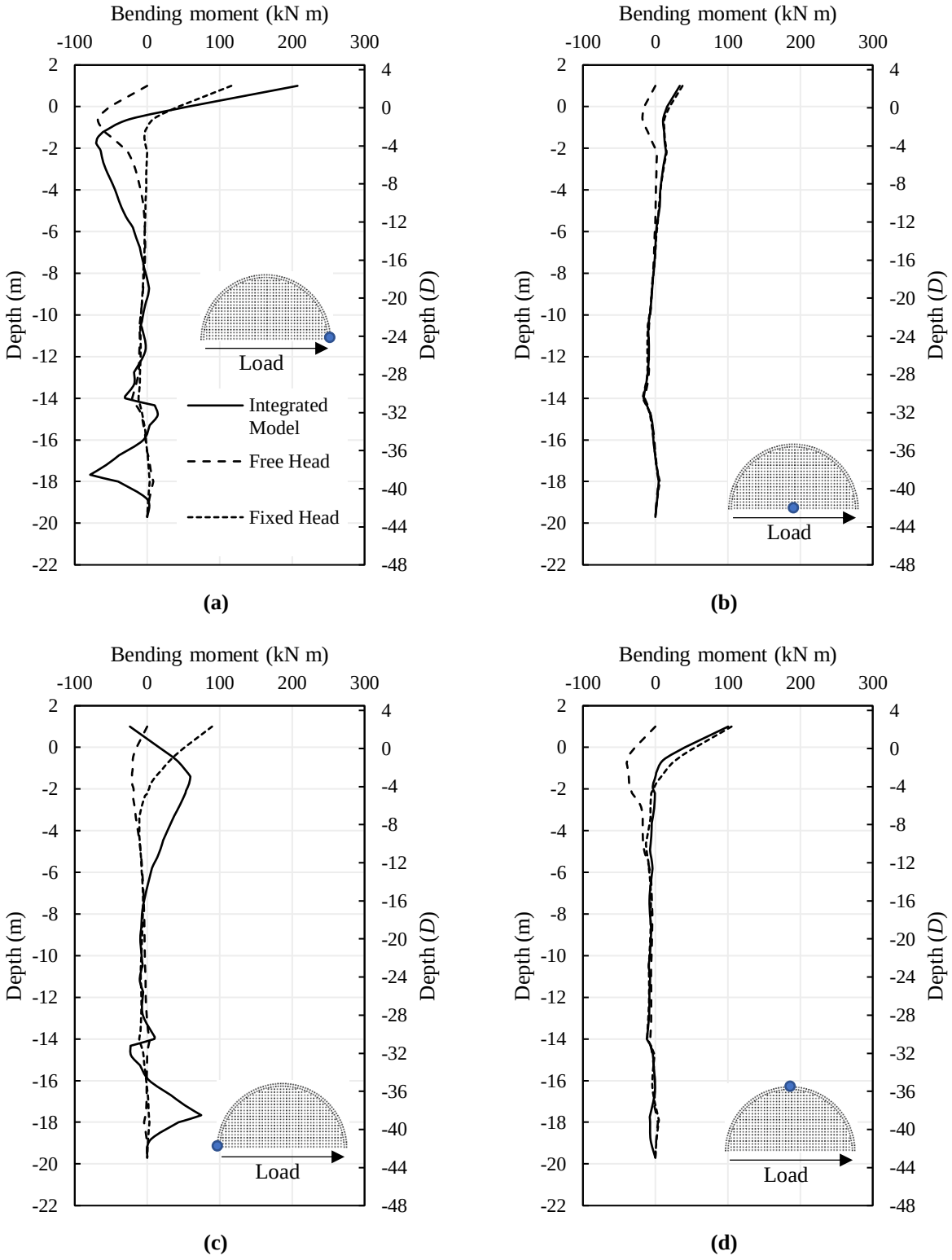

Figure 2-6 Bending moment profiles of the (a) leading pile, (b) central pile, (c) trailing pile, and (d) central perimeter pile from different analysis models

In comparison to the traditional foundation-only models, Fig. 2-6 also shows that the piles in the integrated model generates some significant variations of bending moment at lower portions of the pile, particularly with the leading and trailing piles. The same observation is also made with the shear force distributions, shown in Fig. 2-7. This is likely caused by a combination of numeric irregularities, and discontinuities with changing soil layers. In addition, it may also be created by the addition of the superstructure to the model as the irregularities are not observed in the foundation-only results. This is reflective in the soil lateral displacement contours in Fig. 2-8, which shows that the lateral deflection of the soil extends deeper that the models which consider only the foundation. Of note, the soil lateral movement is significant near the tips of the leading and trailing piles which helps explain why the irregularities are most significant in those piles.

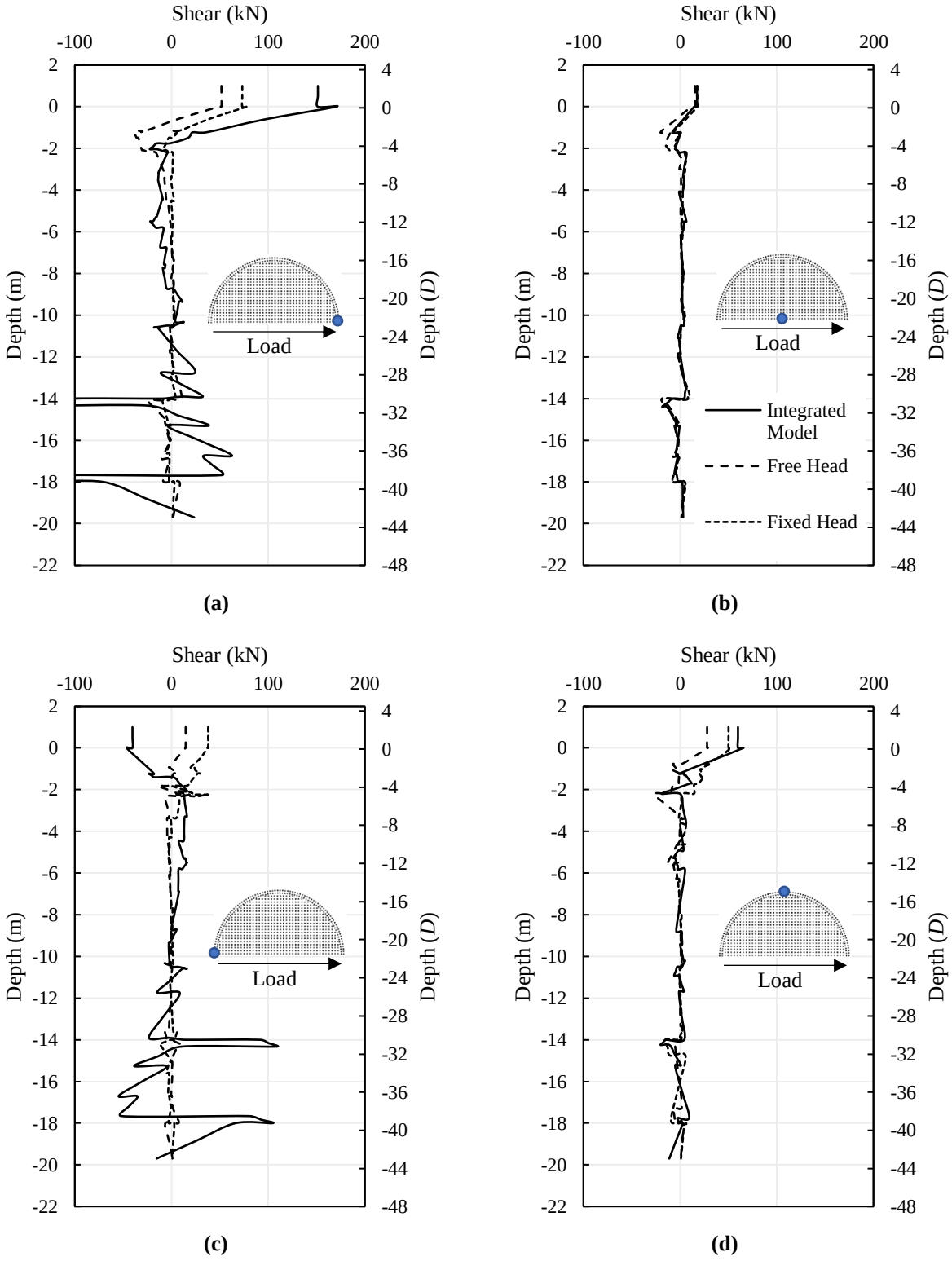

Figure 2-7 Shear force profiles of the (a) leading pile, (b) central pile, (c) trailing pile, and (d) central perimeter pile from different analysis models

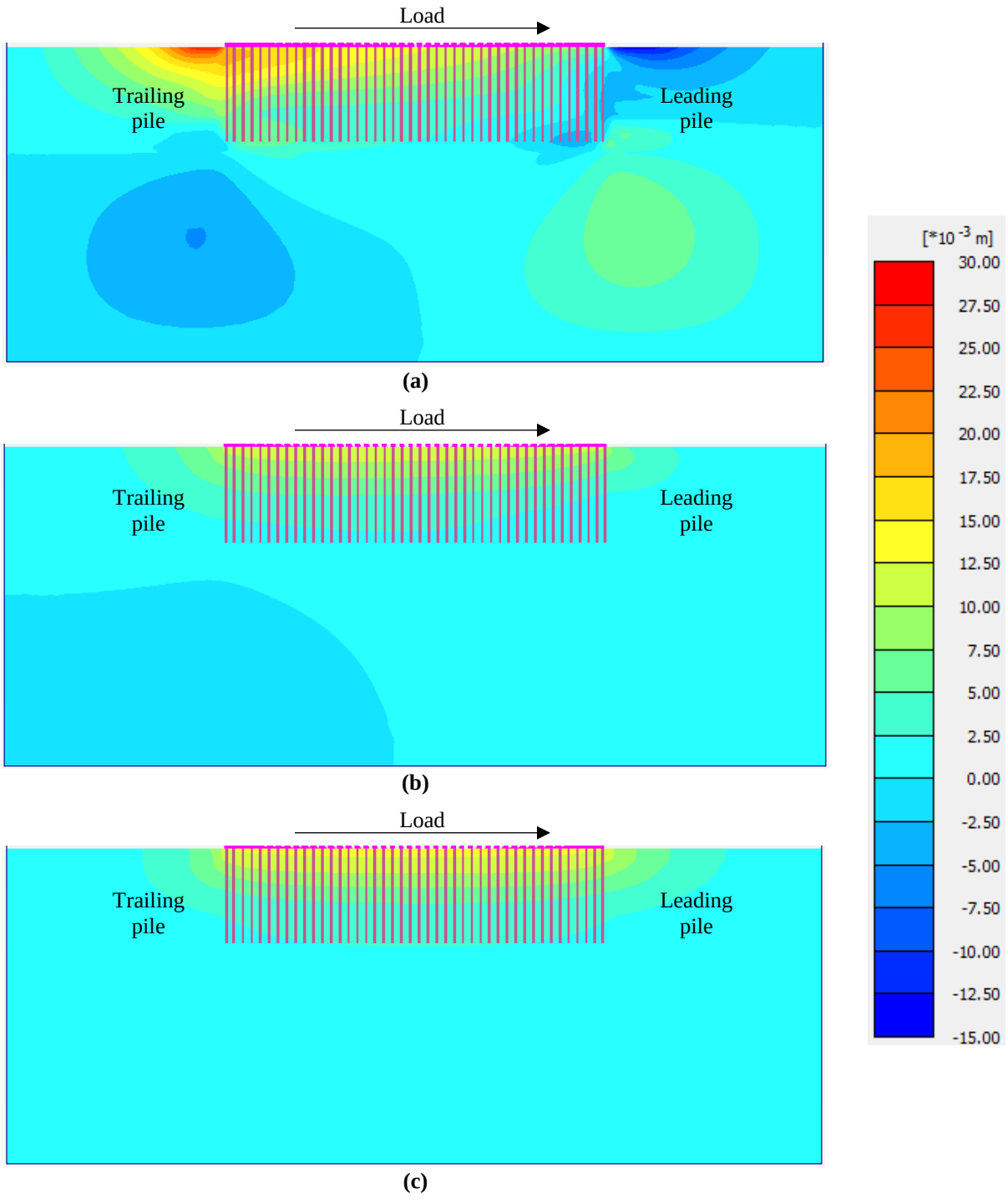

Figure 2-8 Soil lateral displacement contours along the midline from the (a) integrated model, (b) free-head model, and (c) fixed-head model

2.4.2. Effect of quantity of LNG in tank

During the service life of the tank, it is expected to cycle through storing various amounts of LNG. While the tank is designed to store up to 1,000,000 BBL, it is not expected to continually store this amount. Thus, at the time of a

significant lateral load event, the amount of LNG in the tank may not be predictable. This study intends to observe how the added pressure of LNG on the foundation affects the lateral response. Additional 3D FE simulations were performed to compare the lateral foundation response considering an empty tank to a half-filled tank as well as a completely full tank. Applied gravitational pressures to the tank bottom are based on pressures applied during the tank's pre-operational hydrotest at a half-full state and full state using 101.3 kPa and 203.6 kPa, respectively.

Fig. 2-9 compares the shear distribution of piles with varying amounts of LNG pressures. In general, the responses from the three models are similar in behaviour. However, Fig. 2-9(a) illustrates that the addition of LNG pressure minimizes the fluctuation of lateral load carried by the midline piles. In other words, the additional gas pressure may minimize the effect of tank overturning. Fig. 2-10 also shows that as the LNG pressure is applied, the load carried in the center of the tank decreases, along with the maximum loading from the tank walls. However, Fig. 2-9(b) and 2-9(c) show there is little to no effect to the perimeter pile reactions.

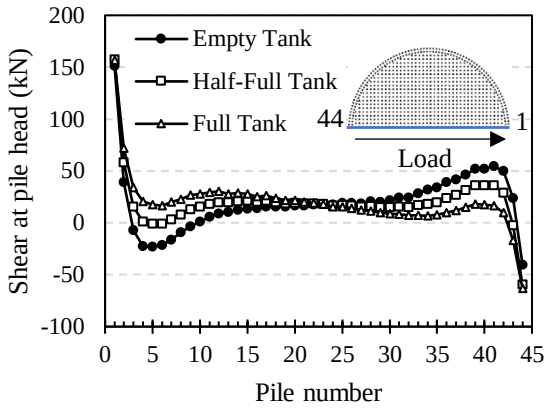

(a)

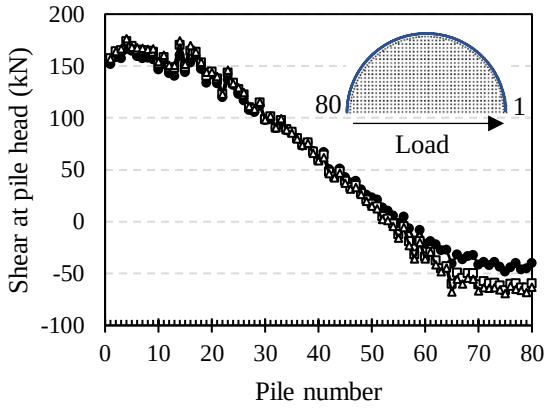

(b)

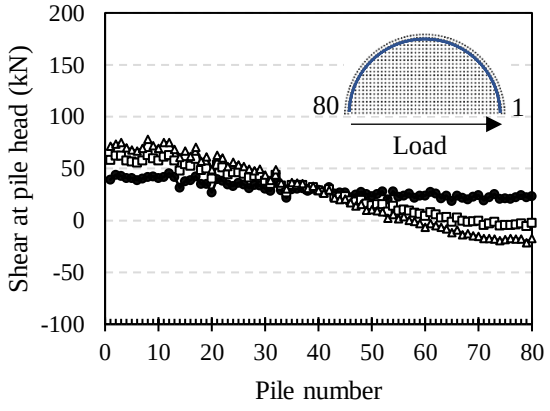

(c)

Figure 2-9 Distribution of shear at pile head for (a) midline piles, (b) outer perimeter piles, and (c) inner perimeter piles from models with varying LNG pressures

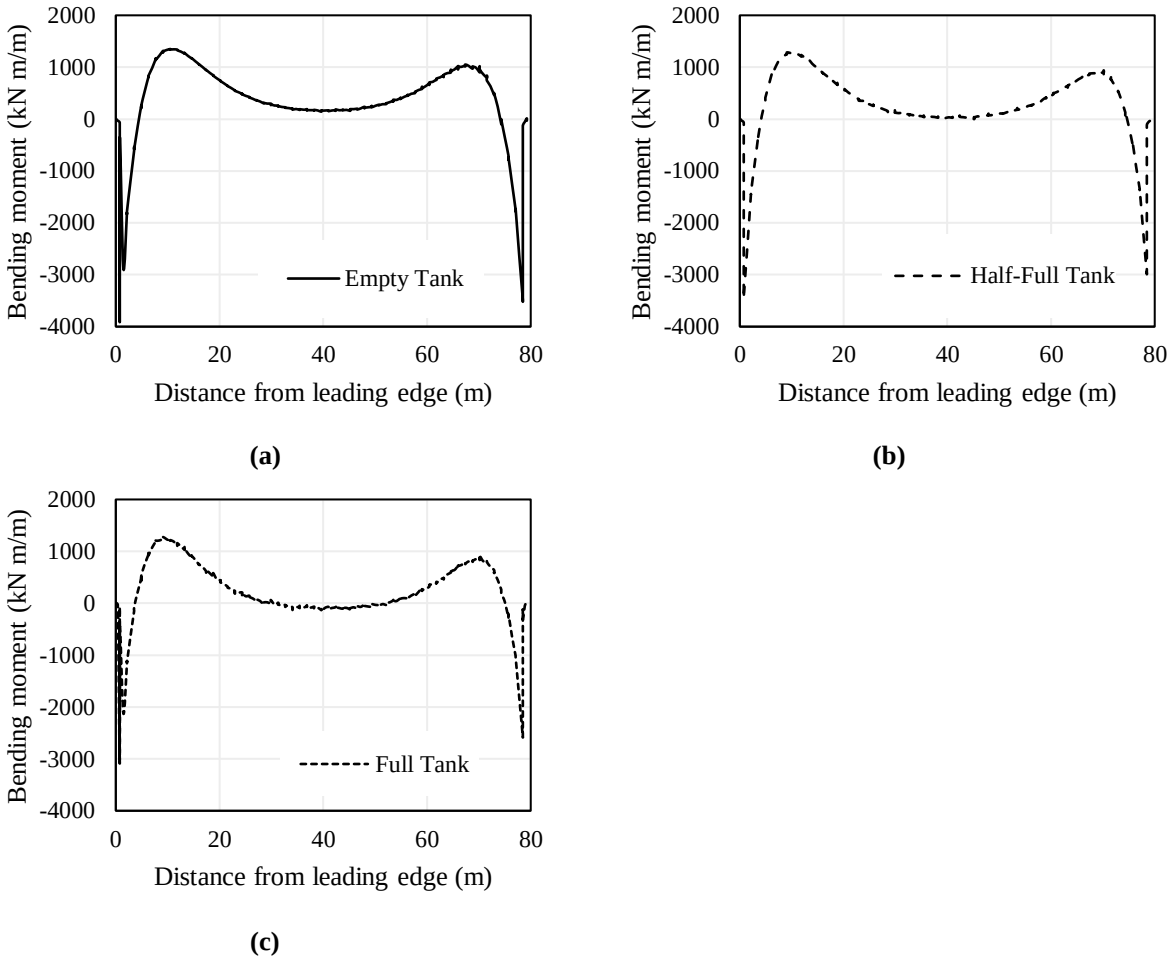

Figure 2-10 Bending moment of tank bottom and pile cap for an (a) empty tank, (b) half-full tank and (c) full tank

The lateral displacements of key piles in the foundation are compared in Fig. 2-11. Overall, the pile head displacements are near identical in all simulations, and the influence depth extends the full length of the embedded pile. However, the addition of LNG pressure increases the subsurface lateral displacement of the leading and trailing piles at a greater depth (Fig. 2-11(a, c)). These same effects are not observed in the central and central perimeter piles as lateral displacement profiles overlap (Fig. 2-11(b, d)).

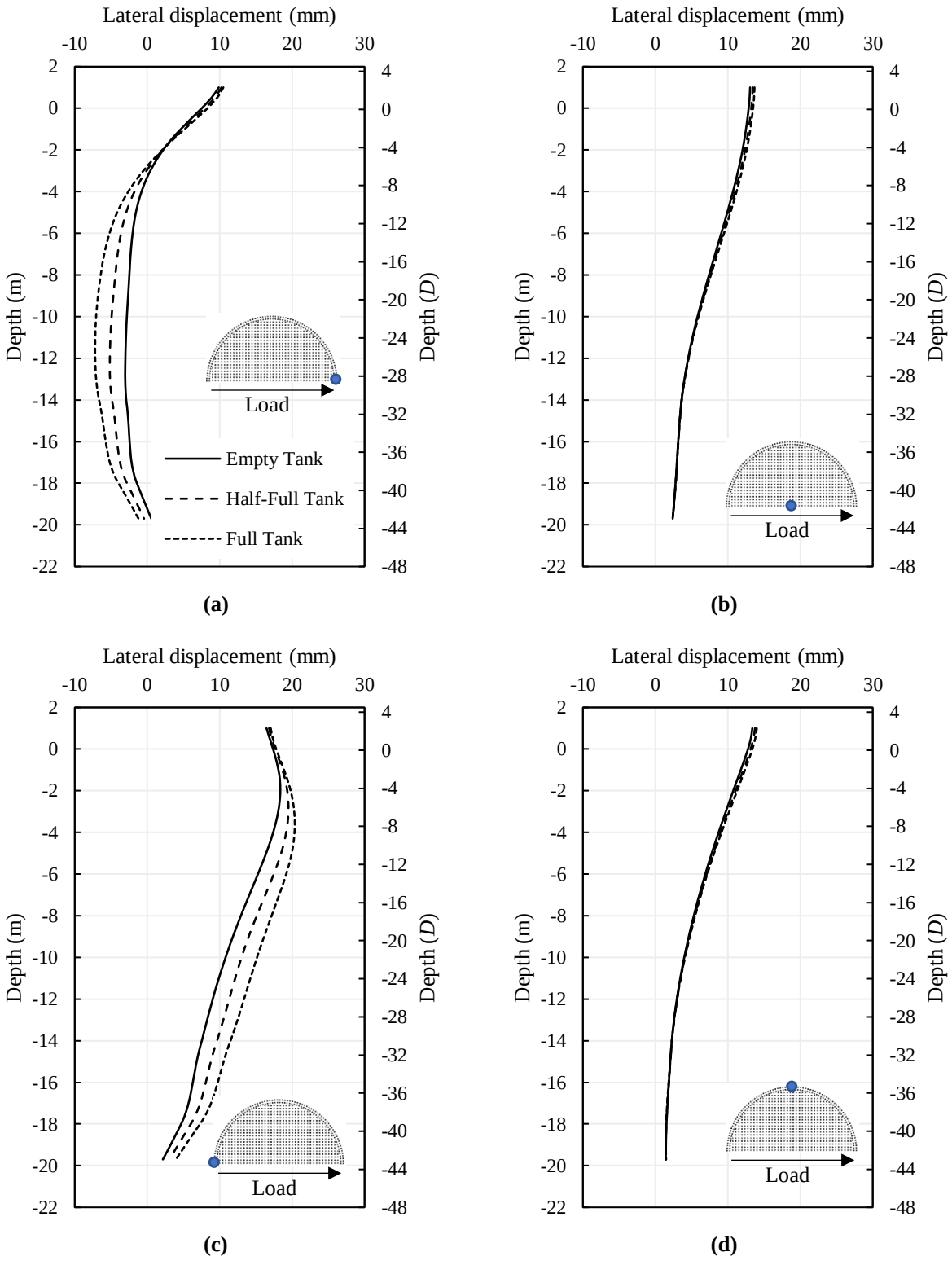

Figure 2-11 Lateral displacement profiles of the (a) leading pile, (b) central pile, (c) trailing pile, and (d) central perimeter pile with varying LNG pressures

Similar observations are also made with the bending moment profiles. In Fig. 2-12, the addition of LNG pressure seems to slightly increase the bending moment carried at the pile head for the leading and trailing piles. This is also in combination with a decrease in the maximum bending moment experienced below ground surface and deepening its location. Although, these effects appear minimal. As with the lateral displacement profiles, the central and central perimeter piles appear unaffected (Fig. 2-12(b, d)).

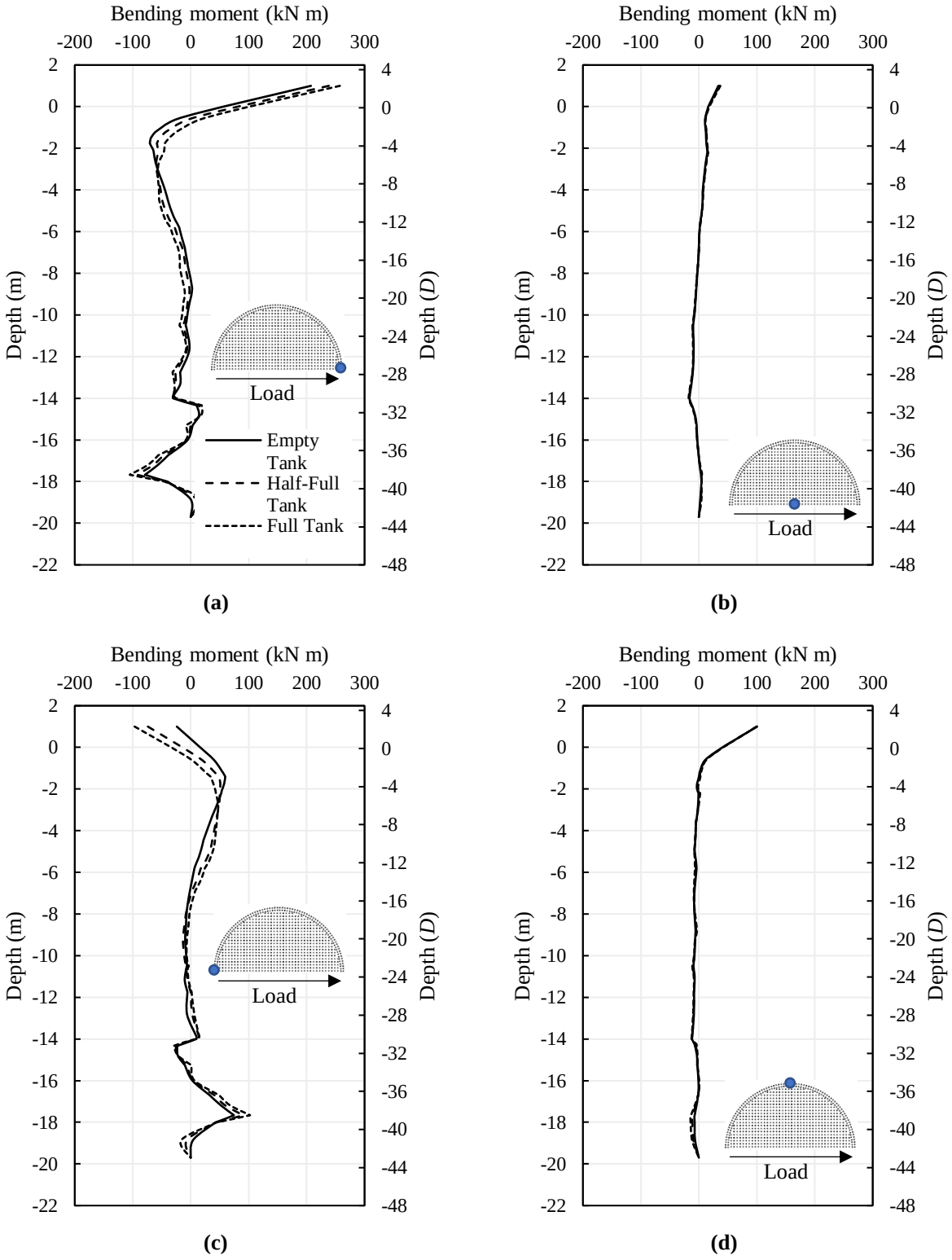

Figure 2-12 Bending moment profiles of the (a) leading pile, (b) central pile, (c) trailing pile, and (d) central perimeter pile with varying LNG pressures

2.4.3. Effect of soil condition

A majority of the parametric analyses in this study considers a multilayered soil condition based on site investigations at the Osaka Gas Senboku Receiving Terminal 1 (Teramoto et al. 2018). However, soil conditions where future LNG tanks may be erected can vary significantly. Thus, it is of importance to study the effect different soil conditions has on the foundation response, particularly with respect to the integrated superstructure-foundation behaviour. This parametric study compares the pile responses in the layered soil to responses of identical foundations in uniform sand with varying densities. In all simulations, the water table is assumed to be at an identical depth of 1.225 m below ground surface. The input soil parameters used for the uniform soil models are identical to those used in the previous study performed by the authors (Jones et al. 2021). The effect of adjusting the relative foundation-soil stiffness is observed using 3D FE models, and results are discussed below.

From the distribution of shear forces in Fig. 2-13 it can be observed that the soil condition can have a significant effect on pile response. In Fig. 2-13(a), all three uniform sand models display a similar load redistribution trend along the midline of piles. Compared to the layered soil results, piles other than the leading-most, central, and trailing-most piles carry a greater portion of load. This is consistent with previous findings of the pile groups in layered soil generating a greater group effect when compared to the behaviour in uniform sand. Less of a soil condition effect is noticeable with the perimeter piles (Fig. 2-13(b, c)).

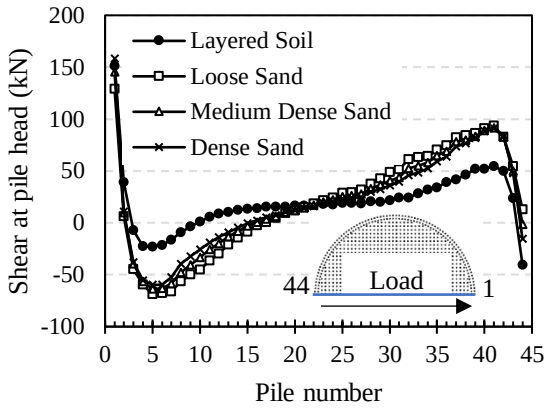

(a)

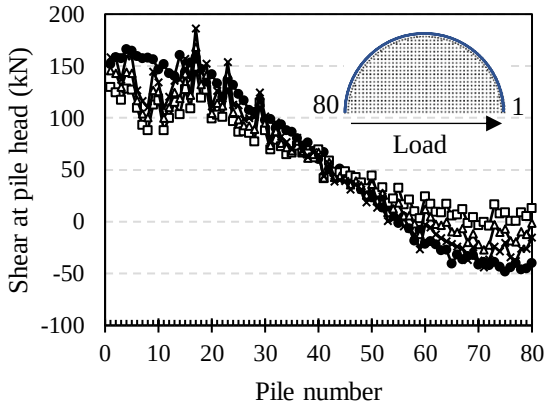

(b)

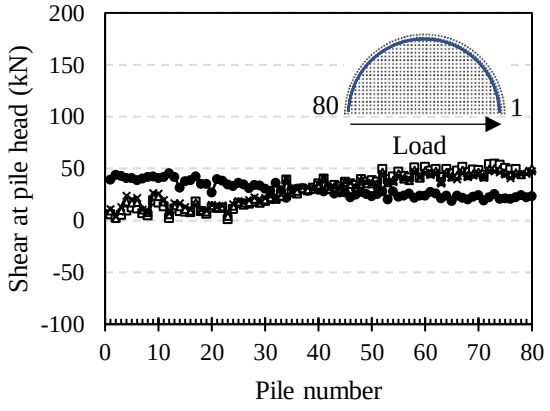

(c)

Figure 2-13 Distribution of shear at pile head for (a) midline piles, (b) outer perimeter piles, and (c) inner perimeter piles from models with varying soil conditions

The soil condition effect is also observed in Fig. 2-14 which shows the lateral displacement profiles of key piles. Between the uniform sand models, the leading pile, central pile, trailing pile, and central perimeter pile all have larger deflections in loose sand. However, three of the four key piles (all except the trailing pile) have even larger deflections when in the layered soil. On average, this trend extends to the rest of the piles in the group. The average pile head displacement of the piles in the layered soil is 13.2 mm. In contrast, the average pile head displacements in the loose, medium dense, and dense sands are 12.7 mm, 9.3 mm, and 7.2 mm, respectively. As the results from this paper indicate that the influence depth extends the entire pile length, it suggests that the weaker soils in the layered deposit affect the behaviour. Another finding in these results is that the shape of the deflected pile appears to be a function of the soil condition. From the four key piles observed in Fig. 2-14, the deflected shape of the piles in the uniform sands are all approximately the same. The only significant difference appears to be the magnitude of deflection. In contrast, the deflected shape from the piles in layered soil appears different, suggesting the change in soil stiffness and properties between layers influenced this result. With the influence depth extending the full length of the pile, it is difficult to pinpoint exactly which layer or layers have this influence. As many in-situ soil conditions have variable soil profiles, it is expected for exact pile deflection shapes to vary.

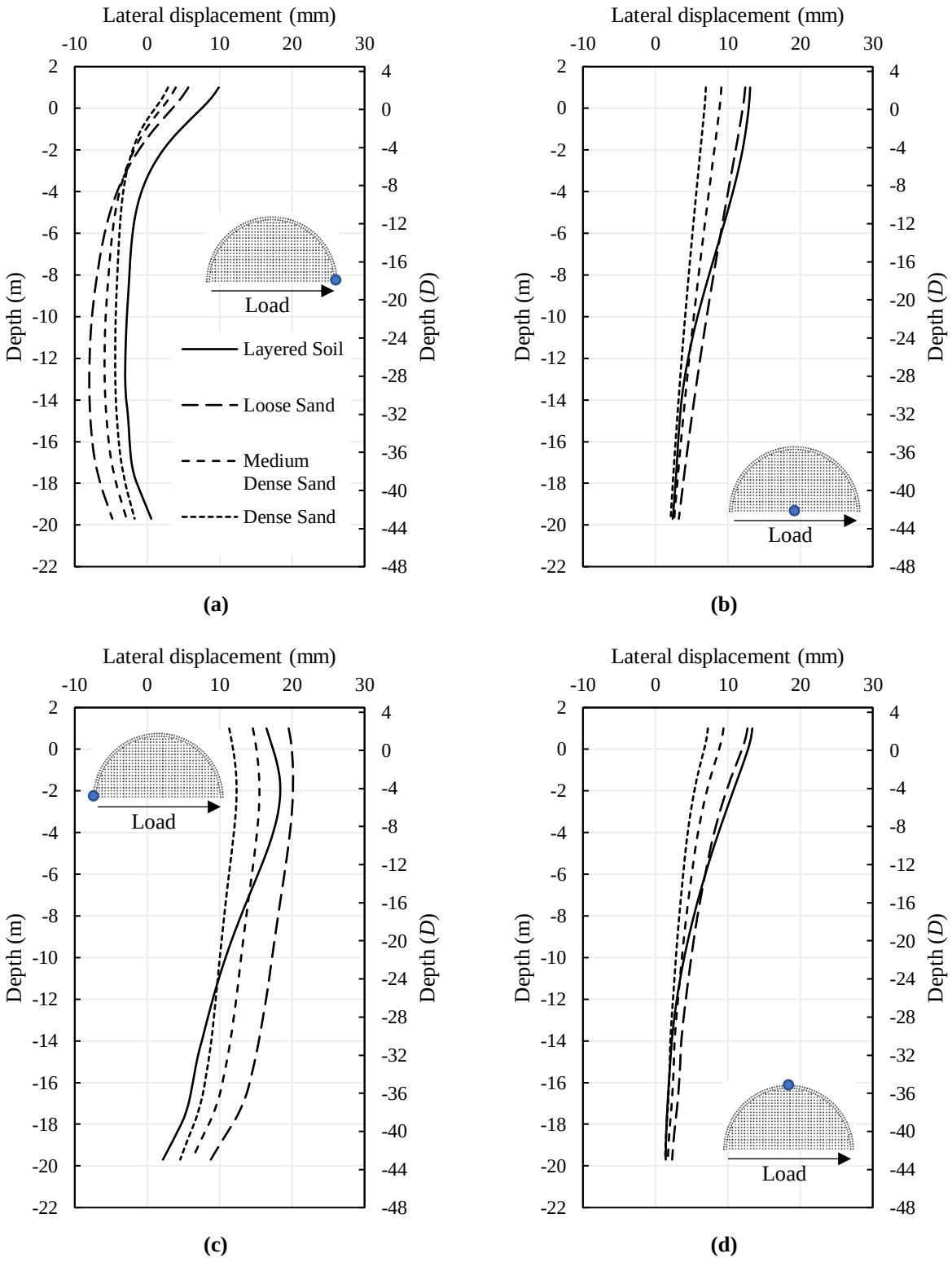

Figure 2-14 Lateral displacement profiles of the (a) leading pile, (b) central pile, (c) trailing pile, and (d) central perimeter pile with varying soil conditions

Fig. 2-15 compares the bending moment profiles in the varying soil conditions observed in the parametric study. The leading pile generates the largest maximum bending moment at the pile head in all soil conditions. In the uniform sand, this maximum bending moment remains approximately unchanged. However, the largest bending moment subsurface increases with increasing sand density (Fig. 2-15(a)). When looking at the results for the leading pile in layered soil, it is observed that the maximum bending moment is larger than all three sand cases. In the trailing pile, the results are somewhat varied where the increasing density of the sand switches the direction of the moment profile (Fig. 2-15(c)). However, the maximum bending moment generated in this pile is largest when placed in the Japanese layered soil. Little to no effect is observed between the four models in the central and central perimeter piles (Fig. 2-15(b, d)).

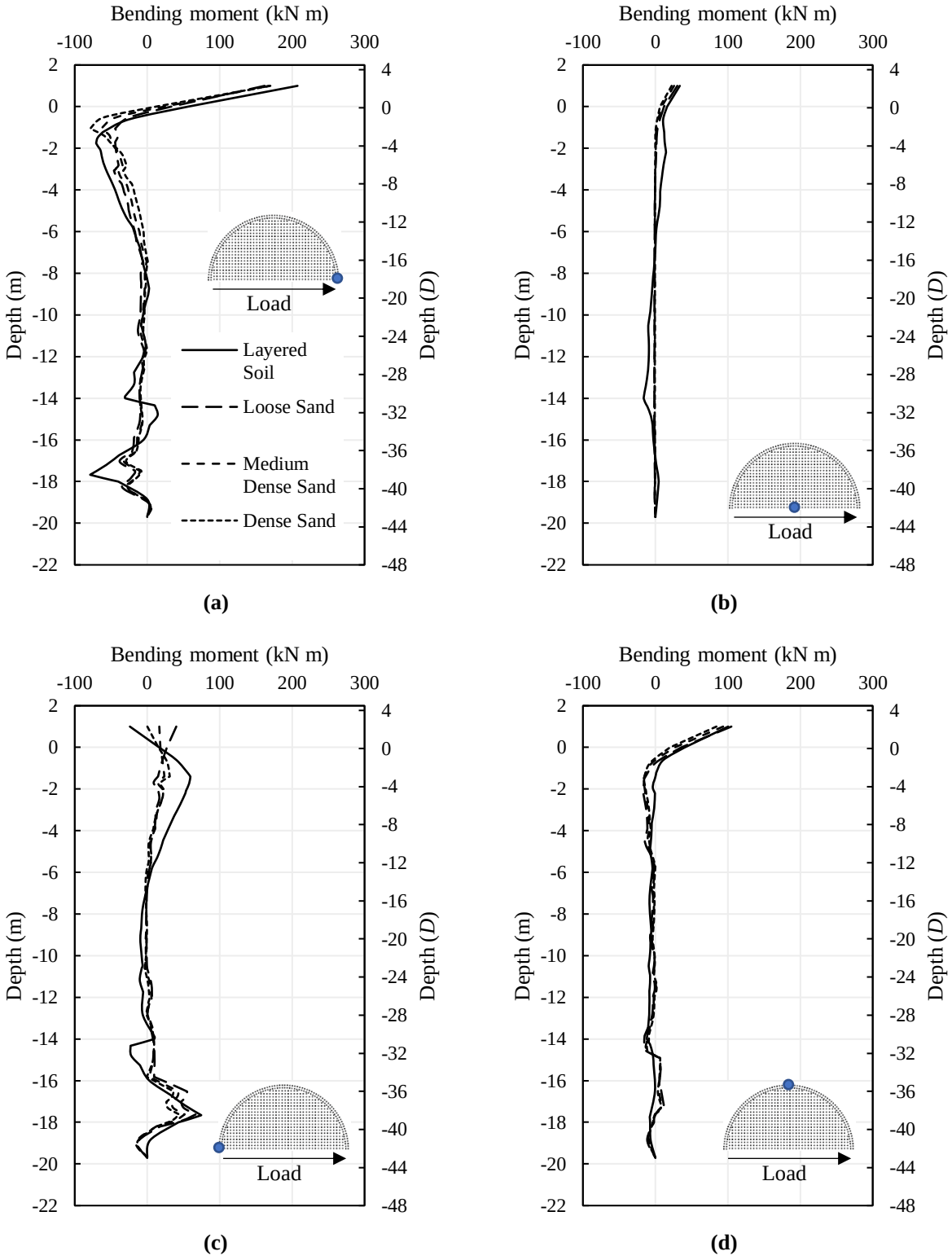

Figure 2-15 Bending moment profiles of the (a) leading pile, (b) central pile, (c) trailing pile, and (d) central perimeter pile with varying soil conditions

2.4.4. Effect of pile spacing

Pile spacing is a known to have an effect of the lateral behaviour of pile groups, and many design recommendations are dependant on this aspect (e.g., AASHTO (2012), FEMA (2012), FHWA (2016)). Closer spacing is known to result in more group interaction, and less soil resistance when compared to individual piles. Pile spacing is also a major aspect which influences the soil-foundation stiffness. While 4*D* is a common spacing used for piles in LNG storage tank foundations, the designing engineers may use a different spacing depending on site conditions. To observe this pile spacing effect, different pile groups are constructed in 3D FE models to support identical LNG tanks and loading conditions. The 1600-pile group with 4*D* spacing is reduced in size to compare to foundations with 780 piles and 476 piles with 6*D* and 8*D* spacings, respectively. The layout of the different foundations with varying spacing are shown in Fig. 2-2.

Shear distribution at the pile heads is shown in Fig. 2-16. Instead of showing the distribution as a function of pile number, as in previous figures, the shear is plotted against the distance from the leading pile. This allows for a better comparison between models as they have a different number of piles along their midlines and perimeters. As expected, the piles along the midline of the foundation as well the piles along the perimeter rows carry more load when the piles have greater spacing. This is because the total load applied to the tank is the same, while fewer piles are available to carry the loading. Fig. 2-16(a) illustrates that this is particularly impactful to the central and trailing piles, and less significant to the leading piles. Fig. 2-16(b) and Fig. 2-16(c) show that the trend in load share in the perimeter piles is identical in all three models. However, greater load is carried by the piles belonging to the groups with greater spacing. Thus, the change in pile spacing had a minimal effect on the load distribution of perimeter pile rows.

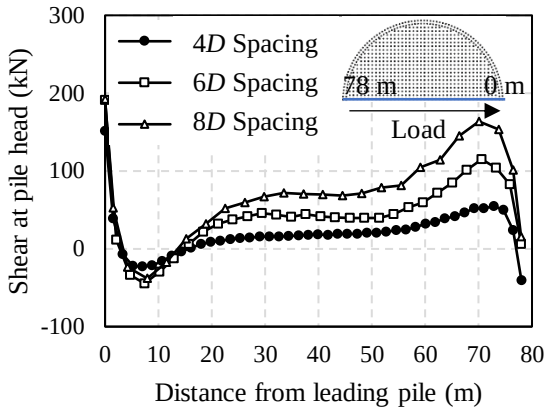

(a)

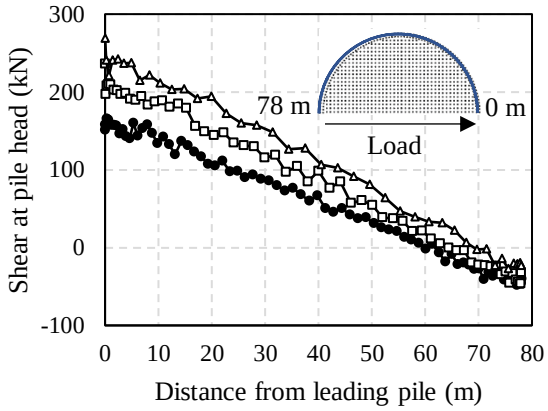

(b)

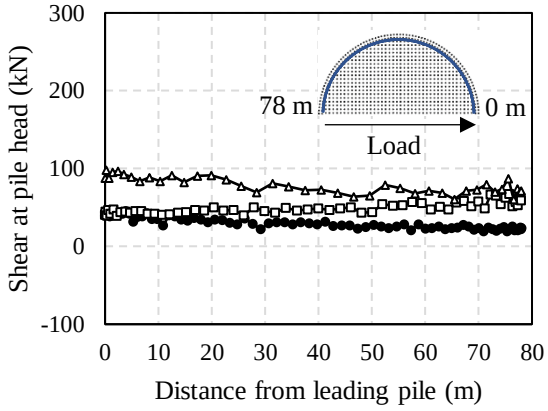

(c)

Figure 2-16 Distribution of shear at pile head for (a) central piles, (b) outer perimeter piles, and (c) inner perimeter piles from models with varying pile spacings

The lateral displacement profiles of key piles in the group did not change significantly with the increase in pile spacing. The leading pile (Fig. 2-17(a)), central pile (Fig. 2-17(b)), and central perimeter pile (Fig. 2-17(d)) show a slightly greater pile head displacement as pile spacing increased. This is consistent with expectations as foundations with reduced stiffness (i.e., fewer piles with larger pile spacing) are expected to deform more. The displacements in the trailing piles are approximately the same in all three models (Fig. 2-17(c)).

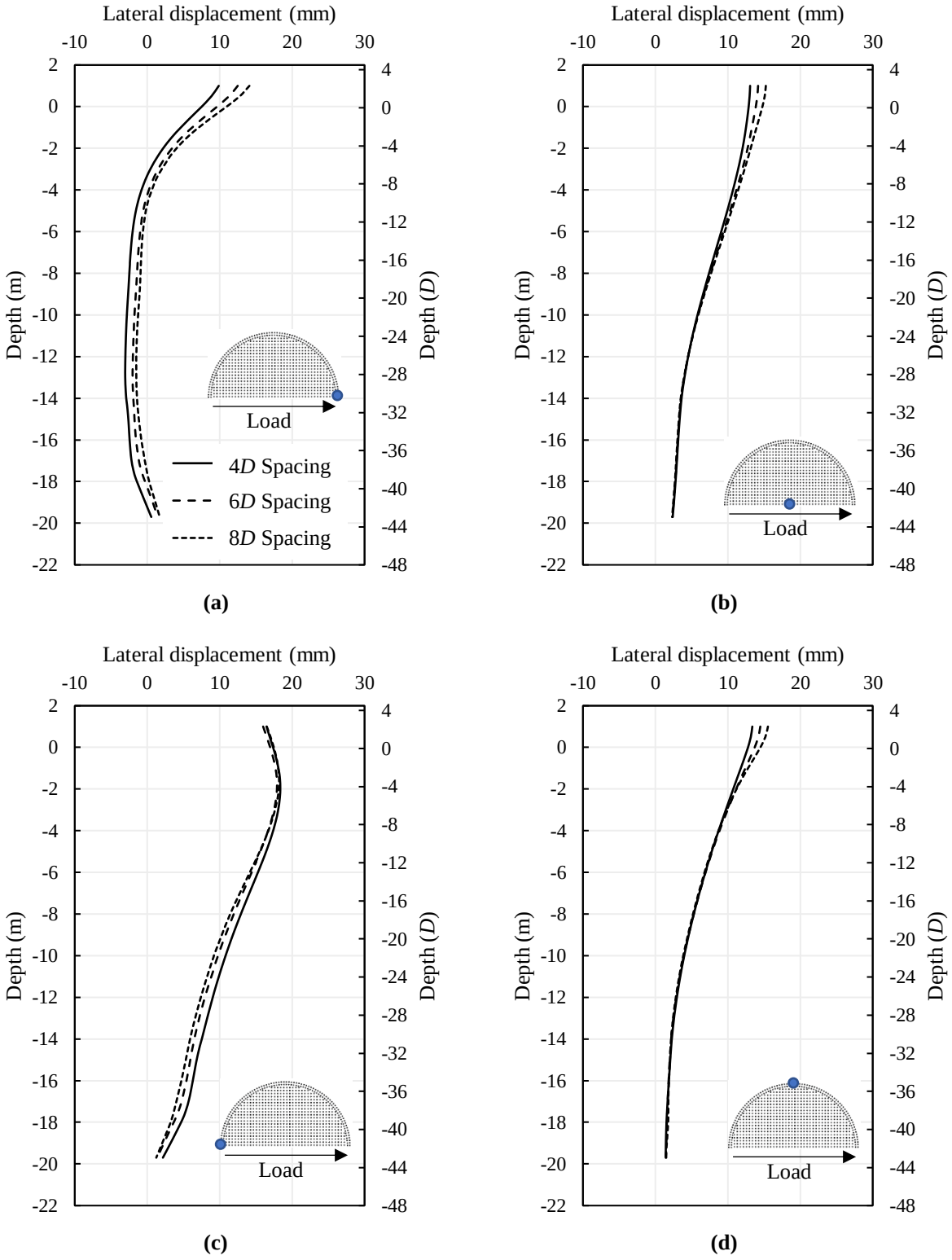

Figure 2-17 Lateral displacement profiles of the (a) leading pile, (b) central pile, (c) trailing pile, and (d) central perimeter pile with varying pile spacings

Fig. 2-18 displays the comparison of bending moment profiles for the models with different pile spacings. As the inter pile spacing increases, the bending moment carried by the leading pile increases both at the pile head, as well as maximum bending moment subsurface. (Fig. 2-18(a)). Similar findings are also observed with the central, trailing, and central perimeter piles, albeit to a lesser magnitude (Fig. 2-18(b, c, d)). Special observation is made with respect to the trailing pile as the bending moment at the pile head is variable in direction, and the maximum bending moment subsurface appears reasonably unchanged. Overall, with fewer piles to carry similar loading, it is expected that greater loading is carried per pile when fewer piles comprise the foundation.

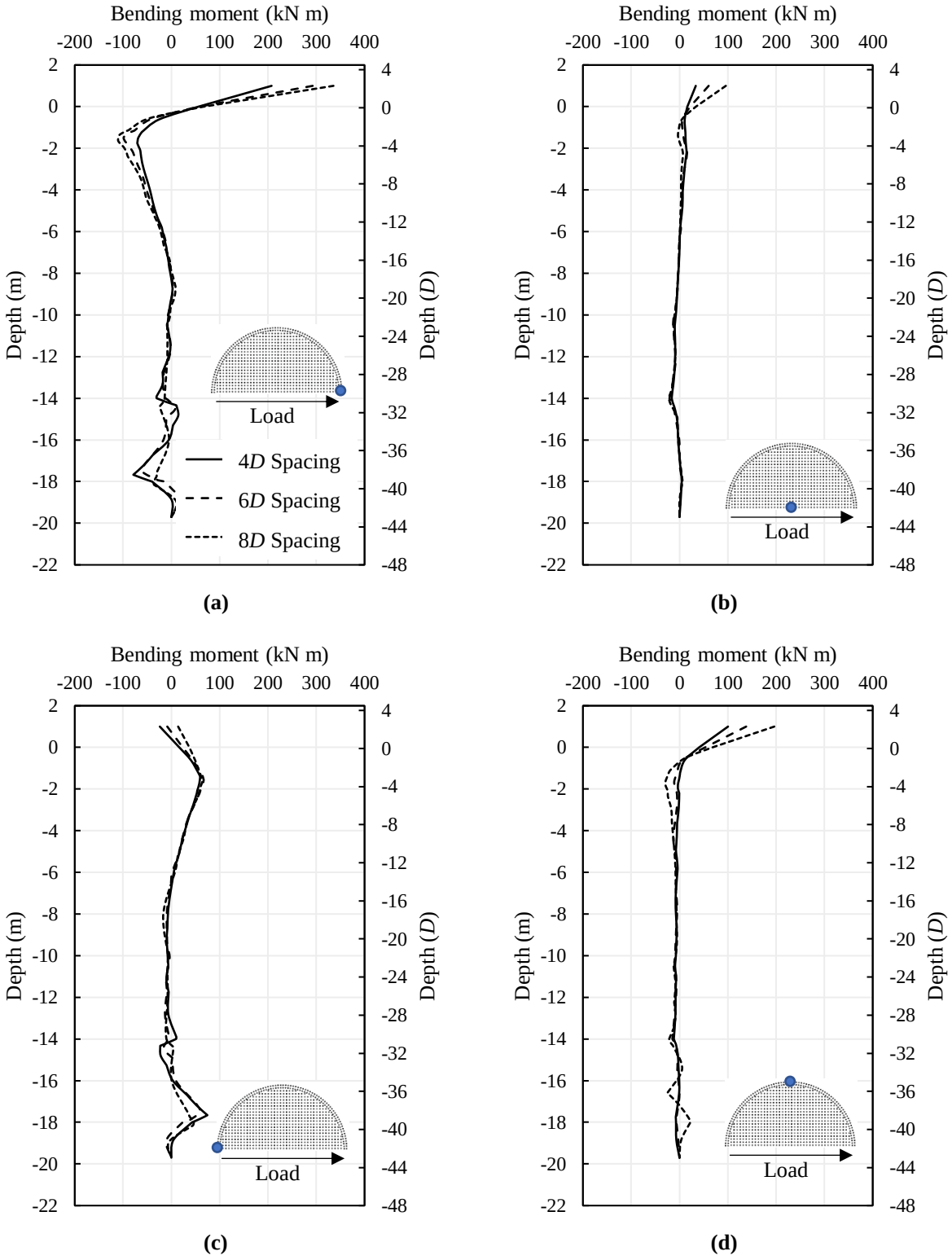

Figure 2-18 Bending moment profiles of the (a) leading pile, (b) central pile, (c) trailing pile, and (d) central perimeter pile with varying pile spacings

2.5. Conclusions

This study investigated the integrated foundation-superstructure behaviour of LNG storage tanks and piled foundations via a comprehensive parametric FE study. A tank and foundation constructed in Savannah, GA, USA was selected for a case study. An integrated analysis approach was adopted, where the full interaction among superstructure, pile foundation and soil was considered in a single computer model. The aim was to develop practical design recommendations based on realistic models. Using the traditional analysis approach, decoupled models (i.e., foundation only) were also developed and analysed for direct comparison to the integrated models. Comparing to the traditional (decoupled) approach, the integrated approach avoids crude assumptions (e.g., boundary conditions) as all elements are coupled during the entire computation. Subsequently, a series of integrated FE models were created to conduct parametric analyses to observe how the different analysis approaches, added LNG pressure, soil condition and pile spacing influence the load distribution to the foundation. Observations were made with respect to the shear, deflection, and bending moment carried by key piles in the arrangements. Based on the results of the study, the following conclusions were made:

(1) The load distribution is not well approximated by the traditional design approach (i.e., decoupled approach). The added weight of the tank and overturning effects created by the lateral loading causes a different trend in load share between piles along the midline of the foundation, as well as the outer ring of perimeter piles. A larger response is generated in midline piles near the tank wall. Overall, the leading and trailing piles are the most significantly affected by the integrated behaviour.

(2) Due to the weight of the tank walls and overturning effects on the tank, the foundation-only approach underestimates the response of the leading pile and overestimates the response of the trailing pile. Changes in the relative stiffness of the foundation can vary the degree of tank overturning, and the response of these piles.

(3) In general, the fixed-head model is most agreeable with the integrated model in comparison to the free-head model. While discrepancies were noted in the leading and trailing piles, it closely predicted the lateral displacement and bending moment profiles of the central and central perimeter piles.

(4) The influence depth of the piles observed in all the parametric analyses extend the full length, or 43D. This is much larger than the approximately 10D depth observed in previous studies. This suggests laterally loaded

pile groups of group sizes close to or larger than observed in this study (476 – 1600 piles) should be designed with consideration to the entire soil profile along the embedded depth.

(5) The addition of LNG pressure to the foundation changes the distribution of load carried by the piles along the midline of the foundation. As more gravitational pressure is applied, the tank overturning effects seem to minimize, and the lateral load carried by the central piles become more uniform. Minimal effects were noted in pile deflection and bending moment profiles.

(6) Changes in soil-foundation stiffness, including varying soil condition and pile spacing, also cause changes to the distribution of pile response carried by the foundation. With the influence depth extending the length of the pile, changes in soil properties along the embedded depth can influence the deflection shape, and the load carried by different piles in the group. Increasing pile spacing results in minimal increases in pile head deflection and load carried by each pile.

References

AASHTO 2012. AASHTO LRFD bridge design specifications. American Association of State Highway and Transportation Officials (AASHTO), Washington, D.C., USA.

Brinkgrieve, R.B.J., Kumarswamy, S., Swolfs, W.M. 2018. Computer program PLAXIS 3D reference manual, Delft University of Technology & PLAXIS bv, The Netherlands.

Brown, D.A., Morrison, C., and Reese, L.C. 1988. Lateral load behavior of pile group in sand. Journal of Geotechnical Engineering (ASCE), **114**(11): 1261–1276.

Dao, T.P.T. 2011. Validation of PLAXIS embedded piles for lateral loading. Delft University of Technology.

FEMA 2012. Foundation analysis and design (No. FEMA P-751), NEHRP recommended provisions: design examples. Federal Emergency Management Agency (FEMA). National Institute of Building Sciences, Building Seismic Safety Council, Washington, D.C., USA.

FHWA 2016. Design and construction of driven pile foundations – volume 1. National Highway Institute U.S. Department of Transportation, Federal Highway Administration, Washington, D.C., U.S.A.

Fraser, R., and Wardle, L. 1976. Numerical analysis of rectangular rafts on layered foundations. Géotechnique, **26**(4): 613–630. doi:https://doi.org/10.1680/geot.1976.26.4.613.

Jones, K., Sun, M., and Lin, C. Numerical analysis of group effects of a large pile group under lateral loading. Computers and Geotechnics (under review)

Ko, J., Cho, J., and Jeong, S. 2017. Nonlinear 3D interactive analysis of superstructure and piled raft foundation. Engineering Structures, **143**: 204–218.

Lin, C., Bennett, C., Han, J., and Parsons, R.L. 2010. Scour effects on the response of laterally loaded piles considering stress history of sand. Computers and Geotechnics, **37**(7–8): 1008–1014.

Lin, C., Bennett, C., Han, J., and Parsons, R.L. 2012. Integrated analysis of the performance of pile-supported bridges under scoured conditions. Engineering Structures, **36**: 27–38.

Lin, G.M., and Lin, C. 2019. Driven pile supported LNG tank in Savannah, Georgia. Deep Foundation Institute Magazine, (2019 Jan/Feb Issue).

Luo, C., Yang, X., Zhan, C., Jin, X., and Ding, Z. 2016. Nonlinear 3D finite element analysis of soil–pile–structure interaction system subjected to horizontal earthquake excitation. Soil Dynamics and Earthquake Engineering, **84**: 145–156. doi:https://doi.org/10.1016/j.soildyn.2016.02.005.

McVay, M., Casper, R., and Shang, T.-I. 1995. Lateral response of three-row groups in loose to dense sands at 3d and 5d pile spacing. Journal of Geotechnical Engineering (ASCE), **121**(5): 436–441.

McVay, M., Zhang, L., Molnit, T., and Peter, L. 1998. Centrifuge testing of large laterally loaded pile groups in sand. Journal of Geotechnical and Geoenvironmental Engineering, **124**(10): 1016–1026. doi:10.1061/(ASCE)1090-0241(1998)124:10(1016).

Rollins, K., Peterson, K., and Weaver, T. 1998. Lateral load behavior of full-scale pile group in clay. Journal of Geotechnical and Geoenvironmental Engineering, **124**(6): 468–478. doi:10.1061/(ASCE)1090-0241(1998)124:6(468).

Ruesta, P., and Townsend, F. 1997. Evaluation of laterally loaded pile group at Roosevelt Bridge. Journal of Geotechnical and Geoenvironmental Engineering, **123**(12): 1153–1161. doi:10.1061/(ASCE)1090-0241(1997)123:12(1153).

Teramoto, S., Niimura, T., Akutsu, T., and Kimura, M. 2018. Evaluation of ultimate behavior of actual large-scale pile group foundation by in-situ lateral loading tests and numerical analysis. Soils and Foundations, **58**(4): 819–837. doi:10.1016/j.sandf.2018.03.011.

Viladkar, M.N., Noorzaei, J., and Godbole, P.N. 1994. Interactive analysis of a space frame-raft-soil system considering soil nonlinearity. Computers & Structures, **51**(4): 343–356. doi:https://doi.org/10.1016/0045-7949(94)90320-4.

Appendix A

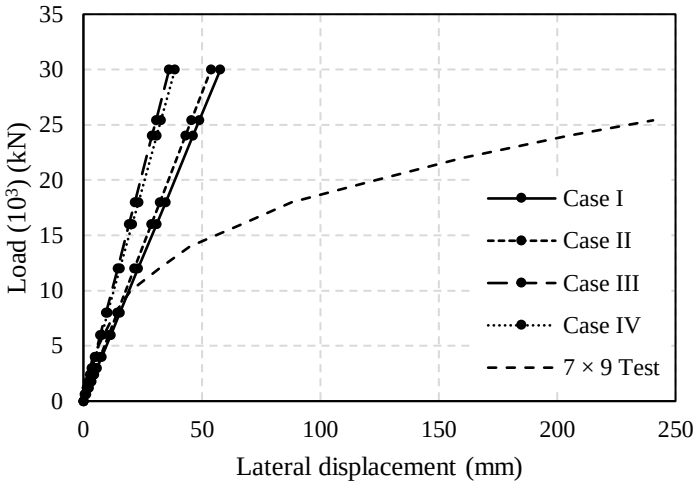

(a)

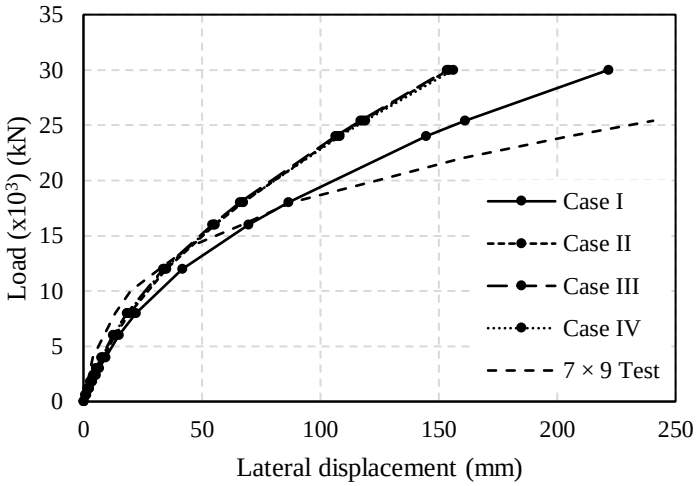

(b)

Figure A-1 Comparison of load-displacement curves between different baseline models in the preliminary study with (a) linear-elastic and (b) Mohr-Coulomb soil models

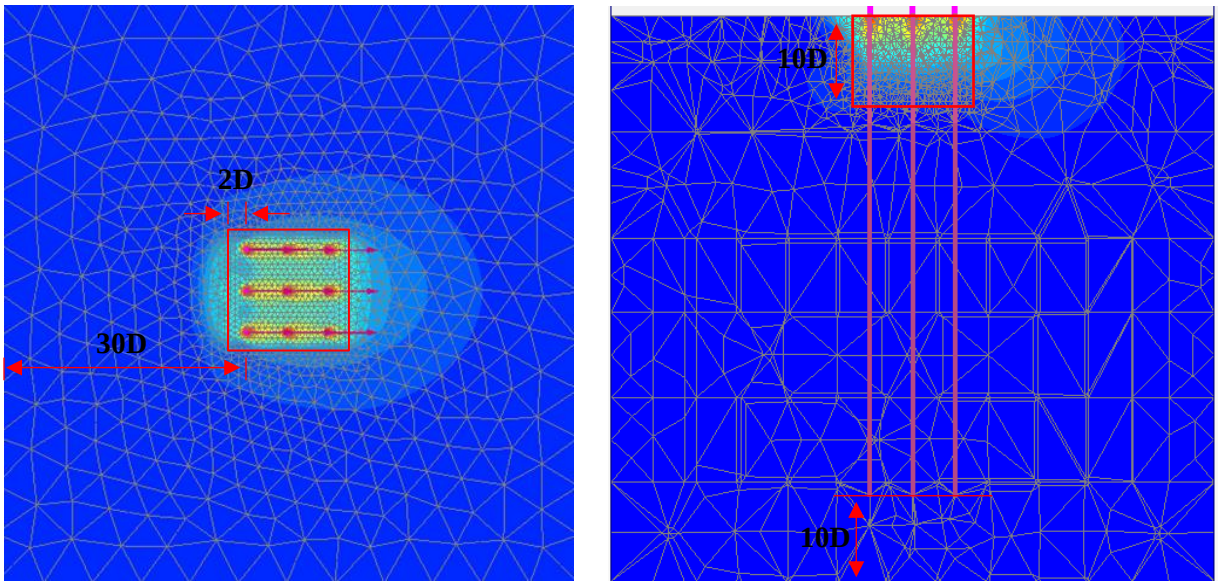

(a) (b)

Figure A-2 Meshing boundaries and local refinement of a 3 × 3 pile group: (a) horizontal; (b) vertical

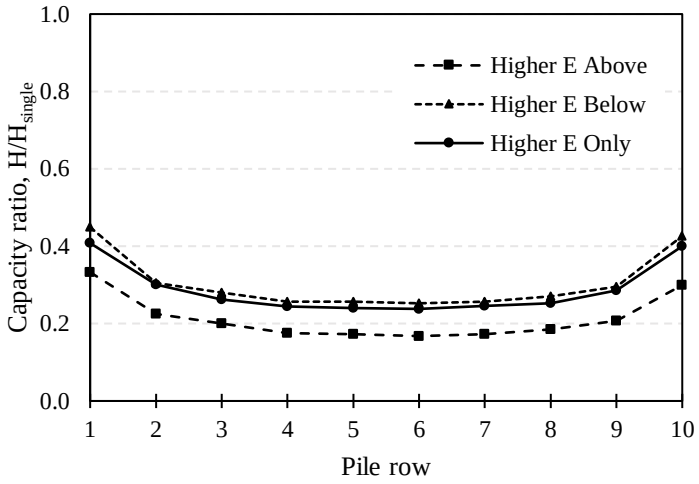

Group Efficiencies:

$$\eta = \frac{H_{total}/N}{H_{single}}$$

Higher *E* Above
$\eta = 0.21$

Higher *E* Below
$\eta = 0.30$

Higher *E* Only
$\eta = 0.29$

Figure A-3 Capacity ratio and group efficiency of a 10 × 10 pile groups in linear elastic soil with different soil modulus profiles

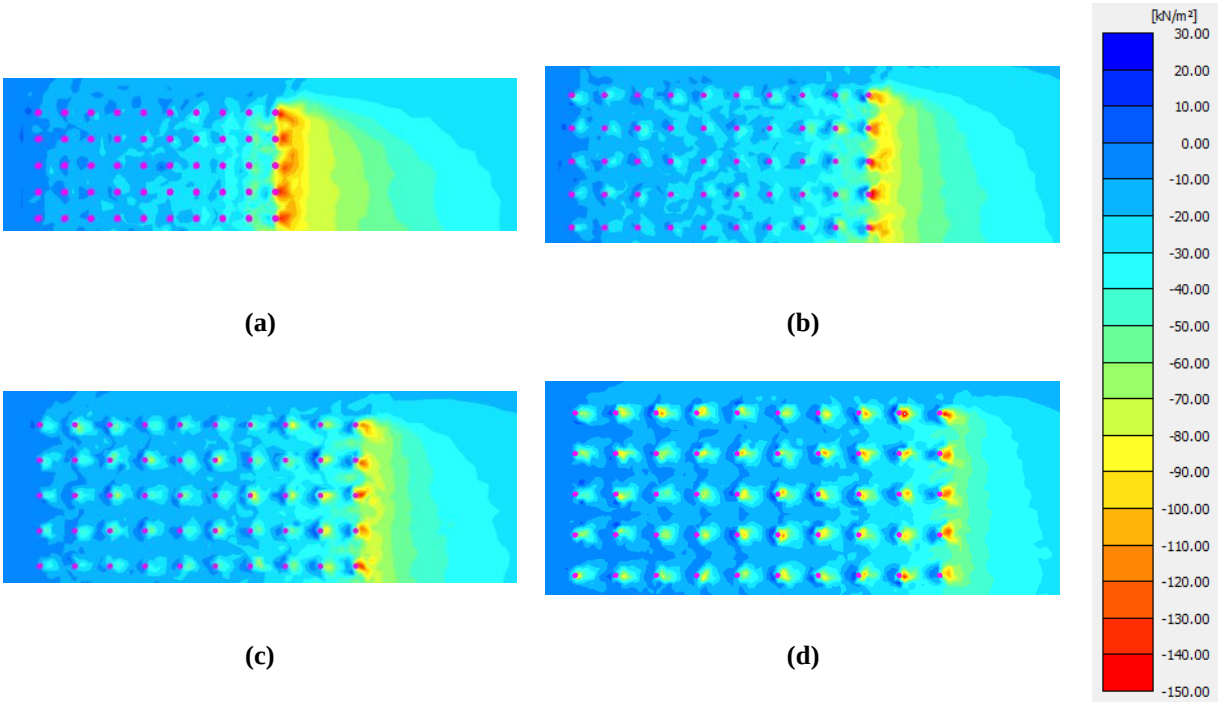

Figure A-4 Plan view of lateral effective stress 3*D* below ground surface of a 10 × 10 pile group with varying pile spacings: (a) *S*=3*D*; (b) *S*= 5*D*; (c) *S*=6*D*; (d) *S*=8*D*

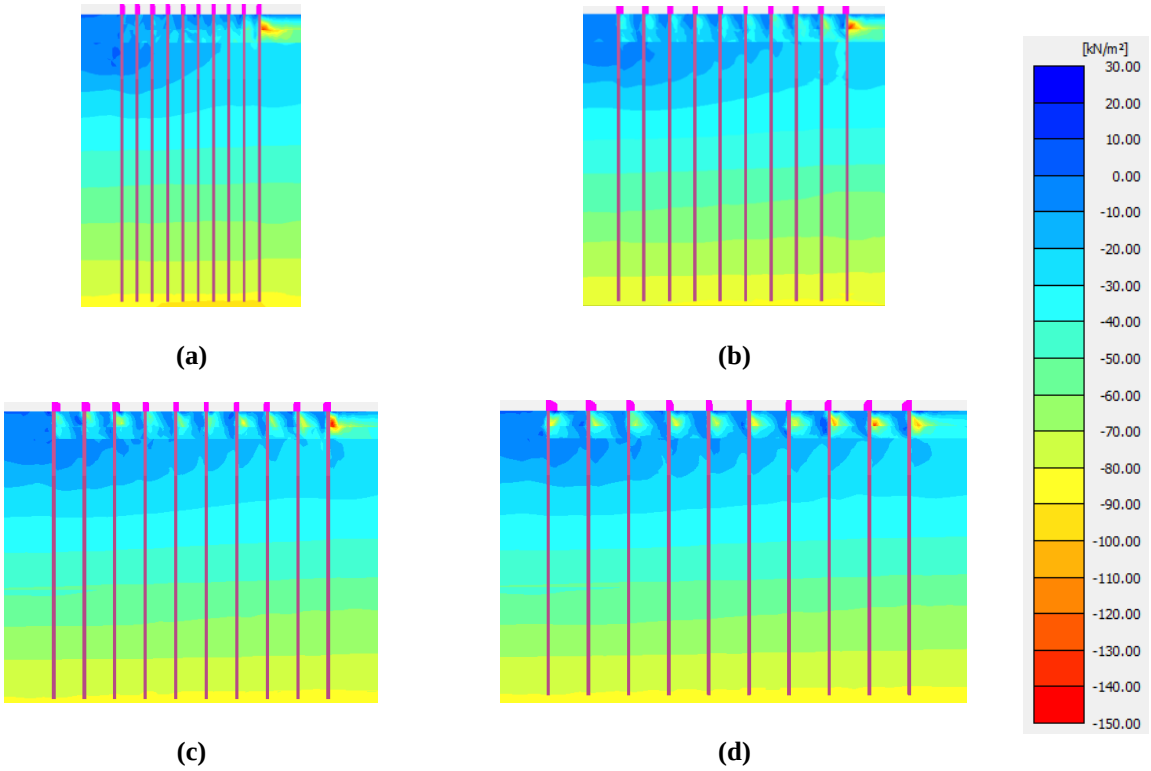

Figure A-5 Cross-sectional view of lateral effective stress of the midline piles in a 10 × 10 pile group in layered soil with varying pile spacings: (a) *S*=3*D*; (b) *S*= 5*D*; (c) *S*=6*D*; (d) *S*=8*D*

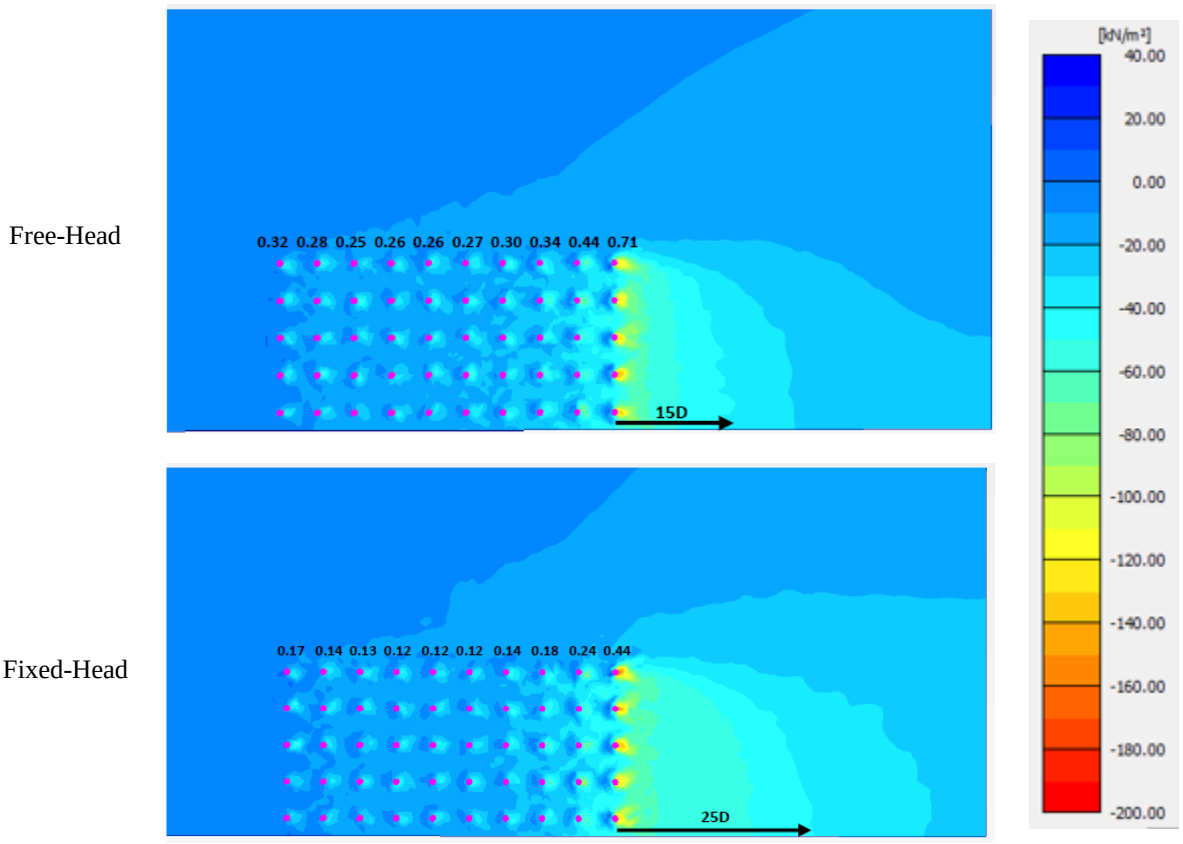

Figure A-6 Plan view of lateral effective stress at a depth of 2.5*D* below the ground surface for 10 x 10 pile group models with free- and fixed-head conditions

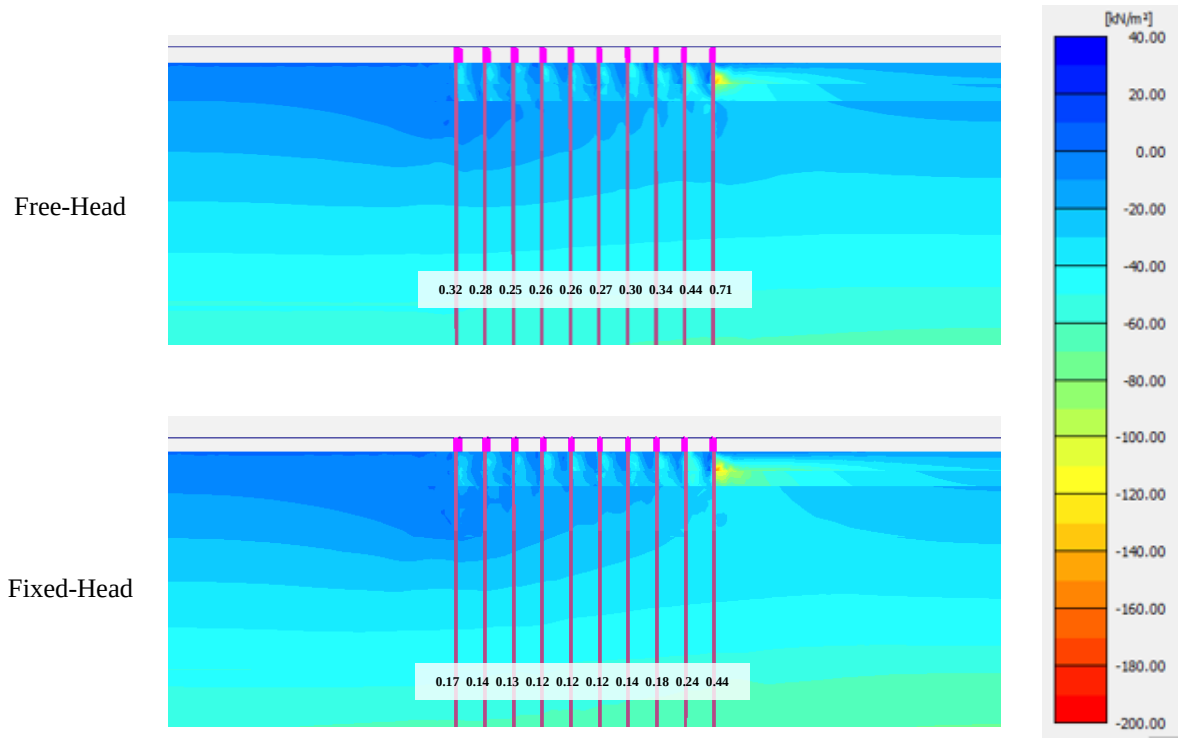

Figure A-7 Cross-sectional view of lateral effective stress for central piles from 10 x 10 pile group models with free- and fixed-head conditions